Remote Techniques for Time - of - Flight Flaw Characterisation

by

Stephen James Davies, B. Sc. (Newcastle - upon - Tyne)

being a thesis submitted for the degree of Doctor of Philosophy
at the University of Warwick

Department of Physics
March (1991)

To Alison

Summary

This thesis describes the investigations conducted into the characterisation of various defects within solids using laser - generation and interferometric detection of ultrasound. Laser - generated ultrasound has advantages over the more commonly used piezoelectric transducers in that it is a reproducible, wide bandwidth, non - contact source which, by using appropriate optics, can be focussed to a point or line source and easily scanned over a surface. Used in association with an interferometric detector enables the possibility of a remote inspection system which would be useful for some applications. The properties of such a system for the characterisation of both bulk and surface - breaking defects are ascertained.

Part of the research project has been concerned with determining the properties of the ultrasound produced in various solids by different laser pulse profiles. The results obtained indicate that the risetime of the ultrasonic compression wave decreases with decreasing incident laser pulse risetime. However the mechanical and thermal properties of the irradiated solid also affects the risetime of the ultrasound. Modelling of the laser - solid interaction was undertaken to understand this phenomenon in more detail.

The wide bandwidth nature of laser - generated ultrasound was used in the characterisation of bulk defects. This has involved determining, using an FFT algorithm, the phase change which occurs when laser - generated ultrasound is scattered from such defects. The aim of the investigation was to assess whether a particular type of defect has a unique phase change which will enable it to be classified. The experimental results obtained compared favourably with the results from theoretical modelling of ultrasonic scattering by defects.

Finally the interaction of laser - generated Rayleigh (surface) waves with surface - breaking defects was considered. Various techniques for the characterisation of surface - breaking defects by analysis of data in the time and frequency domain were utilised. One such technique involved measurement of the Reflection and Transmission coefficients of various surface discontinuities. The phase change of the scattered Rayleigh wave was determined and compared to the theoretical data available. Also, a technique was established whereby certain features on the waveforms recorded on transmission of a Rayleigh wave through a surface - breaking defect could be used to determine the depth of the defect.

Table of Contents

List of Tables and Illustrations

Acknowledgements

The research described in this thesis was made possible by the financial assistance rendered by the Science and Engineering Research Council and the National Non - Destructive Testing Centre, Harwell under a CASE award. Sadly, the policies of the present government towards scientific research will make it yet more difficult for persons like myself to undertake postgraduate research in the future.

My research has benefited from the close collaboration with the National Non - Destructive Testing Centre, Harwell particularly Mr. T. Slesenger whom I thank for his continued interest in what were busy times for him. I would also like to thank my supervisor, Prof. S. B. Palmer, for his interest in and encouragement of my studies. To finalise this vein of academic acknowledgements I would also like to thank Dr. C. Edwards for his ever inquisitive mind.

Away from the contributions made to my academic research there are several people who have contributed, in varying degrees, to my postgraduate studies. The assistance rendered to me by my parents is much appreciated and it would not have been possible to continue my research without them. The Solid State Boys also deserve a mention, namely (and these are their proper names) Greg, Roger, Adrian, Alun and A. C. My time at Warwick would have been much less enjoyable without these characters around, they have been privy to a remarkable metamorphosis. Andrew, Don and John also deserve no less a mention for the many laughs provided in a multitude of ways. Other people around the department too numerous to mention provided interesting sideshows, they know who they are.

To complete the acknowledgements I would like to thank Alison for her love and support. Her contributions to the final product are immeasurable and in some small token of repayment I dedicate this thesis to her.

Declaration

The work described in this thesis is my own except where specifically stated as otherwise and was conducted in the Department of Physics, University of Warwick during the period October 1987 to March 1991. No part of this work has been submitted to this or any other academic institution for admission to a higher degree. Some of the work has already appeared in the form of publications and these are listed below :

Davies, S. J. and Palmer, S. B., J. Nondestr. Test. Eval., **5**, 227 (1990)

Davies, S. J. and Palmer, S. B., Rev. Prog. in Quant. NDE, **10A**, 121 (1990)

Davies, S. J. et al. Rev. Prog. in Quant. NDE, **10A**, 499 (1990)

Chapter One

INTRODUCTION

Recent research using laser - generated ultrasound has concentrated on the potential applications of this unique ultrasonic source particularly in the field of non - destructive testing. The properties of laser - generated ultrasound offer possibilities in extending and improving established inspection techniques and in developing new techniques for the inspection of components in environments where it is not possible to use piezoelectric transducers. In association with these research activities is the development and improvement of non - contacting, broadband, ultrasonic transducers, such as, for example, homodyne and heterodyne interferometers and electromagnetic acoustic transducers, which offer the potential of a purely remote inspection system. Non - contacting generation and detection of ultrasound using lasers has been termed ' laser ultrasonics ' by some research groups.

This thesis describes the investigations undertaken to evaluate the usefulness of laser generation and interferometric detection of ultrasound for the characterisation of defects using the Time - of - Flight Diffraction arrangement. Some of the investigations were undertaken in collaboration with the National Non - Destructive Testing Centre, Harwell who originally developed this particular inspection technique.

The production of ultrasound upon the irradiance of a solid with a laser pulse has been extensively investigated since the early 1960's. In Chapter Two these investigations are reviewed as are the present research activities. This review presents the properties of laser - generated ultrasound in the chronological order in which an

understanding of this phenomenon was obtained. The various applications which utilise laser - generated ultrasound are also reviewed to illustrate its present stage of development.

The basic mechanism for the laser generation of ultrasound is the transferral of a proportion of the incident photon energy to heat energy. This occurs within a region extending from the irradiated solid surface to a depth determined by the electromagnetic skin depth and thermal properties of the solid. Consequently this heat energy results in a localised expansion and, if the incident laser power density is sufficiently large, eventual vapourisation of a portion of the solid resulting in the solid surface being locally stressed. Even if vapourisation does not occur a localised stress field is evolved. Using the form of the stress field in the wave equation (Achenbach (1987)) creates solutions for three possible modes of ultrasonic vibration in thick (≥ 5 mm) samples. These are compressional, shear and Rayleigh (surface) wave motions which a laser source produces simultaneously. On thin (≤ 1 mm) samples, the laser source generates symmetric and antisymmetric Lamb waves. Descriptions of the modes of vibration of these various waves may be found elsewhere (e. g. Viktorov (1967), Bullen and Bolt (1985) and Achenbach (1987)).

Detailed descriptions of the generation of ultrasound by laser pulse irradiation of a solid surface have been given by, for example, Scruby et al. (1981), Cooper (1985) and Aindow (1986). References to other articles on this subject are given in Chapter Two. Investigations into the properties of the ultrasound generated by laser vapourisation of a portion of the solid in relation to the properties of the incident laser pulse and the irradiated solid have, however, been less extensive and this is the purpose of Chapter Three. Experimental measurements of the risetime of the laser - generated ultrasonic compression wave have

indicated that it is proportional to the risetime of the incident laser pulse. However, accurate measurements of the compression wave risetime are hampered by the properties of the detector used. To reduce this effect, a broad bandwidth interferometric detector was used to record the ultrasonic compression wave signal.

A knowledge of the relationship between the laser pulse profile, the properties of the irradiated solid and the resulting ultrasonic compression wave enables an evaluation of the maximum frequency obtainable for a particular laser pulse profile and solid. It is known that a laser source generates frequencies over a much larger bandwidth than ultrasound generated by a piezoelectric transducer. The wide bandwidth nature of the laser source has potential applications in the characterisation of bulk defects and this is the subject of Chapter Four. This chapter is concerned with the determination of the phase change of ultrasound scattered from various bulk defects using the laser source and interferometric detector in the Time - of Flight Diffraction arrangement. This arrangement is discussed with specific relevance to the use of a laser source and interferometric detector to replace the commonly used piezoelectric transducers. The phase behaviour of ultrasonic signals recorded after interacting with slot and hole defects exhibited interesting features which enabled characterisation of such defects.

Various techniques for the characterisation of surface - breaking defects using laser generation and detection of Rayleigh (surface) waves were employed and are described in Chapter Five. Surface - breaking defects on some components are potentially more likely to result in component failure than are bulk defects. Thus it is important to have a technique whereby it is possible to characterise both surface - breaking and bulk defects. Using the laser source, which generates

simultaneously compression, shear and Rayleigh (surface) waves, and an interferometric detector in the Time - of Flight Diffraction arrangement enables the characterisation of both of these types of defects.

Surface - breaking defects are generally characterised from analysis of the scattered Rayleigh wave signal in the time or frequency domain. Techniques are described in this chapter which use both time and frequency domain data to characterise various surface - breaking defects. In addition a new technique for the sizing of surface - breaking defects from analysis of the Rayleigh waveform after transmission through a defect is proposed.

The concluding remarks of Chapter Six consider the potential usefulness of the defect characterisation techniques described in the previous chapters. Increased knowledge of the properties required to produce larger ultrasonic frequencies can be used to tailor the characterisation techniques described to a particular application. Recommendations for future investigations into this particular use of laser ultrasonics for defect characterisation are also given in this chapter.

REFERENCES

Achenbach, J. D. (1987)	'Wave propagation in elastic solids', 1st Ed., 5th print (North Holland) (1987)
Aindow, A. M. (1986)	PhD Thesis, University of Hull (1986)
Bullen, K. E. and Bolt, B. A. (1985)	' An introduction to the theory of seismology ', 4th Ed. (CUP) (1985)
Cooper, J. A. (1985)	PhD Thesis, University of Hull (1985)
Scruby et al. (1981)	Res. Tech. in NDT (Academic Press), Vol. V, (1981)
Viktorov, I. A. (1967)	' Rayleigh and Lamb Waves ', (Plenum Press) (1967)

Chapter Two

LASER GENERATION OF ULTRASOUND : A REVIEW

2. 1 : INTRODUCTION

Since the early 1960's there has been considerable interest in the production of elastic (or stress) waves by the irradiation of a solid with a laser pulse. This interest reached its zenith, in terms of the number of papers published, in the early 1980's. A majority of the research was conducted at the University of Hull in association with AEA Technology, Harwell. Early experiments concentrated on recording the elastic (or stress) wave produced by the interaction of a laser pulse with a solid. More detailed investigations were undertaken in association with mathematical modelling of the source, using some of the theories developed in the field of geophysics, to characterise more fully the laser source. In addition to obtaining an understanding of the laser source, investigations were undertaken to determine areas of applicability. Present research efforts in laser - generated ultrasound concentrate on the areas of application of this remote, non - contacting, broadband, highly repeatable source of ultrasound.

This chapter will give a brief history of the development of laser - generated ultrasound. The mechanisms for the production of ultrasound will also be summarised. They have been described in more detail previously by several authors (e.g. Scruby et al. (1981), Cooper (1985), Aindow (1986), Anssel et al. (1988)). One aspect of the mechanism for the laser - generation of ultrasound will be discussed in Chapter Three.

2. 2 : LASER - GENERATED ELASTIC (OR STRESS) WAVE INVESTIGATIONS IN SOLIDS UP TO 1980

The bulk of the laser - generated elastic (or stress) wave investigations from White (1963a) up to Ledbetter and Moulder (1979) concerned the interaction of Q - switched Ruby (and later Nd:YAG) laser pulses with various solids. Transparent overlays or liquids were used in a majority of the investigations to enhance the production of elastic (or stress) waves. The investigations conducted before 1980 may be broadly divided into two areas.

2. 2. 1 : Investigations of the properties of the elastic wave (mainly the compression wave) produced

Papers which dealt with this particular aspect of a laser / solid interaction include White (1963a), Ready (1965), Percival (1967), Lee and White (1968), Cachier (1971), Hartman et al. (1972), Kubota and Nakatani (1973), Robin (1978) and Ledbetter and Moulder (1979). Theories attempting to explain the production of elastic waves by the laser heating of a solid were also published in conjunction with these experimental reports. The modelling involved calculating the temperature distribution produced as a result of illuminating a surface with a laser pulse. The resulting thermal expansion was related to the thermal stresses using the usual stress - strain relation (White (1963b)). This thermal stress term was inserted into the wave equation and solutions for the compression and shear wave modes obtained. It should be noted that most of the theoretical modelling (except, for

example, Ready (1971), Penner and Sharma (1966), Krahl et al. (1975)) was concerned with the heating of a solid with no change of phase i.e. no ablation at the solid surface. This is in contrast to the majority of the experimental research in which an ablative mode of elastic wave generation was employed. Theoretical descriptions of the interaction of laser radiation with an absorbing solid with no change of phase include White (1963b), Bushnell and McCloskey (1968), Gournay (1966), Bechtel (1975), Budenkov and Kaunov (1977) and Gorodetskii et al. (1978). Modelling of the ablative mode of generation is complex. An attempt to model this mode of elastic wave generation is described in Chapter Three.

From these investigations it was noted that

- the production of the elastic wave is not a consequence of the radiation pressure which is a factor of 10^4 - 10^5 less than the ablative pressure (Askar'yan and Moroz (1963)).
- the amplitude of the bulk elastic wave increased considerably, compared to generation on a free surface, when a constraining layer was placed over the solid surface.
- the laser source could generate elastic waves under difficult environmental conditions where it is not possible to use a piezoelectric probe.
- elastic waves are generated in a variety of solids ranging from opaque to transparent to the incident wavelength (Kubota and Nakatani (1978)). As expected the amplitude of the elastic wave is much reduced with transparent materials.
- a modified wave equation in association with thermal considerations could be used to describe the shape of the elastic wave produced.

- compression, shear and Rayleigh (surface) waves were generated simultaneously by the laser source which propagate at their respective velocities characteristic of a particular solid (Ledbetter and Moulder (1979)).

2. 2. 2 : Investigation of the pressure (stress) produced in a sample, with or without a constraining layer, as a function of the incident laser fluence

Papers which reported on the measurement of the pressure produced by a laser pulse incident on a solid surface include Neumann (1964), Gregg and Thomas (1966), Felix and Ellis (1972), Fox (1974), Felix (1974), Yang (1974), Fairand et al. (1974), Fairand and Clauer (1979), Jones (1971), Anderholm (1970), Peercy et al. (1970) and Metz et al. (1975).

Neumann (1964) noted three types of evaporation which occurred depending on the material illuminated. For metals, such as aluminium or steel with relatively high melting temperatures, a stress was induced by the evaporation of electrons and ions to form a plasma. For a solid, such as lead with a lower melting point, globules are formed which result in a higher momentum imparted to the sample surface. An even higher momentum was imparted to samples such as glazed porcelain as absorption of the laser energy occurred beneath the surface resulting in the explosion of splinters of the material.

Other conclusions reached from these investigations include

- larger pressures were developed when the sample was illuminated in a vacuum rather than in air.

- using a constraining surface or an absorbing liquid in contact with the sample under study can significantly increase the pressure imparted.
- use of a constraining layer also means that larger fluences can illuminate the sample surface before surface damage occurs. The constraining layer can also act as a protective layer for the sample.
- generally the peak stress is linearly dependent on laser fluence (Yang (1974)).
- an optimum intensity exists for a particular material for the maximum momentum transfer. For the elements studied this is ~ 5 x 10^8 W / cm^2 in air which imparts a momentum ~ 5 x 10^{-5} kg m / sec per Joule of absorbed energy. This corresponds to all the material, contained within a disc defined by the laser beam diameter and electromagnetic skin depth being vapourised. It is assumed that thermal conduction of heat is negligible over the time to reach vapourisation. Below this optimum a significant amount of laser energy is conducted away in the material and this does not contribute to vapourisation. At energy densities above the optimum, a significant amount of the energy goes into increasing both the degree of ionisation and the energy per ion. The latter is less efficient in imparting momentum to the surface.
- the risetime of the stress wave closely follows the risetime of the incident laser pulse. When the laser pulse begins to decay, the stress wave decays more slowly (Fairand and Clauer (1979), Bechtel (1975)).

These investigations gave the general properties of laser - generated elastic waves but further investigations were needed to fully characterise the laser source. Knowledge of the laser source was extended further in the 1980's from further investigations of its properties conducted in the main at the University of Hull.

2. 2 : LASER - GENERATED ULTRASOUND - CHARACTERISATION OF THE SOURCE, UNIVERSITY OF HULL GROUP 1980 ONWARDS

This section will summarise the research conducted by the University of Hull group in association with AEA Technology, Harwell from 1980 onwards in the characterisation of the laser source. Research efforts of other groups will be summarised in the next section.

2. 2. 1 : Properties of the laser - generated ultrasound

It was known that the laser source produced simultaneously compression, shear and Rayleigh (surface) waves. However the efficiency of generation of ultrasound into these three acoustic modes had not been quantitatively investigated. To investigate this efficiency, a Q - switched Nd:YAG laser pulse irradiated in air the free surface of a variety of metallic samples. The compression, shear and Rayleigh (surface) waves were detected using a piezoelectric probe and the amplitude of each wave mode recorded as a function of incident laser pulse energy. For power densities at the sample surface insufficient to

generate a plasma, the amplitude of the compression and shear waves increased linearly with increasing power density. The amplitude of the Rayleigh wave also increased with increasing power density. When a plasma was formed just above the sample surface (power density $\geq 10^7$ W / cm^2) it was observed that the generation of the compression wave pulse was enhanced whilst the shear wave amplitude reached a maximum near to the onset of a plasma and then decreased steadily with increasing power density. The amplitude of the Rayleigh wave continued to increase with increasing power density.

In addition to recording the amplitude of the Rayleigh wave as a function of power density, the effect of the laser source shape on the resulting Rayleigh wave was investigated. Using a beam expander and cylindrical lens a line source whose width could be varied was produced. As the width of the line source increased the Rayleigh wave signal broadened indicating that generation of Rayleigh waves occurs at the edges of the illuminated area. The generation of the Rayleigh wave can be further enhanced by placing an aperture just above the surface. This has the effect of producing a sharp edge to the source and also enhances the shear wave production. The broadness of the Rayleigh pulse is also determined by the width of the detector used. For an infinitely thin line source, the Rayleigh pulse will have a time width corresponding to the propagation time across the detecting element. Thus to generate and detect the smallest time width Rayleigh pulse possible, the source and detector must be made as small as possible. This effect has also been investigated by Aharoni et al. (1967).

The variation of the Rayleigh wave amplitude as a function of angle around a line source and a circular source was also investigated. For a particular power density and propagation distance, the circular source showed no variation in Rayleigh wave amplitude with angle. A

line source however, had two distinct maxima propagating in a direction perpendicular to the line source. Using acoustical engineering theory (Olson (1947)), the experimental directivity pattern could be fitted to a theoretical directivity.

When the laser pulse irradiates a thin (≤ 1 mm) sample, symmetric and antisymmetric Lamb waves are generated (Lamb (1917), Viktorov (1967)). Descriptions of laser - generated Lamb waves and their properties have been described by Dewhurst et al. (1987), McKie (1987) and Hutchins et al. (1988a).

2. 2. 2 : Mechanisms for the laser generation of ultrasound

Mechanisms for the production of ultrasound can be divided into two regions corresponding to power densities of $< 10^7$ W / cm^2 and $\geq 10^7$ W / cm^2. Laser generation of ultrasound in the absence of a plasma occurs through thermal mechanisms. A proportion of the photons from the incident laser pulse are absorbed to the electromagnetic skin depth and excite the conduction electrons in a metal to higher energy states. These higher energy state electrons are scattered in various ways by any deformation of the ideal periodic lattice of positive ion cores. Some of the energy goes into increasing the thermal energy of the irradiated region and thus into the generation of coherent acoustic longitudinal and transverse phonons with frequencies above 20 kHz i. e. ultrasound. The acoustic source model consists of a thin heated disc of metal extending into the solid to a depth determined by heat diffusion. The diameter of the source is determined by the laser beam diameter and the depth does not exceed that to which significant heating takes place in the duration of the laser pulse. Elastic waves are generated within this zone by

strains arising from thermoelastic expansion which, from the nature of the source, act radially from the centre outwards in the plane of the surface. Using the differential heat equation in a semi - infinite medium, the temperature distribution and consequently the lateral strain developed across the surface can be calculated. This strain is proportional to the amount of laser energy absorbed from the incident beam and is thus inversely proportional to the wavelength as the absorption decreases with increasing wavelength. Studies of the variation of the amplitude of the compression and shear waves as a function of laser wavelength verified this prediction.

At higher power densities, the thermoelastic generation is supplemented by the ablation of electrons and ions forming a plasma, with consequent expansion of the plasma away from the surface of the metal. This causes a momentum pulse to be transmitted to the solid, as described by previous studies, which enhances the production of the compression wave pulse. The shear wave pulse is not enhanced, which implies a decoupling of laser energy to lateral thermal gradients within the solid due to the presence of the plasma. A small ablation pit, ~ μm deep, is formed by this process. Although the amplitude of the ultrasound generated is increased, this damage may make it impracticable to use for some applications.

Investigations of the effect of various coatings on the metal surface upon the amplitude of the various wave modes were also conducted. Coatings such as oil, resin and grease as well as a constraining layer were used. For all the coatings used, an enhancement in the amplitude of the various acoustic modes of > 20 dB was observed. The various modifications to the surface effectively result in a buried source at the coating / metal surface boundary. A stress free boundary at the metal surface no longer exists and this results in the

development of normal stresses. This occurs at all incident power densities. The nature of the source is different and more closely resembles the plasma regime source. Ablation of the coatings was observed at power densities sufficient to form a plasma.

2. 3. 3 : Modelling of the various sources

The **thermoelastic** source of ultrasound (typical power densities $< 10^7$ W / cm^2 for a metal in the near infrared / visible wavelength region) is considered to have a Heaviside step function time dependence radial stress distribution over the timescales of interest. Physically this can be thought of as the rapid expansion of a thin disc followed by a slower rate of contraction after the laser pulse. Using this force distribution it is possible to calculate the surface and epicentral displacements. The calculation of the surface displacement of a point radial loading of a half space with Heaviside time dependence has been described by, for example, Cooper (1985). The stress distribution was written in terms of three orthogonal components of displacement in cylindrical coordinates with the vertical term tending to zero. These equations are solved using Laplace and Hankel integral transforms and then inverse transformed, using a Cagniard - de - Hoop inversion method, to obtain the real solution of the displacement of the surface of a half - space as a function of time. The theoretically predicted surface displacement for a point radial force with Heaviside time - dependence is shown in Fig. 2. 1. The compression wave arrival is too small to be seen on this scale. The discontinuity at the Rayleigh wave arrival time disappears when a detector with a finite frequency response and sensing

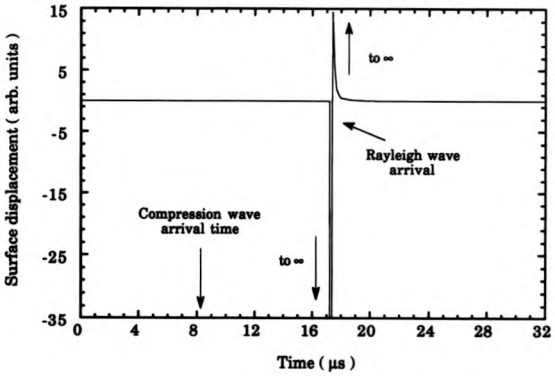

Figure 2. 1 : Theoretical surface displacement for a Thermoelastic source and point detector 50 mm away from the source (after Cooper (1985))

region is used. Cooper (1985) has shown experimental waveforms which agree with this theoretical prediction.

Cooper (1985) used the same method to obtain the epicentral displacements for a thermoelastic source and this is shown in Fig. 2. 2a. Rose (1984) considered the point source as a Surface Centre Of Expansion (SCOE) and obtained a formal solution using a Green's function formalism. Scruby et al. (1980) and Dewhurst et al. (1982) also used a Green's function formalism to obtain the epicentral displacement due to a thermoelastic source. The waveforms obtained by this method are the same as those obtained by Cooper (1985). An example of the experimental epicentral waveform obtained with a thermoelastic source is shown in Fig. 2. 2b. Note the relatively small positive spike before it goes negative at the compression wave arrival time.

The theoretical modelling of the thermoelastic source described above took no account of the thermal diffusion into the solid. Doyle (1986) and McDonald (1990) considered the effect of thermal diffusion on the predicted epicentral displacement using a Green's function formalism to determine whether it was a significant contribution. The theoretical epicentral waveform obtained by this method had an initial positive spike at the compression wave arrival time. The ratio of spike height to the compression wave step was ~ 0.7 which agrees with the ratio obtained experimentally by Scruby et al. (1981). Thus thermal diffusion was considered to be a major cause of the initial positive spike of the epicentral waveform.

Physically the appearance of the initial positive displacement at the epicentre can be understood by considering the contribution arising at a particular time from a small depth below the irradiated surface. The source can be considered to propagate, in a diffuse manner, into the bulk. This causes a small time delay between the direct compression

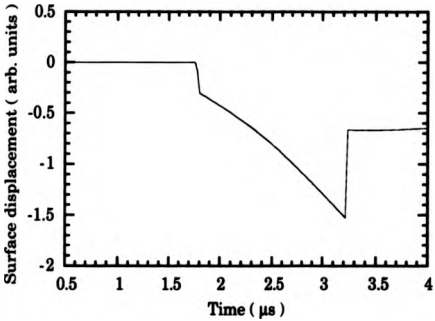

Figure 2.2a : Theoretical Thermoelastic Epicentral displacement in Stainless Steel.

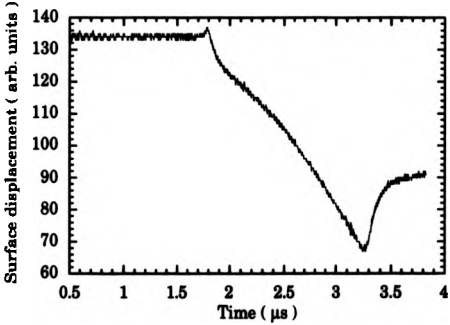

Figure 2. 2b : Thermoelastic epicentral displacement recorded on 10 mm thick Stainless Steel sample.

pulse and the pulse that is reflected at the surface boundary, so that there is incomplete cancellation and pulses appear at the compression arrival. As the risetime of the incident laser pulse decreases the amplitude of this positive spike increases.

The source of ultrasound in the **Plasma** regime (typical power densities $\geq 10^7$ W / cm^2 for a metal in the near infrared / visible wavelength region) has a stress distribution which may be simply modelled as the transient response of an elastic half - space due to the application of a normal, point force at the surface with arbitrary time dependence. Its time dependence consists of the recoil force of evaporating surface material and a longer timescale decreasing force due to the pressure exerted over an increasing circular area by the expanding gas. The plasma regime driving force is investigated in more detail in Chapter Three.

The response of the surface to a normal driving force with Heaviside time dependence has been derived by Pekeris (1955) and is shown in Fig. 2. 3a for a source to detector displacement of 50 mm on an aluminium surface. If the source size, detector size, bandwidth and decreasing driving force are taken into account then the constant negative displacement after the Rayleigh wave arrival is replaced by a displacement tending towards zero over a longer timescale than the initial rise. This is shown in Fig. 2. 3b for a plasma regime laser - generated Rayleigh wave propagating in aluminium and detected using a modified Michelson interferometer situated 50 mm away from the source. Note that the first part of the Rayleigh pulse is now positive as opposed to negative for the thermoelastically produced Rayleigh wave.

The epicentral displacement for a normal driving force with Heaviside time dependence has been obtained by Knopoff (1958) and Sinclair (1979). The epicentral displacement for a normal driving force

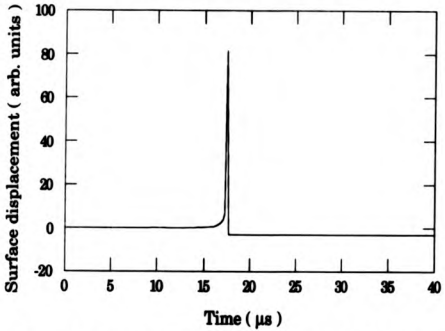

Figure 2. 3a : Theoretical Surface displacement in aluminium for Plasma regime source (after Pekeris (1955))

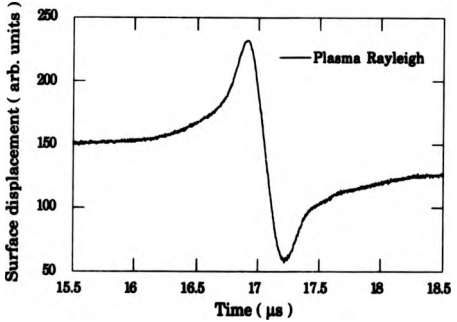

Figure 2. 3b : Experimental Rayleigh wave generated in Plasma regime on aluminium surface.

with δ - time dependence is obtained by differentiating Knopoffs' solution and this is shown in Fig. 2. 4a. Figs. 2. 4b and 2. 4c show experimental epicentral waveforms for a weak and strong plasma generated above the surface of a 10 mm thick Stainless Steel sample. This source produces outward displacements whereas the thermoelastic source causes inward displacements. Note that for a relatively weak plasma the thermoelastic contribution is still significant. Experimental epicentral waveforms for a normal driving force with Heaviside time dependence have been obtained using a CO_2 laser (Taylor et al. (1990)). The mechanism for the production of ultrasound in metals at the CO_2 wavelength (10.6 μm) is different from those described here and further details may be found elsewhere (Taylor (1990)).

By varying the incident power density and using various coatings on the surface it is possible to tailor the force function ranging from a Heaviside to a δ - function time dependence. The profile of the force function for a particular arrangement is investigated in Chapter Three where the plasma regime source of ultrasound is discussed in more detail.

2. 3. 4 : Directivities

The directivity of the compression and shear waves generated in the thermoelastic regime and plasma regime has been described by Cooper (1985) using a method similar to that described by Lord (1966) and Rose (1984). These are shown in Figs. 2. 5 and 2. 6 for the thermoelastic and plasma regime sources respectively. Experimental verification of these directivities were obtained by, for example, the University of Hull group and the agreement between theory and

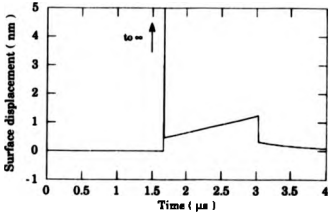

Figure 2. 4a : Theoretical Epicentral displacement for a ∂ - function normal force in Stainless Steel

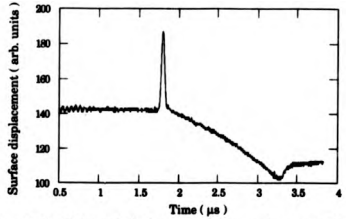

Figure 2. 4b : Epicentral displacement of ultrasound generated in weak Plasma regime in 10 mm thick Stainless Steel sample

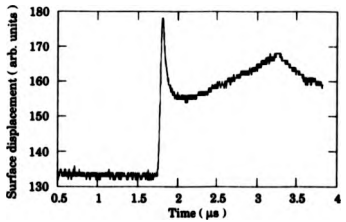

Figure 2. 4c : Epicentral displacement of ultrasound generated in Plasma regime in 10 mm thick Stainless Steel sample

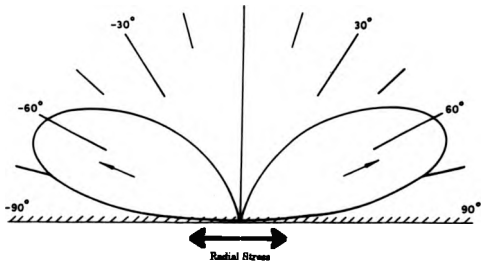

Figure 2. 5a : Theoretical directivity of compression wave for thermoelastic regime source in aluminium (after Cooper (1985))

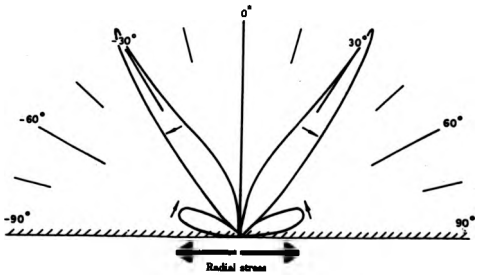

Figure 2. 5b : Theoretical directivity of shear wave for thermoelastic regime source in aluminium (after Cooper (1985))

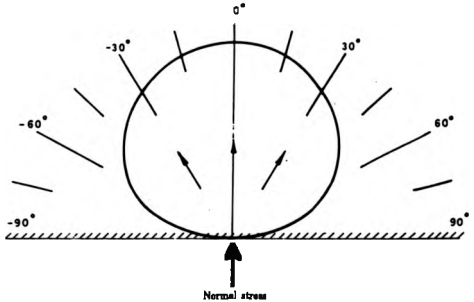

Figure 2. 6a : Theoretical directivity of compression wave for plasma regime source in aluminium (after Cooper (1985))

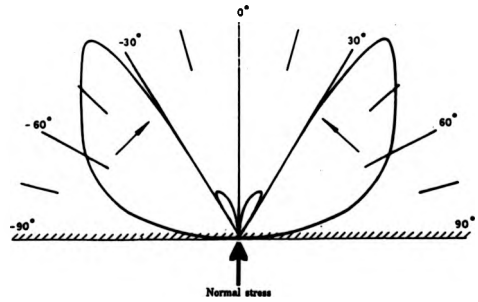

Figure 2. 6b : Theoretical directivity of shear wave for plasma regime source in aluminium (after Cooper (1985))

experiment was good. The partition of the total ultrasonic energy in the thermoelastic and plasma regimes into the various acoustic modes as a function of Poisson' s ratio has been determined by Rose (1984) and Cooper (1985).

2. 3. 5 : Non - contacting Ultrasonic Transducers

In association with the investigations into the properties of laser - generated ultrasound came the development of non - contacting ultrasonic transducers. Examples of such transducers include the capacitance transducer (Scruby and Wadley (1978), Aindow et al. (1987), Kim et al. (1989)), the ElectroMagnetic Acoustic Transducer or EMAT (Hutchins and Wilkins (1985)) and a homodyne (single frequency) or heterodyne (multi - frequency) interferometer (Monchalin (1986)). The majority of the experimental investigations described in this thesis have used a modified Michelson interferometer to detect the acoustic transients (McKie (1987), Lesne et al. (1987), Sontag and Tam (1986)) whose output voltage can be directly related to surface displacement. Absolute displacement transducers are useful in the comparison of experimental waveforms with the theoretical predictions. Other interferometers such as the Knife - edge (Stegeman (1976), Monchalin (1985)) and Fabry - Perot Interferometers (Monchalin (1985), Monchalin et al. (1989a)) have also been developed. Use of laser generation and interferometric detection of ultrasound offers a unique non - contacting technique of probing a particular material. One advantage of a non- contacting technique of generation / detection over piezoelectric probes is that no stress is applied to the surface by the generating / detecting element. Interferometers may also

be constructed with a very wide bandwidth (~ 400 MHz) based on a modified Michelson design using avalanche photodiodes and wide bandwidth amplifiers (Edwards (1989)). The disadvantage at present in using interferometers is that, in most cases, flat, polished surfaces must be available to detect the ultrasound. Rough surface interferometers have been developed (Paul et al. (1987)) and techniques have been described for obtaining as much of the scattered light off the surface as possible (Monchalin (1985)).

Thomsen et al. (1986) have described a technique for the detection of acoustic transients generated by a picosecond laser from measurements of the reflectivity of the sample surface. The reflectivity of the surface changes when an acoustic pulse arrives and this is measured using the same picosecond laser to probe the surface. Changes in the reflectivity of 10^{-6} - 10^{-3} were measured in various semiconductor materials.

2. 4 : OTHER LASER - GENERATED ULTRASOUND INVESTIGATIONS - 1980 ONWARDS

Since the detailed investigations of the mechanisms for the laser - generation of ultrasound by the University of Hull group, a few papers have been published on the theory of generation. Rudd (1983) calculated the sound power and efficiency of generation for three mechanisms of ultrasonic generation : Radiation pressure, Thermoelastic generation and the Plasma regime source. Sullivan et al. (1988) considered the thermoelastic generation of ultrasound using a numerical finite element technique. Aussel et al. (1988) considered both the

thermoelastic and plasma mechanisms for ultrasonic generation. They showed experimental data to support their theory which is similar to that obtained by the University of Hull group. Bresse and Hutchins (1988) considered the acoustic radiation fields from wide or finite size sources which is a more realistic approach to the experimentally obtainable source. Other theoretical descriptions are given by Krylov et al. (1986), Aleshkevich et al. (1987), Askar'yan and Yurkin (1987) and Kolomenskii (1988).

Some of the experimental investigations of laser - generated ultrasound have used lasers with different wavelengths and pulse profiles on different materials to demonstrate the mechaniam. These investigations are summarised in Table 2. 1.

Author / Year	Laser / Wavelength	Pulse width / Energy	Power Density / Fluence	Material studied	Aim of investigation
Ghosh and Hurst (1988)	Excimer 248 nm and 193 nm	?	Fluence : 10 mJ/cm^2 - 10 J/cm^2	Polymethylmeth acrylate (PMMA)	Demonstrate ultrasonic generation on PMMA and effect of etching.
Neubrand and Hess (1989)	Excimer 248 nm	25ns / 10mJ	10^6 W/cm^2 Thermo	Aluminium	Demonstration of Rayleigh waves
Tam and Coufal (1983)	Nitrogen 337.1 nm	1.2ns and 10ns/ < 1mJ	Fluence : 120 J/cm^2 and 0.25 J/cm^2	Various metals	Generation and detection of short acoustic pulses.
Bourkoff and Palmer (1985)	Dye 580 nm	6ns / (20 - 210) uJ	< 90 MW/cm^2	Various solids	Noncontact characterisation of samples of small size.
Sessler et al. (1985)	?	70 ps / (1 - 10) mJ	(0.14 - 1.4) GW/cm^2	Quartz and Polymers	Generation of subnanosecond acoustic pulses.
Eesley et al. (1987)	Dye 595 nm	5ps / <2mW	~10^3 W/cm^2	Metal films	Generation of picosecond acoustic pulses in metal films.

Thomsen et al. (1984)	Dye laser 620 nm	1ps / 1nJ	50 MW/cm^2	Various polymers	Generation of coherent acoustic phonons.
Grahn et al. (1989)	Dye laser 620 nm	0.2ps / 0.2nJ	300 MW/cm^2	Various solids	Generation and detection of picosecond ultrasonic waves.
Bazylev et al. (1989)	Ruby / 694nm	4ns / <6mJ	?	Quartz and aluminium	Generation of ultrasound using Ruby laser.
Fassbender et al. (1989)	Ruby / 694nm	30ns / 600mJ	Various :Thermo. to Ablative	Aluminium	Finding optimum intensity for which a compression wave is produced.
Zhang et al. (1989)	Ruby / 694nm	30ns / 600mJ	Various : Thermo. to Ablative	Aluminium	Study of laser - generated shear waves.
Tittman et al. (1987)	Nd:YAG / 1.06μm	10ns / 700mJ	10^8 W/cm^2	Water	Investigation of the laser source.
Sarrafzadeh et al. (1986)	Nd:YAG / 1.06μm	60ns / 9mJ	?	Railroad Steel	Demonstration of laser ultrasound.
Kanemitsu et al. (1988)	Nd:YAG / 1.06μm	30ps / 50mJ	10^{13} W/cm^2	Glass	Generation of picosecond ultrasound in glass.

Kanemitsu et al. (1989)	Nd:YAG / 1.06μm	30ps / 50mJ	Various : Thermo. to Ablative	Various solids	Study of picosecond ultrasound in solids.
Harada et al. (1989)	Nd:YAG / 1.06μm	30ps / 50mJ	10^{11} W/cm^2	Silicon	Generation of picosecond ultrasound in silicon.
Dewhurst and Al'Rubai (1989)	Nd:YAG / 1.06μm	30ps / 8mJ	10^{12} W/cm^2	Thin sheet aluminium	Generation of picosecond ultrasound in various metals
Canella et al. (1989)	Nd:YAG / 1.06μm	2.5ns / 275mJ	10^9 W/cm^2	Steel and aluminium	Laser ultrasound in metals
Monchalin et al. (1989b)	Nd:YAG / 1.06μm	?	?	Aluminium	Rayleigh and Lamb waves.
Wang and Meng (1989)	CO_2 / 10.6μm	80ns / 1J	Various : Thermo. to Ablative	Aluminium	Use of CO_2 laser to generate ultrasound.
Taylor et al. (1990)	CO_2 / 10.6μm	100ns / 1J	Various : Thermo. to Ablative	Various solids	Different mechanism for laser generation of ultrasound using CO_2 laser.

Table 2.1: Summary of laser - generated ultrasound investigations

Other research has concentrated on using the laser pulse with appropriate optics to achieve a mode of operation to suit a particular application. An example has been described by Wagner et al. (1988) who repetitively Q - switched a pulse from a Nd:YAG laser with the result that a series of pulses could irradiate a solid and hence produce a series of ultrasonic pulses. These ultrasonic pulses were equally spaced in time and this resulted in a narrowband ultrasonic pulse of frequency determined by the time spacing between each individual laser pulse. It is thus possible to generate a narrow band ultrasonic pulse with a modulation frequency the same as the optimum frequency sensitivity of an interferometer.

McKie et al. (1989) used a lenticular lens array to generate up to seven simultaneous line sources from a single Q - switched laser pulse. This had a similar effect to that described by Wagner et al. (1988) above in that a series of ultrasonic pulses were generated and recorded at an angle of 60° and 80° from the plane of the sample surface. The theoretical analysis uses equations derived by Rose (1984) for the thermoelastic source. This is a rather dubious theory to use in this case as the plasma regime was used for the generation of ultrasound.

Another variation on the use of multiple sources is to develop a laser array such that the laser source moves over the surface of a sample. A moving thermoacoustic array has been considered theoretically by, for example, Westervelt and Larson (1973), Chotiros (1988) and Berthelot (1989). By varying the speed at which the thermoacoustic source moves over the surface it is possible to generate a plane wave in a particular direction. Also as the incident laser energy is spread over a larger area it is possible to remain within the thermoelastic regime using larger laser pulse energies.

The use of laser arrays on solid surfaces for non - destructive testing has been considered by Addison et al. (1987). Bruinsma and Vogel (1988) directed an incident laser pulse into several optical fibres of differing length. They demonstrated that the directivity of the laser array source could be changed by varying the distance between successive fibre ends on the surface of the sample.

Ishikawa et al. (1990) set up an interference pattern on a sample surface by splitting an incident laser beam into two and directing the two beams onto the same region of the sample surface. This resulted in the production of ultrasound (coherent acoustic phonons) with frequencies ranging from ~ 80 MHz up to ~ 1 GHz. By changing the crossing angle of the laser beams it is possible to change the fringe spacing and hence the frequency of ultrasound produced. This effect has also been described by Cachier (1971) and Nelson et al. (1982).

VonGutfeld et al. (1983a, 1983b) described a technique for increasing the efficiency of the thermoelastic generation of ultrasound by effectively increasing the area over which the laser energy is distributed. This was accomplished using an acoustic holographic lens structure which is basically a grated mask with absorbing and non - absorbing strips evaporated onto the sample surface.

Cielo et al. (1985) described another method for increasing the area over which the laser energy is distributed. Using a positive axicon lens, an annular source was produced, on a sample surface, 0.2 mm wide with a diameter of 15 mm. This annular source produces a convergent Rayleigh wave which has its maximum amplitude at the centre of the annulus. The amplitude of the Rayleigh wave at the centre of the annulus was a factor of twenty larger than the Rayleigh wave produced from a line source with the same incident laser energy. The

application of this type of source to the non - destructive testing of materials will be described later.

2.5 : OTHER THEORIES ON THE GENERATION OF ACOUSTIC PULSES IN SOLIDS USING LASER BEAMS

This section will briefly summarise theories for the production of acoustic pulses using laser beams by mechanisms other than those described previously. Most of the theories developed have been for the production of acoustic pulses in semiconductors. Gusev and Petrosyan (1987) developed a theory for the excitation of one - dimensional longitudinal acoustic phonons in a semiconductor whose energy gap is smaller than the quantum energy of the incident light pulse. In another paper, Gusev et al. (1988) considered the excitation of plane acoustic pulses in the nonlinear absorption of light near the surface of a crystal. These theories, along with other experimental and theoretical investigations in the area of laser optoacoustics of condensed matter by the Moscow State University, have been summarised in a paper by Akhmanov et al. (1989).

Adkhamov (1988) considered theoretically the optical generation of sound by two - frequency laser pumping in a piezoelectric semiconductor. It was proposed that hypersound (~ 10 GHz) could be generated and used to measure the attenuation characteristics of a semiconductor at these frequencies. Deev and Pyatakov (1988) described the generation of acoustic waves by the action of a pulsed laser beam on a space - charge grating formed in a bismuth germanate crystal. It was stated that a special kind of photoacoustic effect with memory occurs in

such a photorefractive crystal which could have applications to acoustooptical signal processors.

Zakharova and Ryzhii (1989) described the generation of acoustic lattice vibrations in a surface layer of a semiconductor when the density of an electron - hole plasma is largely governed by Auger processes. Whilst Dharamsi and Hassam (1989) described a method for generating pico - and subpicosecond optoacoustic pulses by a mechanism based upon the phenomenon of ' electronic expansion ' (or photostriction). The creation of electron - hole pairs changes the lattice constant of a solid which consequently generates acoustic signals which could be a magnitude shorter than those generated by other mechanisms.

2.6 : APPLICATIONS OF LASER - GENERATED ULTRASOUND

The areas of application of laser - generated ultrasound have been investigated to varying degrees since 1963. Before these areas are outlined, the properties of laser - generated ultrasound are summarised:

- Remote, non - contacting source of ultrasound which means that it can be used to generate ultrasound on hot or rough samples and in hostile environments.
- It is a reproducible, from shot to shot, source of ultrasound.
- It is a broadband source of ultrasound which makes precise time resolution possible. Its broadband nature is investigated further in Chapter Three and used in Chapter Four.

- Ultrasound is generated by three mechanisms : Thermoelastically, ablatively or beneath a constrained layer. Each of these mechanisms results in slightly different source characteristics. Thus a particular mechanism for ultrasonic generation may be chosen to suit a particular application. The ablative production of ultrasound results in some surface damage. This may make it inappropriate to use for some applications.
- The laser pulse can be focussed to a virtual point source. Thus it may be used to generate ultrasound on very small samples or on areas inaccessible to piezoelectric probes.
- It produces simultaneously compression, shear and Rayleigh (surface) waves. On thin samples ($\leq$ 1 mm thick) it produces symmetric and antisymmetric Lamb waves.
- It has a set directivity for the various acoustic modes. This may be modified to suit a particular application using optics.
- Using appropriate optics it can be used to produce a train of pulses at a particular frequency.
- Owing to its non - contact nature it does not stress the surface of the sample in which ultrasound is generated. It also avoids the problem of material degradation if a couplant is used.
- It has the ability to monitor changes as a function of pressure and temperature.
- Used in association with interferometric detection (termed ' laser ultrasonics ' by Monchalin et al. (1988a, 1988b)) a completely remote generation and detection system is available.
- By virtue of its remoteness it allows faster scanning of a surface to be achieved.

- Using a high repetition rate laser it is possible to generate ultrasound in a series of components on, for example, a production line.

2. 6. 1 : Non - Destructive Testing (NDT)

The immediate and most obvious application of laser - generated ultrasound was in the ultrasonic non - destructive testing of materials. Essentially the techniques used are the same (see, for example, Krautkramer and Krautkramer (1977), McGonnagle (1962), Silk et al. (1987)) except that the piezoelectric probes are replaced by the laser source and a remote detector. In a majority of practical applications in industry, piezoelectric probes are sufficient for the detection and characterisation of defects. Laser ultrasonics (laser generation and interferometric detection) can, by virtue of its properties, improve the already established techniques. It also allows further applications to be found which are not possible with piezoelectric probes. One disadvantage of laser ultrasonics for non - destructive testing is the surface damage caused when ultrasound is generated in the plasma regime. This may be acceptable on some components.

The earliest descriptions of the use of laser - generated ultrasound in locating flaws within a sample were given by Bondarenko et al. (1976) and VonGutfeld and Melcher (1977). Bondarenko et al. (1976), using laser - generated ultrasound and interferometric detection, noted that the technique could be used for thickness gauging, high resolution flaw detection and for the determination of velocity and elastic moduli of materials. VonGutfeld and Melcher (1977) demonstrated the flaw detection capabilities of laser - generated ultrasound by scanning the

source over an aluminium cylinder containing several drilled holes. With the source and detector directly in line with a defect a change in the signal shape was observed. The effect of various constraining layers on the amplitude of the ultrasonic signal was also investigated. Other early papers which give examples of the use of laser - generated ultrasound in the location of flaws within a sample include Bar - Cohen (1979), Calder and Wilcox (1980) and VonGutfeld (1980).

In addition to non - destructive testing, Calder and Wilcox (1980) demonstrated that laser ultrasonics could be used to measure the acoustic velocity in a liquid metal column at the point of melting. Such measurements are useful in obtaining a more complete evaluation of the thermodynamic state of the liquid metal. VonGutfeld (1980) proposed a scheme for medical diagnostics by using laser absorption at a rubber - water interface in order to perform acoustic tomography. To date this has not received any further investigation.

The University of Hull group also investigated the use of laser - generated ultrasound in the non - destructive testing of materials e. g. Aindow et al.(1983), (1984), Cooper et al. (1985). In addition to locating defects using body waves extensive investigations into the interaction of laser - generated Rayleigh waves with surface - breaking defects were conducted (e. g. Cooper et al. (1986)). These investigations are summarised in Chapter Five. Aindow et al. (1984) using laser generation and interferometric detection on the same surface scanned over a series of flat - bottomed holes with different depth / diameter ratios. An oscillation of the recorded signal was observed with a frequency characteristic of a particular depth of the flat - bottomed hole beneath the surface. Rayleigh waves were also used to determine the location of a particular defect.

Other papers reporting on the use of laser - generation and interferometric detection for non - destructive testing include Sarrafzadeh et al. (1986) who directed the generating laser beam to the sample surface using a fibre optic cable. The acoustic transients were detected by a fibre - optic interferometer. Such a system provides the basis for a safe, portable laser ultrasonic system. Generation of ultrasound using an optical fibre directed laser pulse has been described by, for example, Burger et al. (1987), Prause and Hering (1987) and Peters et al. (1989).

Monchalin et al. (1988a, 1988b) have concentrated on developing a laser ultrasonic system for industrial applications. One drawback in the implementation of laser ultrasonics in an industrial environment for non - destructive testing is the relatively poor surface finish of some of the components to be tested. A confocal Fabry - Perot Interferometer has been developed which has been shown to operate on rough surfaces. However on totally absorbing surfaces, the interferometer can not be used. To overcome this problem the incident Nd:YAG laser pulse, in addition to generating ultrasound, was used to clean (by ablating some of the absorbing coating) the irradiated area thus allowing the Fabry - Perot Interferometer to be used. This cleaning - for - receiving arrangement was used in the thickness gauging of seamless pipes and in locating internal flaws.

Hutchins and Hauser (1987), Hutchins et al. (1987, 1989a) and Hu et al. (1989) have reported on the use of laser - generated ultrasound and EMAT detection. Initial investigations, Hutchins and Hauser (1987), demonstrated the use of a laser - EMAT system in defect detection and location. Later papers used ultrasonic tomographic reconstruction to produce images of the internal structure of objects containing defects. The technique was demonstrated using a cylindrical

aluminium sample containing a central cylindrical hole. Experiments were conducted with the hole containing air and various solid inserts.

Other ultrasonic signal processing techniques such as the Synthetic Aperture Focussing Technique or SAFT (Seydel (1982), Doctor et al. (1986) and Hutchins et al. (1990)) and the Split Spectrum Processing (SSP) technique (Rose et al. (1988), Shanker et al. (1989) and Aussel (1990)) will in future be applied to waveforms recorded using laser generation and interferometric detection. Investigations into the use of laser - generated ultrasound and interferometric detection to characterise defects are described in Chapter Four and Five.

Kuei Jen et al. (1985) and Cielo et al. (1987), using the annular source described previously, characterised piezoelectric ceramics used in piezoelectric transducers. They illustrated that it was possible to determine from the Rayleigh waveform whether or not the piezoelectric sample had a surface electrode on it. Cielo et al. (1987) compared the various techniques available for the characterisation of samples such as piezoelectric ceramics.

Lorenz et al. (1989, 1990), Scruby (1989) and Scruby et al. (1990) reported on the non - contact inspection of surface coatings. Lorenz et al. (1989, 1990) used the dispersive properties of the broadband laser - generated Rayleigh waves to determine the layer thickness from phase velocity data. Scruby (1989) and Scruby et al. (1990) recorded oscillations in the ultrasonic waveform which occurred directly after the Rayleigh wave arrival to determine the coating thickness. Scruby et al. (1990) also investigated the effect of a hardened region at the surface of an iron sample on the shape of the Rayleigh wave as well as the degree of anisotropy in a variety of composites.

Symmetric and antisymmetric Lamb waves generated by a laser in samples $\leq$ 1 mm thick may be used to locate flaws in pipelines.

Harker (1988) and Lesne et al. (1990) describe the methods used to detect defects using this wave mode. The use of Lamb waves to measure sample thickness will be discussed in a later section.

2. 6. 2 : Laser ultrasonic velocity and attenuation measurements : Determination of Elastic constants and Grain size

The elastic constants and moduli of a solid can be determined from measurements of the compression and shear wave velocities. In an isotropic solid the velocities are the same when measured in any propagation direction, whilst the velocities are direction dependent in an anisotropic solid. If a single crystal is used, various ultrasonic wave modes may be propagated in a direction parallel to each of the crystal axes and the calculated velocities used to determine the elastic constants of the crystal (Musgrave (1970)).

Using a laser source and interferometric detection it is possible to have an essentially point source and detector. This property, in association with the high resolution of the laser - generated ultrasound, make it possible to obtain accurate measurements of the travel time of the various acoustic modes. Accurate techniques for the measurement of velocity using piezoelectric probes at temperatures ranging from 0 K up to ~ 500 K are possible (Butler et al. (1979), Carnevale et al. (1964), Eccleston (1990)). Above these temperatures it becomes impractical to use piezoelectric probes and laser ultrasonics is a practicable alternative. It must be noted that laser ultrasonics could be used to measure the velocity within samples ranging in temperature from 0 K up to the samples vapourisation temperature.

Various examples on the use of laser - generated ultrasound to measure the velocity of anisotropic solids at ambient temperatures have been given by Castagnede et al. (1989). Ultrasonic slowness curves were constructed for fibreglass / polyester and silicon < 100 > samples using an iso - angular scanning geometry. Good agreement between the experimental and theoretical values were obtained.

Monchalin et al. (1987), Brun and Pons (1987), Dewhurst et al. (1988) and Aussel and Monchalin (1989) described measurements of the ultrasonic velocities in various samples using laser ultrasonics at ambient and elevated temperatures. Dewhurst et al. (1988) measured the velocity of compression waves as a function of temperature in aluminium, iron and steel samples up to the melting point temperature. A significant change in the velocity - temperature profile was observed in the iron sample at its Curie temperature. The use of ultrasonic velocity and attenuation measurements to locate the transition temperatures is an established technique (Truell et al. (1969)). Current techniques use piezoelectric probes cemented to a crystal. It is possible that laser ultrasonics will be used in the future especially on superconducting crystals as, using velocity and attenuation measurements, it is possible to determine the bandgap of the superconducting crystal (Truell et al. (1969)).

Aussel and Monchalin (1989) measured the acoustic velocities of a variety of solids using a crosscorrelation technique. The diffraction correction owing to the finite size of the laser source and detector was estimated and subtracted from the time delay measurements. This resulted in obtaining a greater accuracy for the elastic moduli values.

Measurement of the laser - generated ultrasonic attenuation in various solids ranging from porous solids to metals have been described by Telschow (1988), Hutchins et al. (1989b), Aussel and Monchalin

(1989), Scruby (1989) and Paul et al. (1989). Ultrasonic attenuation measurements are well suited for the microstructure characterisation of materials. The wide bandwidth nature of ultrasound generated by a laser can be used to investigate materials with large and small grain sizes. Paul et al. (1989) used the Rayleigh approximation to describe the scattering of the laser - generated ultrasound. The total attenuation spectrum obtained from various steel plates was related to the average grain size using this approximation. The grain size was calculated and compared to the metallographically determined grain size. Other investigations in this field include Greenough et al. (1987) who used laser - generated Rayleigh waves to assess the structural change in metallic amorphous ribbons.

2. 6. 3 : Determination of Thin Film Thickness

The short temporal width of the laser - generated ultrasonic compression wave pulse may be used to determine the thickness of films ≤ 1 mm thick. This is not possible using a piezoelectric probe as the temporal width of the ultrasound produced in this manner is typically ~ 1 μs. If the ultrasound is generated so as to reflect back and forth between the thin film surfaces, overlapping of successive echoes occurs which can not be resolved without data processing. Use of a laser to generate non - overlapping compression waves to determine the thin film thickness has been described by Hutchins et al. (1980) and Tam (1984).

Hutchins et al. (1980) used a Nd:YAG laser to generate compression waves in a liquid layer. Timing between successive echoes enabled the thickness of the liquid layers to be determined independent

of the liquid containment vessel. Tam (1984) demonstrated the use of ~ 1 ns wide compression wave pulses in the measurement of thin film thickness. The film thicknesses ranged from 14 μm to 262 μm and good agreement between calculated and measured thicknesses was obtained. This technique also has application in the measurement of bond thickness in adhesively bonded samples (Segal and Ross (1980)).

Another method for obtaining the thickness of thin films is to record the symmetric and antisymmetric Lamb waves generated by a laser source. Dewhurst et al. (1987) have demonstrated the use of Lamb waves in determining the thickness of metal sheets down to ~ 30 μm thick. Taylor (1990) using a CO_2 laser and modified knife - edge detector has demonstrated the CO_2 laser production of Lamb waves in acetate sheets.

2. 6. 4 : Use as a Standard Source

The highly repeatable nature of the laser source and its ability to change its source characteristics makes it an ideal tool to use as a standard source. Use of the laser source as a standard source has been described by Hutchins et al. (1981), Scruby et al. (1981) and Hutchins and Tam (1986). In Acoustic Emission studies, the laser source can be used to model a particular crack mode. Thus it is possible to generate a waveform using the laser source similar to that received in an Acoustic Emission study. The properties of the incident laser pulse and irradiated surface identify the type of source, which in turn can be used to determine the crack mode stress intensity. It is also used to calibrate acoustic emission transducers (Scruby et al. (1981), Scruby (1989)).

Another area in which the laser source as a standard source may be used is in the characterisation of other transducers. This involves comparing the ultrasonic signals produced from a different source with a laser source (Cooper et al. (1984), Brun and Pons (1987) and Dewhurst et al. (1987)).Using a wide bandwidth non - contact detector such as an interferometer, it is possible to record and compare the ultrasound produced by other transducers with that produced by a laser source. Comparison of the signals allows the determination of the effective stress distribution representative of the transducer used. Interferometers may also be used to characterise the ultrasonic field of piezoelectric transducers (Scruby (1989)).

2. 6. 5 : Acoustic Microscopy

Acoustic Microscopy as a technique for the characterisation of a surface is described by, for example, Lemons and Quate (1979). Discussions on the use of a laser pulse to replace the ZnO transducers and coupling medium (usually water) in generating high frequency ultrasound may be found in Hutchins and Tam (1986), Lyamshev (1987), Favro et al. (1988) and Hauden et al. (1989). Use of an interferometer to detect the ultrasound would greatly enhance the technique. To generate the high frequencies, a laser with a short (~ ps) pulse width is required.

2. 6. 6 : Miscellaneous Applications

In addition to the applications of laser - generated ultrasound described already, there are several other applications which can not be as conveniently classified. This section gives a summary of the other applications published.

Yang (1974) proposed that the generation of stress waves in thin metallic films by a Q - switched laser pulse could be used in the detonation of insensitive high explosives. This made use of the high pressures developed by irradiating a metallic surface through a constraining layer with a laser pulse. Fairand and Clauer (1979) suggested that the high pressures generated could be used to produce significant changes in the in - depth microstructure and mechanical properties of metal alloys. This aids in the understanding of the pressure required to alter the properties of materials. More recently, Bournot et al. (1987) have investigated the surface hardening of aluminium, titanium and steel after a high pressure shock wave was generated using a Nd:YAG laser. This process could be used to harden materials without affecting the surface quality of metals.

Hutchins and Tam (1986) described a method for the potential monitoring of annealing processes by observing the laser - generated acoustic signal. Of particular interest was the laser annealing of silicon during its manufacture. Another use they described was the determination of charge distribution in dielectrics. The laser pulse was used to provide reproducible short duration pressure transients within the dielectric. This pressure pulse produced a local electric field (which was determined from measurement of the current in an external circuit) which could be related to the charge density.

Harata and Sawada (1988) have used laser - generated ultrasound in the determination of candle flame parameters. A laser - induced grating (Harata et al. (1987)) was used to generate the ultrasound which was optically detected using Bragg diffraction of another laser probe. Measurement of the ultrasonic velocity enabled the flame temperature to be determined by assuming the flame to be an ideal gas. This research has application in the remote monitoring of real combustion diagnostics.

Johnson et al. (1987), Johnson (1988) and Carlson and Johnson (1988) considered theoretically, using finite element techniques, and experimentally the laser generation of ultrasound in a weld pool. The aim of these investigations is to develop a truly automated welding system using information obtained from ultrasonic measurements as a feedback device to the welding process. Using a laser to do the welding has the additional advantage that it will also generate ultrasound in the weld pool. This, in addition to non - contacting detection of the ultrasound, will provide a powerful control on the welding process.

Tankovsky and Palal (1989) generated resonant elastic modes in bonded materials and in optical fibres by the thermoelastic mechanism. The acoustic spectra excited were observed to be unique for a particular material. This could have applications in the control or evaluation of the elastic parameters of optical fibres.

One application for which no papers have at present been published is in the use of laser ultrasound for the determination of Residual Stress (Pao et al. (1984), Allen and Sayers (1984), Pritchard (1987)). Precise measurement of the velocity as a function of propagation direction within a particular sample could be achieved using a point source and detector. The change in velocity with angle in rolled steel has a magnitude ~ 10^{-4}. Time measurements must be made

to this accuracy or greater if an accurate determination of the residual stress within a material is to be determined.

2. 6. 7 : Future Applications

Laser ultrasonics is a technique which seeks application in an industrial environment. Owing to the large expense and safety requirements for a portable laser ultrasound system, it seems unlikely that it will replace those areas of application where the use of piezoelectric transducers is sufficient. Thus laser ultrasonics may be developed for applications in which it is not possible to use piezoelectric transducers such as in hostile environments or on awkwardly shaped components.

One area of application which may be developed in the near future is the active testing of products, such as hot rolled steel or plastics, along a production line. The ultrasonic information may be used as an active feedback element in the manufacturing process. It may also be used to test small components such as solder joints on printed circuit boards. The possibilities for the use of laser ultrasonics are limited only by the needs of industry and the imagination of the researchers in this field.

2.7 : REFERENCES

Addison, R. C. et al. (1987)	IEEE Ultra. Symp. Proc., 1109 (1987)
Adkhamov, A. A. (1988)	Sov. Phys. - Acoust., **34**, 125 (1988)
Aharoni, A. et al. (1987)	Ultra. Int. Conf. Proc., 623 (1987)
Aindow, A. M. et al. (1983)	Ultra. Int. Conf. Proc., 20 (1983)
Aindow, A. M. et al. (1984)	NDT Int., 17, 329 (1984)
Aindow, A. M. (1986)	PhD Thesis, University of Hull (1986)
Aindow, A. M. et al. (1987)	J. Phys. E : Sci. Instrum., **20**, 204 (1987)
Akhmanov, S. A. et al. (1989)	Infrared Phys., **29**, 815 (1989)
Aleshkevich, V. A. et al. (1987)	Sov. Phys. - Acoust., **33**, 457 (1987)
Allen, D. R. and Sayers, C. M. (1984)	Ultrasonics, **22**, 179 (1984)
Anderholm, N. C. (1970)	Appl. Phys. Lett., **16**, 113 (1970)
Askar' Yan, G. A. and Moroz, E. M.	Sov. Phys. - JETP, **16**, 1638 (1963)
Askar' Yan, G. A. and Yurkin, A. V.	Sov. Phys. - Acoust., **33**, 219 (1987)
Aussel, J. D. (1990)	Ultrasonics, **28**, 229 (1990)
Aussel, J. D. et al. (1988)	Ultrasonics, **26**, 245 (1988)
Aussel, J. D. and Monchalin, J. P.	Ultrasonics, **27**, 165 (1989)

Bar - Cohen, Y. (1979)	Brit. J. NDT, **21**, 76 (1979)
Bazylev, P. V. et al. (1989)	Sov. J. NDT, **25**, 253 (1989)
Bechtel, J. H. (1975)	J. Appl. Phys., **46**, 1585 (1975)
Berthelot, Y. H. (1989)	J. A. S. A., **85**, 1173 (1989)
Bondarenko, A. N. et al. (1976)	Defektoskopiya, **6**, 85 (1976)
Bourkoff, E. and Palmer, C. H. (1985)	Appl. Phys. Lett., **46**, 143 (1985)
Bournot, Ph. et al. (1987)	SPIE : High Power Lasers, **801**, 308 (1987)
Bresse, L. F. and Hutchins, D. A.	Rev. Prog. Quant. NDE, **7A**, 629 (1988)
Bruinsma, A. J. A. and Vogel, J. A.	Appl. Opt., **27**, 4690 (1988)
Brun, A. Le and Pons, F. (1987)	Proc. 4th Europ. Conf. NDT, **2**, 1593 (1987)
Budenkov, G. A.and Kaunov, A. D.	Ninth World Conf. on NDT Proc., **4A**, 14 (1977)
Burger, C. P. et al. (1987)	J. Nondest. Eval., **6**, 57 (1987)
Bushnell, J. C. and McCloskey, D. J.	J. Appl. Phys., **39**, 5541 (1968)
Butler, B. et al. (1979)	Ultrasonics, **17**, 249 (1979)
Cachier, G. (1971)	J. A. S. A., **49**, 974 (1971)
Calder, C. A. and Wilcox, W. W.	Mat. Eval., **38**, 86 (1980)
Canella, G. et al. (1989)	Non - Destruct. Test. (Proc. 12th World Conf.), 643 (1989)
Carlson, N. M. and Johnson, J. A.	Rev. Prog. Quant. NDE, **7**, 1485 (1988)
Carnevale, E. H. et al. (1964)	J. A. S. A., **36**, 1678 (1964)

Castagnede, B. et al. (1989)	Ultra. Int. Conf. Proc., 71 (1989)
Chotiros, N. P. (1988)	J. A. S. A., **83**, 2145 (1988)
Cielo, P. et al. (1985)	Ultrasonics, **23**, 55 (1985)
Cielo, P. et al. (1987)	Nondestruct. Charact. of Mat. II, Proc., 733 (1987)
Cooper, J. A. et al. (1984)	IEE Proc., **131**,Pt. A, 275 (1984)
Cooper, J. A. (1985)	PhD Thesis, University of Hull (1985)
Cooper, J. A. et al. (1985)	Ultra. Int. Conf. Proc., 207 (1985)
Cooper, J. A. et al. (1986)	Phil. Trans. R. Soc. Lond., **A320**, 319 (1986)
Deev, V. N. and Pyatakov, P. A.	Sov. Phys. - Acoust., **34**, 358 (1988)
Dewhurst, R. J. et al. (1982)	J. Appl. Phys., **53**, 4064 (1982)
Dewhurst, R. J. et al. (1987)	Appl. Phys. Lett., **51**, 1066 (1987)
Dewhurst, R. J. et al. (1988)	J. Appl. Phys., **63**, 1225 (1988)
Dewhurst, R. J. and Al' Rubai, W. S.	Ultrasonics, **27**, 262 (1989)
Dharamsi, A. N. and Hassam, A. B.	J. A. S. A., **85**, 1560 (1989)
Doctor, S. R. et al. (1986)	NDT Int., **19**, 163 (1986)
Doyle, P. A. (1986)	J. Phys. D : Appl. Phys., **19**, 1613 (1986)
Eccleston, R. S. (1990)	personal communication

Edwards, C. (1989)	personal communication
Eesley, G. L. et al. (1987)	Appl. Phys. Lett., **50**, 717 (1987)
Fairand, B. P. et al. (1974)	Appl. Phys. Lett., **25**, 431 (1974)
Fairand, B. P. and Clauer, A. H.	J. Appl. Phys., **50**, 1497 (1979)
Fassbender, S. et al. (1989)	Mat. Sci. Eng., **A122**, 37 (1989)
Favro, L. D. et al. (1988)	Rev. Prog. Quant. NDE, **7A**, 225 (1988)
Felix, M. P. (1974)	Rev. Sci. Instrum., **45**, 1106 (1974)
Felix, M. P. and Ellis, A. T. (1972)	Appl. Phys. Lett., **21**, 532 (1972)
Fox, J. A. (1974)	Appl. Phys. Lett., **24**, 461 (1974)
Ghosh, A. P. and Hurst, J. E. (1988)	J. Appl. Phys., **64**, 287 (1988)
Gorodetskii, V. S. et al. (1978)	Sov. J. Quantum Electron., **8**, 1345 (1978)
Gournay, L. S. (1966)	J. A. S. A., **40**, 1322 (1966)
Grahn, H. T. et al. (1989)	IEEE QE - **25**, 2562 (1989)
Greenough, R. D. et al. (1987)	J. Appl. Phys., **62**, 4728 (1987)
Gregg, D. W. and Thomas, S. J.	J. Appl. Phys., **37**, 2787 (1966)
Gusev, V. E. and Petrosyan, E. G.	Sov. Phys. - Acoust., **33**, 135 (1987)
Gusev, V. E. et al. (1988)	Sov. Phys. - Acoust., **34**, 269 (1988)

Harada, Y. et al. (1989)	J. Phys. D : Appl. Phys., **22**, 569 (1989)
Harata, A. et al. (1987)	Jpn. J. Appl. Phys. Suppl., **26**, 41 (1987)
Harata, A. and Sawada, T. (1988)	Jpn. J. Appl. Phys. Suppl., **27**, 223 (1988)
Harker, A. H. (1988)	' Elastic waves in solids ', (Adam Hilger) (1988)
Hartman, W. F. et al. (1972)	J. Appl. Mech., **39**, 119 (1972)
Hauden, D. et al. (1989)	Ultra. Int. Conf. Proc., 152 (1989)
Hu, J. K. et al. (1989)	Mat. Eval., **47**, 736 (1989)
Hutchins, D. A. et al. (1980)	Acoust. Lett., **4**, 95 (1980)
Hutchins, D. A. et al. (1981)	Appl. Phys. Lett., **38**, 677 (1981)
Hutchins, D. A. and Wilkins, D. E.	J. Appl. Phys., **58**, 2469 (1985)
Hutchins, D. A. and Tam, A. C.	IEEE - UFFC, **33**, 439 (1986)
Hutchins, D. A. and Hauser, F.	NDT Character. of Mat. II Proc., 725 (1987)
Hutchins, D. A. et al. (1987)	IEEE Ultra. Symp. Proc., 1037 (1987)
Hutchins, D. A. et al. (1988a)	J. A. S. A., **85**, 747 (1989)
Hutchins, D. A. et al., (1988b)	Ultra. Meth. in Eval. of Inhomog. Mat. (NATO Advanced Study Institute) Series E, No. 126, 353 (1989)
Hutchins, D. A. et al., (1988c)	J. A. S. A., **85**, 1441 (1989)
Hutchins, D. A. et al. (1990)	Nondestr. Test. Eval., **5**, 85 (1990)

Ishikawa, K. et al. (1990)	Opt. Comm., **76**, 81 (1990)
Johnson, J. A. et al. (1987)	J. Nondestruct. Eval., **6**, 147 (1987)
Johnson, J. A. (1988)	Rev. Prog. Quant. NDE, **7**, 1477 (1988)
Jones, E. D. (1971)	Appl. Phys. Lett., **18**, 33 (1971)
Kanemitsu, Y. et al. (1988)	J. Appl. Phys., **63**, 4751 (1988)
Kanemitsu, Y. et al. (1989)	Jpn. J. Appl. Phys. Suppl., **28**, 234 (1989)
Kim, K. Y. et al. (1989)	Rev. Sci. Instrum., **60**, 2785 (1989)
Knopoff, L. (1958)	J. Appl. Phys., **29**, 661 (1958)
Kolomenskii, Al. A. (1988)	Sov. Phys. - Acoust., **34**, 504 (1988)
Krautkramer, J. and H. (1977)	' Ultrasonic Testing of Materials ', 2nd Ed., (Springer) (1977)
Krehl, P. et al. (1975)	J. Appl. Phys., **46**, 4400 (1975)
Krylov, V. V. et al. (1986)	Sov. Phys. - Acoust., **41**, 46 (1986)
Kubota, K and Nakatani, Y (1973)	Jpn. J. Appl. Phys., **12**, 888 (1973)
Kusi Jen, C. et al. (1985)	J. Am. Ceram. Soc., **68**, C - 146 (1985)

Lamb, H. (1917)	Proc. Roy. Soc. (Lond.), **A93**, 114 (1917)
Ledbetter, H. M. and Moulder, J. C.	J. A. S. A., **65**, 840 (1979)
Lee, R. E. and White, R. M. (1968)	Appl. Phys. Lett., **12**, 12 (1968)
Lemons, R. A. and Quate, C. F. (1979)	Physical Acoustics, Vol. XIV (1979)
Lesne, J. L. et al. (1987)	SPIE Vol. **863**, 13 (1987)
Lesne, J. L. et al. (1990)	Nondestr. Test. Eval., **5**, 171 (1990)
Lord, A. E. (1966)	J. A. S. A., **39**, 650 (1966)
Lorenz, M. et al. (1989)	Non - Destruct. Test. (Proc. 12th World Conf.), 1449 (1989)
Lorenz, M. et al. (1990)	Nondestr. Test. Eval., **5**, 187 (1990)
Lyamshev, L. M. (1987)	Sov. Phys. - Usp., **30**, 252 (1987)
McGonnagle, W. J. (1962)	' Non - Destructive Testing ', 2nd Ed., (Gordon and Breach) (1962)
McDonald, F. A (1990)	Appl. Phys. Lett., **56**, 230 (1990)
McKie, A. D. W. (1987)	PhD Thesis, University of Hull (1987)
McKie, A. D. W. et al. (1989)	Ultrasonics, **27**, 323 (1989)
Metz, S. A. et al. (1975)	J. Appl. Phys., **46**, 1634 (1975)
Monchalin, J. P. (1985)	Appl. Phys. Lett., **47**, 14 (1985)
Monchalin, J. P. (1986)	IEEE UFFC - **33**, 485 (1986)

Monchalin, J. P. et al. (1987)	NDT Charact. of Mat. II Proc., 717 (1987)
Monchalin, J. P. et al. (1988a)	IEEE Ultra. Symp. Proc., 1041 (1988)
Monchalin, J. P. et al. (1988b)	Rev. Prog. Quant. NDE, **7**, 1607 (1988)
Monchalin, J. P. et al. (1989a)	Appl. Phys. Lett., **55**, 1612 (1989)
Monchalin, J. P. et al. (1989b)	J. Nondestr. Eval., **8**, 121 (1989)
Musgrave, M. J. P. (1970)	' Crystal Acoustics ', (Holden - Day) (1970)
Nelson, K. A. et al. (1982)	J. Appl. Phys., **53**, 1144 (1982)
Neubrand, A. and Hess, P. (1989)	Mat. Sci. and Eng., **A122**, 33 (1989)
Neumann, F. (1964)	Appl. Phys. Lett., **4**, 167 (1964)
Olson, H. F. (1947)	' Elements of acoustical engineering ', 2nd Ed., (Van Nostrand) (1947)
Pao, Y. H. et al. (1984)	Physical Acoustics Vol. XVII, (1984)
Paul, M. et al. (1987)	Appl. Phys. Lett., **50**, 1569 (1987)

Paul, M. et al. (1989)	Non. Destruct. Test. (Proc. 12th World Conference), 261 (1989)
Peercy, P. S. et al. (1970)	Appl. Phys. Lett., 16, 120 (1970)
Pekeris, C. L. (1955)	Proc. N. A. S., 41, 469 (1955)
Penner, S. S. and Sharma, O. P.	J. Appl. Phys., 37, 2304 (1966)
Percival, C. M. (1967)	J. Appl. Phys., 38, 5313 (1967)
Peters, B. R. et al. (1989)	Proc. 1989 SEM Spring Conf., 794 (1989)
Prause, L. and Hering, P. (1987)	Laser und Optoelektronik (1987)
Pritchard, S. E. (1987)	NDT Int., 20, 57 (1987)
Ready, J. F. (1965)	J. Appl. Phys., 36, 462 (1965)
Ready, J. F. (1971)	' Effects of High Power Laser Radiation', (Academic Press), (1971)
Robin, J. E. (1978)	J. Appl. Phys., 49, 5306 (1978)
Rose, J. L. et al. (1988)	Mat. Eval., 46, 114 (1988)
Rose, L. R. F. (1984)	J. A. S. A., 75, 723 (1984)
Rudd, M. J. (1983)	Rev. Prog. Quant. NDE, 2B, 1763 (1983)
Sarrafzadeh, A. et al. (1986)	'Acousto - Ultrasonics : Theory and Applications', (Ed. J. C. Duke) (1986)
Scruby, C. B. and Wadley, H. N. G.	J. Phys. D : Appl. Phys., 11, 1487 (1978)

Scruby, C. B. et al. (1980)	J. Appl. Phys., **51**, 6210 (1980)
Scruby, C. B. et al. (1981)	Res. Tech. in NDT (Academic Press), Vol. V, (1981)
Scruby, C. B. (1989)	Ultrasonics, **27**, 195 (1989)
Scruby, C. B. et al. (1990)	Nondestr. Test. Eval., **5**, 97 (1990)
Segal, E. and Rose, J. L. (1980)	Res. Tech. in NDT (Academic Press), Vol. IV, (1980)
Sessler, G. M. et al. (1965)	J. Appl. Phys., **56**, 119 (1965)
Seydel, J. A. (1982)	Res. Tech. in NDT (Academic Press), Vol. VI, (1982)
Shankar, P. M. et al. (1989)	IEEE UFFC, **36**, 101 (1989)
Silk, M. G. et al. (1987)	' The reliability of Non - destructive Inspection ', (Adam Hilger) (1987)
Sinclair, J. E. (1979)	J. Phys. D : Appl. Phys., **12**, 1309 (1979)
Sontag, H. and Tam, A. C. (1986)	IEEE UFFC - **33**, 500 (1986)
Stegeman, G. I. (1976)	IEEE SU - **23**, 33 (1976)
Sullivan, J. M. et al. (1988)	IEEE Ultra. Symp. Proc., 481 (1988)
Tam, A. C. (1984)	Appl. Phys. Lett., **45**, 510 (1984)
Tam, A. C. and Coufal, H. (1983)	Appl. Phys. Lett., **42**, 33 (1983)
Tankovsky, N. and Pelzl, J. (1989)	Ultra. Int. Conf. Proc., 301 (1989)
Taylor, G. S. (1990)	PhD Thesis, University of Warwick (1990)

Taylor, G. S. et al. (1990)	Ultrasonics, **28**, 343, (1990)
Telschow, K. (1988)	Rev. Prog. Quant. NDE, **7**, 1211 (1988)
Thomsen, C. et al. (1984)	Phys. Rev. Lett., **53**, 989 (1984)
Thomsen, C. et al. (1986)	Phys. Rev. B, **34**, 4129 (1986)
Tittmann, B. R. et al. (1987)	IEEE Ultra. Symp. Proc., 1121 (1987)
Truell, R. et al. (1969)	' Ultrasonic Methods in Solid State Physics ', (Academic Press) (1969)
Viktorov, I. A. (1967)	' Rayleigh and Lamb Waves ', (Plenum Press) (1967)
VonGutfeld, R. J. and Melcher, R. L.	Appl. Phys. Lett., **30**, 257 (1977)
VonGutfeld, R. J. (1980)	Ultrasonics, **18**, 175 (1980)
VonGutfeld, R. J. et al. (1983a)	Appl. Phys. Lett., **42**, 1018 (1983)
VonGutfeld, R. J. et al. (1983b)	Rev. Prog. Quant. NDE, **2B**, 1797 (1983)
Wagner, J. W. et al. (1988)	Appl. Opt., **27**, 4696 (1988)
Wang, M. R. and Meng, H. C. (1989)	J. Appl. Phys., **66**, 205 (1989)
Westervelt, P. J. and Larson, R. S.	J. A. S. A., **54**, 121 (1973)
White, R. M. (1963a)	J. Appl. Phys., **34**, 2123 (1963)
White, R. M. (1963b)	J. Appl. Phys., **34**, 3559 (1963)

Yang, L. C. (1974) J. Appl. Phys., **45**, 2601 (1974)

Zakharova, A. A. and Ryzhii, V. I. Sov. Phys. - Semicond., **23**, 1223 (1989)

Zhang, S. Y. et al. (1989) submitted to Res. in NDE (1989)

Chapter Three

PROPERTIES OF ULTRASOUND GENERATED IN THE PLASMA REGIME

3. 1 : INTRODUCTION

Previous investigations, Table 3. 1, have indicated that the properties of the plasma regime laser - generated ultrasound are dependent upon the properties of the incident laser pulse. Accurate measurement of the profile of the ultrasonic pulse generated by a point source can only be achieved if a point ultrasonic detector with a bandwidth greater than the bandwidth of the incident laser pulse profile is used. Using finite size and bandwidth detectors affects the recorded profile and corrections must be made to obtain the profile of the compression wave. The detectors used in the investigations summarised in Table 3. 1 had bandwidths less than or the same order of magnitude as the incident laser pulse bandwidth. This makes direct comparison between the results difficult.

The properties of the ultrasonic compression wave may also be affected by the properties of the solid in which the ultrasound is generated. The aim of this investigation is to determine, both theoretically and experimentally, whether the properties of the plasma regime laser - generated ultrasonic compression wave are dependent solely on the properties of the incident laser pulse, or on the properties of the material in which the ultrasound is generated or a combination of the two.

Author (s)	Laser used	Pulse Duration	Energy / Pulse	Material in which ultrasound is generated	Ultrasonic pulse risetime / width	Detector used
Jones (1971)	Nd : YAG (1060 nm)	(2 - 4) ps	(10 - 20) J	Aluminium	≤ 1 ns risetime	X - cut Quartz
Peercy et al. (1970)	Nd : YAG	(2 - 4) ps	(10 - 20) J	Various solids	≤ 1 ns risetime	X - cut Quartz
Dewhurst and Al' Rubai (1989)	Nd : YAG	30 ps	8 mJ	Aluminium	1.7 ns risetime	PVDF
Harada et al. (1989)	Nd : YAG	30 ps	100 mJ	Silicon	3 ns FWHM	ZnO
Tam (1984)	Nitrogen (337 nm)	0.5 ns	1.5 mJ	Stainless Steel	0.8 ns FWHM	ZnO
Tam and Coufal (1983)	Nitrogen	1.2 ns, 10 ns	0.6 mJ, 1 mJ	Various metals	~ 5 ns FWHM and ?	PVF Foil
Bourkoff and Palmer (1985)	Tunable Dye	6 ns	(20 -210) μJ	Various	?	Interferometer
Fassbender et al. (1989)	Ruby (694 nm)	30 ns	600 mJ	Aluminium and Steel	~ 10 ns risetime	Capacitance detector

Table 3. 1 : Summary of the results obtained from experiments conducted using fast risetime laser pulses.

The first part of the chapter outlines the theoretical modelling for the derivation of the pressure (stress) produced by the plasma regime source of ultrasound. Expressions for the pressure produced, in terms of the properties of the incident laser pulse and the mechanical and thermal properties of the irradiated solid, are derived in an attempt to determine the properties of the ultrasonic compression wave generated by this mechanism.

In association with the theoretical modelling, experimental measurements of the ultrasound generated using lasers with different pulse profiles and wavelengths in various solids were performed. Wide (~ 100's MHz) bandwidth modified Michelson interferometers were used as detectors which reduced, to some extent, the affect of the detecting transducer upon the profile of the ultrasound recorded.

3. 2 : THEORETICAL CONSIDERATIONS

Consider the processes involved in the production of a pressure upon a solid surface in the plasma regime (Power densities $I \geq 10^7$ W / cm^2) from the onset of the laser pulse. The various stages involved are described and the magnitude of each contribution to the final pressure is estimated. The pressure developed will propagate through the solid as ultrasound. The relationship between pressure (stress) and the resulting ultrasound has been described elsewhere (e. g. Aindow (1986)).

3 : Properties of ultrasound generated in the plasma regime

3. 2. 1 : Absorption of incident photons

A proportion of the laser pulse energy is absorbed by the solid to the electromagnetic skin depth. The absorptivity, T_{op}, and electromagnetic skin depth, δ_{em}, are given by (Bleaney and Bleaney (1978))

$$T_{op} = \frac{4}{\mu_o \sigma c \delta_{em}} = \frac{4}{c}\sqrt{\frac{\pi \mu_r \upsilon}{\sigma \mu_o}} \qquad (3.1)$$

$$\delta_{em} = \frac{1}{(\sqrt{\pi \sigma \upsilon \mu_r \mu_o})} \qquad (3.2)$$

where μ_o, $_r$ are the vacuum and relative permeabilities respectively,
c, υ are the velocity and frequency of the incident radiation,
and σ is the electrical conductivity of the irradiated medium.

The absorptivity and skin depth for a Nd:YAG laser pulse incident upon an aluminium surface using these equations is ~ 7 % and ~ 5 nm respectively. The absorptivity may be greater for optically polished machined materials. The number of aluminium atoms exposed to the laser pulse in a small disc given by this skin depth and a spot size of, for example, 2 mm diameter is 9.5×10^{14}.

The energy of the photons is absorbed by electrons in the conduction band which are thus raised to higher energy states. Energy is transferred from these electrons by collisions with other electrons and

with phonons, so that the solid tends to reach an equilibrium at a higher temperature. In order that a single instantaneous temperature may be defined at every point, the light must not cause a substantial change in the internal energy of the region where absorption occurs during the relaxation times involved, which are ~ (10^{-12} - 10^{-13}) s. Provided this condition is satisfied it is possible to discuss classically the effects of thermal conductivity on the temperature distribution in the solid.

3. 2. 2 : Heating up to the vapourisation point

The heating of a disc of material up to its vapourisation temperature by a laser pulse has been described by, for example, Dabby and Paek (1972). The authors derived expressions for the time needed for the front surface of a solid to reach the vapourisation temperature in terms of the laser pulse power density and material properties. The initial temperature distribution was also derived and a term introduced to approximate this complex expression. The derivation described in this section follows that given by Dabby and Paek (1972). Except where specifically stated, the equations used are those given by these authors. The calculations for the various temperature and velocity profiles have been performed by the present author using these equations.

The following assumptions were made in their derivation :

- the laser beam intensity, I, in W / cm^2, is sufficient to eventually cause vapourisation of the front surface of the material.
- the gas that is created due to the vapourisation of the material is transparent to the incident laser energy.
- heat losses due to reradiation are negligible.

- the thermal constants and optical absorption coefficient, b, in cm^{-1}, are independent of the laser beam intensity and the temperature of the solid.
- the effects of radial heat conduction and the liquid phase can be ignored. The liquid phase is not of great significance as normally the latent heat of fusion is very much less than the latent heat of vapourisation.

In order to derive the initial temperature distribution the heat equation when no vapourisation occurs is solved. In terms of normalised variables this may be written as (Dabby and Paek (1972))

$$\frac{\partial \theta}{\partial \tau} - \frac{\partial^2 \theta}{\partial \alpha^2} = \frac{B}{\lambda} \exp(-B\alpha) \qquad (3.3)$$

where $\theta = \frac{T}{T_v}$ - the dimensionless temperature (3.4)

where T is the temperature of the irradiated material (in °K) and T_v is the vapourisation temperature.

$\tau = \frac{K C_p}{\rho K L_v^2} t$ - the dimensionless time (3.5)

where C_p is the Specific Heat Capacity (in J / g °K),

ρ is the Density of the solid (in g / cm^3),

K is the Thermal Conductivity of the solid (in J / cm s °K),

L_v is the Latent Heat of Vapourisation of the solid (in J / g),

and t is the time from the onset of the laser pulse (in secs).

$s = \frac{IC_p}{KL_v}(z - Z)$ - the dimensionless distance (3. 6)

where z is the depth variable and Z is the depth to which material has been removed (Z' is the velocity of the front surface, in this instance Z' = 0).

$B = \frac{KbL_v}{IC_p}$ - the dimensionless Absorption parameter(3. 7)

and $\lambda = \frac{C_p T_v}{L_v}$ - the dimensionless Heating parameter (3. 8)

subject to $\theta = 0$ at $\tau = 0$

$\frac{\partial \theta}{\partial s} = 0$ at $s = 0$

$\theta = 0$ at $s = \infty$

Defining, for convenience, $\theta' = B\lambda\theta$ (3. 9)

$s' = Bs$ (3. 10)

$\tau' = B^2\tau$ (3. 11)

The solution of (3. 3) is

$$\theta' = 2\sqrt{\tau'}\,\mathrm{ierfc}\left(\frac{s'}{2\sqrt{\tau'}}\right) - \exp(-s') + \frac{1}{2}\exp(\tau')\left\{\exp(-s')\,\mathrm{erfc}\left(\sqrt{\tau'} - \frac{s'}{2\sqrt{\tau'}}\right) + \exp(s')\,\mathrm{erfc}\left(\sqrt{\tau'} + \frac{s'}{2\sqrt{\tau'}}\right)\right\} \quad (3.12)$$

where erfc is the complamentary error function,

and ierfc is the complementary error function integral.

The time, τ_v, when vapourisation begins is obtained by solving (3. 12) subject to $\theta = 1$ at $s = 0$ or $\theta' = B\lambda$ at $s' = 0$ giving

$$\lambda B = \left(\frac{2}{\sqrt{\pi}}\right)\sqrt{\tau_v'} + \exp(\tau_v')\,\mathrm{erfc}(\sqrt{\tau_v'}) - 1 \qquad (3.13)$$

In Fig. 3. 1 τ_v' as a function of $B\lambda$ is plotted. For large values of τ_v', i. e. $\mathrm{erfc}(\sqrt{\tau_v'})$ tending to zero, the graph has a constant gradient of $2/\sqrt{\pi}$.

Using this information and equation (3. 13), the author has determined the approximate time to reach vapourisation which was found to be

$$t_v \sim \frac{\pi}{4}\frac{K\rho C_p T_v^2}{I^2} \qquad (\text{secs}) \qquad (3.14)$$

$$\text{for } \frac{Kb^2 t_v}{\rho C_p} > 2.$$

Using (3. 4) - (3. 13) and Fig. 3. 1 it is possible to calculate the time when vapourisation begins for different solids. These times are shown in Table 3. 2 for various solids and it is observed that generally it takes ~ 10^{-11} seconds to reach the vapourisation temperature for a power density, I, of ~ 10^9 W / cm^2. The exceptions are copper and silicon which take ~ 10^{-10} s to reach their vapourisation temperatures. The author is not aware of any published technique whereby the time to reach vapourisation can be measured experimentally. In reality, the thermal conductivity, K, (assumed constant in this case) exhibits a much larger variation in its magnitude with varying temperature than the other thermal and mechanical properties of the illuminated solid (Kaye and Laby (1989)). As the temperature of the body increases the thermal

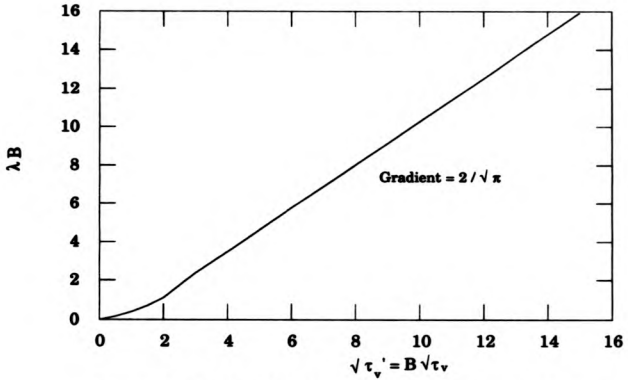

Figure 3. 1 : Graph showing the variation of λB as a function of dimensionless time τ_v'

Material	Thermal Conduct. : K (J / cm s °K)	Absorption coeff. : b (cm $^{-1}$)	Vap. Temp. : T_v (°K)	Lat. Heat of Vap. : L_v (x10^3 J / g)	Density : ρ (g / cm^3)	Specific Heat Cap. : C_p (J / g°K)	λB (= $\frac{KbT_v}{I}$)	Time required for vap. : t_v (x 10^{-11} s)
Aluminium	2.01 @ 293 K	1.1 x 10^6 @ 0.95 μm	2793	10.8	2.71	0.913 @ 293K	6.18	3.66
Brass (70 % Cu)	1.10	0.87 x 10^6 (Cu)	2863 (Cu)	4.7 (Cu)	8.50	0.37	2.74	4.34
Copper	3.85	0.87 x 10^6	2863	4.7	8.93	0.385	9.59	10.0
Soft Solder (50Pb / 50Sn)	0.65 (Tin)	~ 10^6	~ 2500	~ 1.7	9.00	0.176	~ 1.63	1.15
Stainless Steel	1.50	0.78 x 10^6	~ 3030 (Fe)	6.3 (Fe)	7.93	0.51	3.55	7.40
Mild Steel	0.63	0.78 x 10^6	~ 3030 (Fe)	6.3 (Fe)	7.86	0.42	1.49	3.45
Silicon	1.60	0.03 x 10^6	3473	12.8	2.3	0.7	0.17	33.8

Table 3.2 : Values used to calculate the times to reach vapourisation for various solids for an incident power density, I, of 10^9 W / cm^2 (data taken from Kaye and Laby (1969))

conductivity tends to decrease resulting in a faster time to reach vapourisation temperature.

Aussel et al. (1988) also gave an equation for the time to reach vapourisation which included terms referred to as the coefficient of light energy absorption of the material, A, the laser power density, W, and the initial temperature of the material, T_i. This was given as

$$t_r = \frac{\pi}{4}\frac{K\rho C_p}{(AW)^2}(T_v - T_i)^2 \qquad (3.15)$$

Note the similarity with equation (3. 14). If the quantity (A W) is taken to be equivalent to the power density, I, then the two equations are virtually equivalent.

The lasers used in the experimental investigation of the risetime of the laser - generated ultrasound, except for the picosecond laser, had pulse profiles with risetimes of ~ ns. For the calculations performed in this chapter, the incident laser pulse is assumed to have a rectangular profile of 10 ns duration and 1 ns rise and fall times so that the power density, I, may be assumed to remain constant over the duration of the laser pulse. The time to reach vapourisation is thus two order of magnitudes less than the laser pulse risetime and hence, for the laser pulse risetimes considered, the time to reach vapourisation may be considered to be independent of the laser pulse risetime. In effect it can be assumed that, as soon as the laser pulse reaches its maximum intensity, vapourisation has commenced. Lasers, with pulse risetimes the same order of magnitude as the time to reach vapourisation or less, would show a more significant variation in the time to reach vapourisation with risetime.

At the instant vapourisation begins, the exact temperature distribution in the solid is (Dabby and Paak (1972))

$$\theta'(\tau_v', s') = 2\sqrt{\tau_v'}\,\text{ierfc}\left(\frac{s'}{2\sqrt{\tau_v'}}\right) - \exp(-s') + \frac{1}{2}\exp(\tau_v')\left\{\exp(-s')\,\text{erfc}\left(\sqrt{\tau_v'} - \frac{s'}{2\sqrt{\tau_v'}}\right) + \exp(s')\,\text{erfc}\left(\sqrt{\tau_v'} + \frac{s'}{2\sqrt{\tau_v'}}\right)\right\} \quad (3.16)$$

This is a difficult expression to use and so it was approximated with

$$T = T_v(1 + qZ)\exp(-qZ) \qquad \text{at } t = 0 \qquad (3.17)$$

where q is a fitted parameter and the expression represents the temperature distribution at the instant that vapourisation occurs. Figs. 3.2 and 3.3 show the exact and approximated initial temperature distributions calculated by the author for aluminium and mild steel at the instant that vapourisation occurs. The relevant thermal and mechanical properties of these metals are given in Table 3.2. For aluminium, the best fit curve was obtained for $q = 3.5 \times 10^5\ cm^{-1}$ and for mild steel the best fit curve was obtained for $q = 5.5 \times 10^5\ cm^{-1}$.

3. 2. 3 : Vapourisation of material

Dabby and Paak (1972) continued their analysis to determine the temperature profile in the solid and the velocity with which material can be removed by vapourisation from a solid surface. The temperature and velocity were derived by perturbing the temperature profile around the

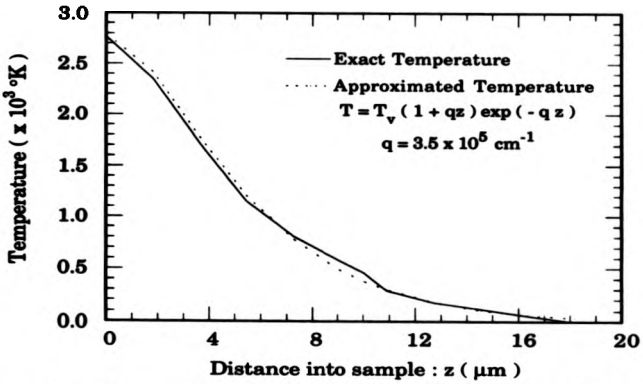

Figure 3. 2 : Exact and approximated initial temperature distribution for aluminium at the instant that vapourisation occurs.

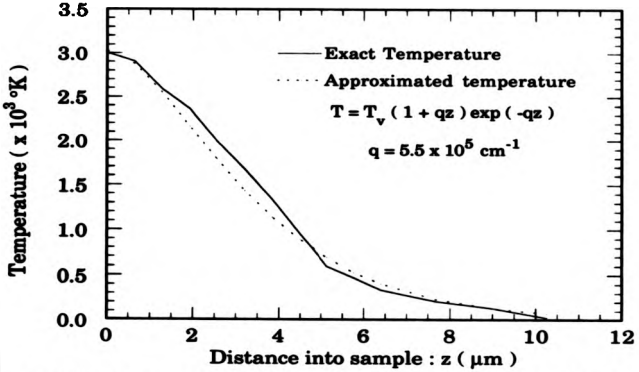

Figure 3. 3 : Exact and approximated initial temperature distributions for mild steel at the instant that vapourisation occurs.

initial (inner solution) and steady - state (outer solution) front - surface velocities.

The front - surface energy balance requires the energy given to the vapourised material to be equal to the energy conducted from the solid i. e.

$$\rho L_v Z' = K \frac{\partial T}{\partial z} \qquad \text{at } z = Z \qquad (3.18)$$

Energy given to vapourised material — Energy conducted from the solid

In order to determine the temperature profile within the material (region $z > Z$), the heat conduction equation with a distributed laser heat source moving with the front surface is used. Thus,

$$\rho C_p \frac{\partial T}{\partial t} = bI\exp(-b(z - Z)) + K \frac{\partial^2 T}{\partial z^2} \qquad (z > Z) \qquad (3.19)$$

Solving (3. 18) and (3. 19) with appropriate boundary conditions will yield the temperature and velocity. The appropriate boundary conditions are

$$T = T_v \qquad \text{at } z = Z$$

and

$$T = 0 \qquad \text{at } z = \infty$$

Two initial conditions are required for (3. 18) and (3. 19). The first assumes that at time t = 0 the drilling process begins, i. e. the time to reach the vapourisation temperature is not included. Thus

$$Z = 0 \quad \text{at } t = 0$$

The second assumes that the initial temperature distribution is given by (3. 17). Thus at $t = 0$, $T = T_v (1 + qz) \exp(-qz)$.

Transforming (3. 17) - (3. 19) into a moving dimensionless reference frame gives

$$\frac{\partial \theta}{\partial \tau} - u \frac{\partial \theta}{\partial s} - \frac{\partial^2 \theta}{\partial s^2} = \frac{B}{\lambda} \exp(-Bs) \qquad (3.20)$$

and

$$u = \lambda \left[\frac{\partial \theta}{\partial s} \right]_{s=0} = \frac{\rho L_v}{I} Z' \text{ - a normalised velocity term} \qquad (3.21)$$

subject to

$$\text{at } \tau = 0 \qquad \theta = (1 + Q s) \exp(-Q s) \qquad (3.22a)$$

$$\text{at } s = 0 \qquad \theta = 1 \qquad (3.22b)$$

$$\text{at } s = \infty \qquad \theta = 0 \qquad (3.22c)$$

where

$$Q = \frac{K q L_v}{I C_p} \text{ - a normalised initial parameter} \qquad (3.23)$$

Initially $\partial\theta / \partial s$ at $s = 0$ is zero. Thus the normalised inner velocity u_i is zero for small values of τ. Substituting this value of u_i into (3. 20) gives

$$\frac{\partial\theta_i}{\partial\tau} - \frac{\partial^2\theta_i}{\partial s^2} = \frac{B}{\lambda}\exp(-Bs) \qquad (3.24)$$

where θ_i is the temperature based upon the initial velocity (inner solution) and is subject to the conditions given in (3. 22).

Equation (3. 24) is solved by taking the Laplace transform with respect to τ, solving the resulting second order differential equation and taking the inverse transform. This is given as (in a different form to that given by Dabby and Paak (1972))

$$\begin{aligned}\theta_i(\tau, s) = {} & \left(1 + \frac{1}{\lambda B}\right)\operatorname{erfc}\left(\frac{s}{2\sqrt{\tau}}\right) \\ & + \frac{\exp(B^2\tau - Bs)}{\lambda B}\left\{1 - \frac{1}{2}\operatorname{erfc}\left(\frac{s}{2\sqrt{\tau}} - B\sqrt{\tau}\right)\right\} \\ & - \frac{\exp(B^2\tau + Bs)}{2\lambda B}\operatorname{erfc}\left(\frac{s}{2\sqrt{\tau}} + B\sqrt{\tau}\right) - \frac{\exp(-Bs)}{\lambda B} \qquad (3.25) \\ & + [\exp(Q^2\tau - Qs)](2Q^2\tau - Qs - 1)\left\{\frac{1}{2}\operatorname{erfc}\left(\frac{s}{2\sqrt{\tau}} - Q\sqrt{\tau}\right) - 1\right\} \\ & + \frac{1}{2}[\exp(Q^2\tau + Qs)](2Q^2\tau + Qs - 1)\operatorname{erfc}\left(\frac{s}{2\sqrt{\tau}} + Q\sqrt{\tau}\right)\end{aligned}$$

For the values of τ and s used in the examples given later, (3. 25) has been simplified to

$$\theta_i(\tau, s) = \left(1 + \frac{1}{\lambda B}\right) \operatorname{erfc}\left(-\frac{s}{2\sqrt{\tau}}\right) - \frac{\exp(-Bs)}{\lambda B} \qquad (3.26)$$

Knowing θ_i, the dimensionless initial velocity u_i can be recalculated as (Dabby and Paek (1972))

$$u_i = \lambda \left[\frac{\partial \theta_i}{\partial s}\right]_{s=0} \qquad (3.27)$$

$$= 1 - \exp(B^2\tau) \operatorname{erfc}(B\sqrt{\tau}) + 2\lambda Q^2\tau \exp(Q^2\tau) \operatorname{erfc}(Q\sqrt{\tau}) - \frac{2\lambda}{\sqrt{\pi}} Q^2 \sqrt{\tau} \qquad (3.28)$$

The steady - state temperature distribution can be obtained by setting $\partial\theta / \partial\tau = 0$ in (3. 20) and solving with u constant. It is found that the steady - state normalised temperature profile θ_{ss} in the moving normalised reference frame is

$$\theta_{ss} = \exp(-vs) - \frac{1}{\lambda(B-v)} \left(\exp(-Bs) - \exp(-vs)\right) \qquad (3.29)$$

where v is the steady - state value of u.

The steady - state temperature is a travelling temperature wave independent of the initial temperature distribution. The value of v can be determined by replacing u with v and θ with θ_{ss} in (3. 21) and solving for v. The normalised steady - state velocity is

$$v = \frac{1}{(1+\lambda)} \qquad (3.30)$$

Figs. 3. 4 and 3. 5 show the dimensionless temperature calculated by the author as a function of the depth (z - Z) into the irradiated solid at different dimensionless times, τ, for aluminium and mild steel. These curves show temperatures inside the material that are higher than the surface temperature T_v. Due to the distributed heat generation by the laser, the temperature throughout the solid will tend to rise. Vapourisation of the front surface occurs removing energy from the region near the front surface. Dabby and Paek (1972) stated that this cooling mechanism causes the maximum temperature to lie below the surface. If sufficient heat generation occurs within the solid, the removal of energy by vapourisation of the front surface may not be rapid enough to prevent the inner portion of the material from reaching temperatures that are substantially higher than the surface vapourisation temperature.

The maximum dimensionless temperature reached by aluminium is ~ 1.2 whilst for mild steel it is ~ 1.6 when each solid is irradiated with a power density, I, of 10^9 W / cm^2. The maximum temperature reached by a particular solid upon heating by a laser pulse is dependent upon its specific heat capacity and thermal conductivity. The specific heat capacity and thermal conductivity constants for aluminium are (from Table 3. 2) 0.913 J / g °K and 2.01 J / cm s °K at

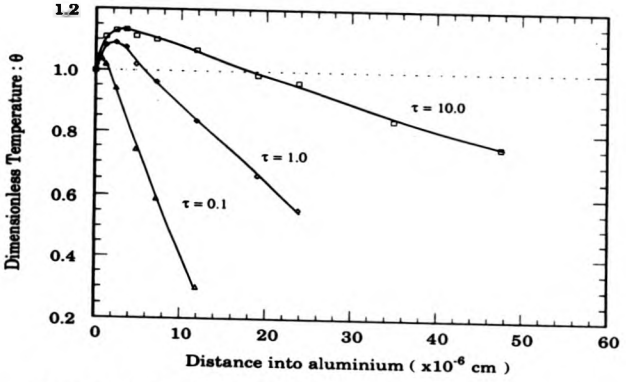

Figure 3. 4 : Graph illustrating the temperature versus distance into aluminium variation at different normalised times.

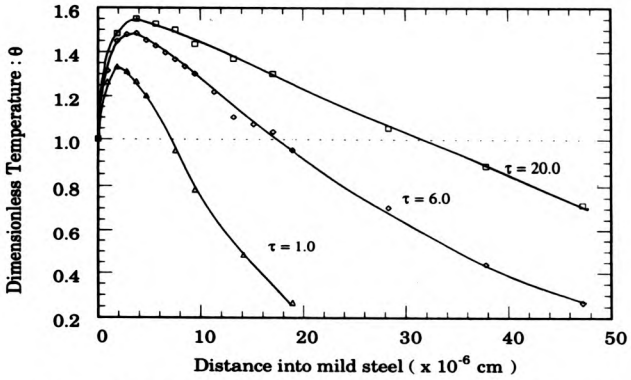

Figure 3. 5 : Graph illustrating the temperature versus distance into mild steel variation at different normalised times.

293 °K respectively. The respective values for mild steel are 0.42 J / g °K and 0.63 J / cm s °K. Solids with large specific heat capacities and thermal conductivities are capable of absorbing a large amount of heat energy with little rise in temperature and dissipating the absorbed energy within its volume at a fast rate. Aluminium, with a higher specific heat capacity and thermal conductivity than mild steel, would thus have lower temperatures developing within its bulk than mild steel as predicted by Dabby and Paak (1972) and shown in Figs. 3. 4 and 3. 5.

The effect of the differences in the thermal conductivities of aluminium and mild steel on the temperature profiles is illustrated more clearly in Figs. 3. 6 and 3. 7. These figures show the absolute velocities of the vapourisation front, calculated by the author using equation (3. 28), as a function of time over the duration of the laser pulse for aluminium and mild steel respectively. The absolute velocity of the vapourisation front in aluminium is approximately one order of magnitude greater than for mild steel. It is also an order of magnitude greater than the compression wave velocity for aluminium which is $\sim 0.6 \times 10^6$ cm / s. This shock wave propagates into the solid over the duration of the laser pulse and then reduces to zero at an equivalent rate over a time equivalent to the laser pulse duration. A similar shock wave was reported in silicon (thermal conductivity = 1.6 J / cm s °K) by Harada et al. (1999).

If the temperature reached is great enough to cause vapourisation of the material at depths below the surface, tremendous pressures arising from the vapourised materials will develop that would explosively remove the intervening material. Material removal will also continue after the laser pulse ends. This is investigated further in the next section. This mechanism of material removal by vapourisation

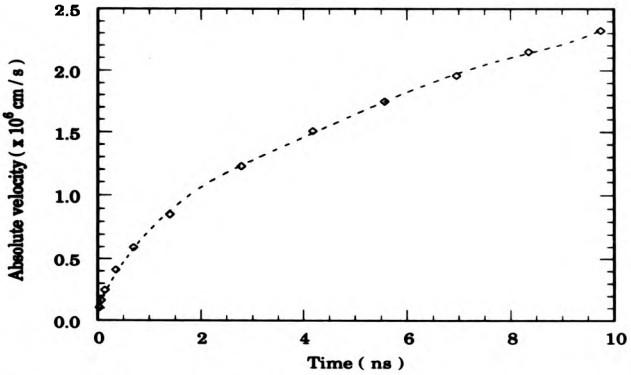

Figure 3. 6 : Absolute velocity of vapourisation front in aluminium as a function of time over the duration of the laser pulse.

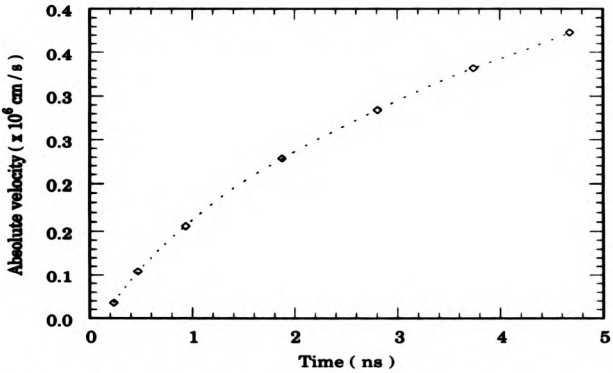

Figure 3. 7 : Absolute velocity of vapourisation front in mild steel as a function of time over the duration of the laser pulse.

upon heating of a solid by a laser pulse, using the heat conduction model followed, has also been described qualitatively by Ready (1963).

3. 2. 4 : Pressure developed as a result of vapourisation

The temperature distribution equations of Dabby and Paek (1972) are used in this section to derive the pressure developed as a result of vapourisation. The superheated region immediately beneath the surface which is above the vapourisation temperature may be treated as a highly condensed gas. The depth to which this region extends as a function of time may be obtained using equation (3. 26). The number of particles (ions and electrons) in this highly condensed gas region may be assumed to be equivalent to the solid state density number for the following reason. Before vapourisation of the material occurs, the ions and electrons are confined to the superheated region. Thus this region must contain the same number of ions and electrons in the highly condensed gas state as in the solid state. This region is modelled, in this instance, as a disc with a diameter of 0.2 cm and extending to a depth below the surface which corresponds to the depth at which the temperature is above the vapourisation temperature.

The number of atoms, N_{atoms}, in a disc 0.2 cm in diameter and of thickness, ∂s, is given by

$$N_{atoms} = \frac{\pi N_A \rho \partial s}{100X} \qquad \text{- number of atoms} \qquad (3.31)$$

where N_A is Avogadro's Number (= 6.02×10^{23} / mol),

and X is the atomic weight (in g) of the majority elements in a particular material.

In a highly condensed gas state, the number of ions is equivalent to the number of contributing atoms, i. e. $N_{ions} = N_{atoms}$, and for each atom it is assumed that an electron is contributed to the gas. Thus $N_{elec} = N_{ions}$ (Krehl et al. (1975)).

The pressure, ∂P_{ions}, owing to N_{ions} ions contained within a disc of thickness ∂s and of constant temperature T is given by

$$\partial P_{ions} = \frac{10 N_{ions} kT}{\pi \partial s} \quad (N / cm^2) \qquad (3.32)$$

where k is Boltzmann's constant (= 1.38×10^{-23} J / °K)

The integer term, 10, is used to present the pressure units on the same scale as the size of the source and represents part of the volume term.

The electrons contribute an equivalent pressure and thus the total pressure, $\partial P_{total} = \partial P_{ions} + \partial P_{elecs}$, is given by

$$\partial P_{total} = \frac{20 N_{ions} kT}{\pi \partial s} \quad (N / cm^2) \qquad (3.33)$$

Using (3. 31) for N_{ions} gives

$$\partial P_{total} = \frac{0.2 N_A \rho kT}{X} \quad (N / cm^2) \qquad (3.34)$$

For aluminium at 2800 °K, ∂P_{total} = 468 N / cm^2, atmospheric pressure at S. T. P. is 10. 1 N / cm^2. Over a 0.2 cm source diameter the force

developed is ~ 15 N which compares favourably to a value of 20 N estimated by Cooper (1985). The pressure that is developed results in two events:

(i) on the free surface side, because the vapourisation pressure is very much greater than the atmospheric pressure, there is an immediate explosion of material. Note that in a vacuum this explosion would be greater as observed by Krehl et al. (1975).

(ii) This equal and opposite pressure on the other face of the disc shaped source stresses the material. This stress is propagated through the material as ultrasound.

The temperature, T, is a function of time and distance into the sample as given by (3. 26). The temperature profile above the vapourisation temperature may be represented by

$$T = T_v \theta_i (\tau, s) H \{ \theta_i (\tau, s) - 1 \} \qquad (3. 35)$$

where $H \{ \theta_i (\tau, s) - 1 \} = 1$ for $\theta_i (\tau, s) \geq 1$

$= 0$ for $\theta_i (\tau, s) < 1$

and is the Heaviside function.

The total pressure at a particular time, τ, is given by

$$P_{total} (\tau) = \frac{0.2 N_A \rho k T_v}{X} \int_0^S \theta_i(\tau,s) ds \quad (N / cm^2) \qquad (3. 36)$$

where S is the depth to which the highly condensed gas region extends in a time τ and this condition negates the use of the Heaviside term in the integral equation.

The derivation of equation (3. 36) may be understood by referring to Fig. 3. 8.

Substituting equation (3. 26) into (3. 36) gives

$$P_{total}(\tau) = \frac{0.2N_A\rho kT_v}{X}\left[\left(1+\frac{1}{\lambda B}\right)\int_0^S \operatorname{erfc}\left(\frac{s}{2\sqrt{\tau}}\right)ds - \frac{1}{\lambda B}\int_0^S \exp(-Bs)ds\right] \qquad (3.37)$$

Thus,

$$P_{total}(\tau) = \frac{0.2N_A\rho kT_v}{X}\left[\left(1+\frac{1}{\lambda B}\right)\left(S\operatorname{erfc}\left(\frac{S}{2\sqrt{\tau}}\right) + 2\sqrt{\frac{\tau}{\pi}}\left(1-\exp\left(-\frac{S^2}{4\tau}\right)\right)\right) + \frac{1}{\lambda B^2}\left(\exp(-BS)-1\right)\right] \qquad (3.38)$$

After the duration of the laser pulse there still exists a region in which the temperature is above the vapourisation temperature. Laser heating of the surface is suspended and the material begins to cool down at a rate assumed to be equivalent to the rate at which the material is heated up. Hence vapourisation of material continues after the laser pulse has ended for a time of approximately twice the duration of the laser pulse. This continues until the temperature within the material decays to

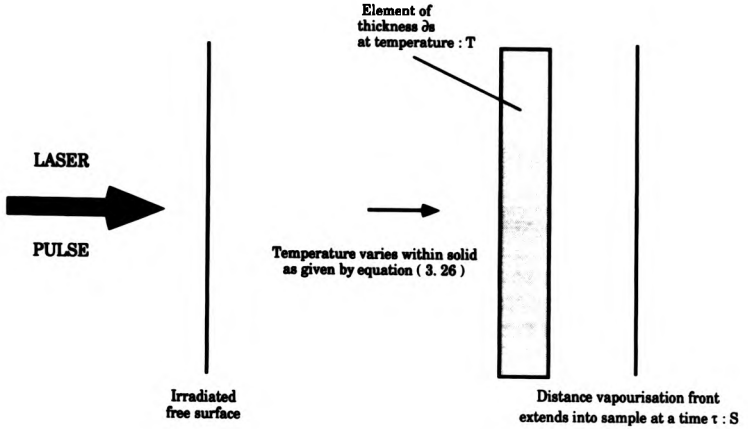

Figure 3. 8 : Diagram to illustrate how the pressure within a highly condensed gas region of thickness S is calculated.

below its vapourisation temperature. Fairand and Clauer (1979) measured the pressure produced by the vapourisation of aluminium and showed that the pressure decayed to zero from its peak value over approximately twice the duration of the laser pulse.

Fig. 3. 9a and 3. 10a are the pressure profiles for aluminium and mild steel as a function of time over the duration of the laser pulse and its decay back down to zero pressure calculated using the expression derived by the author. The peak pressure developed on the aluminium surface is ~ 400 N / cm^2 whilst it is ~ 2800 N / cm^2 for mild steel. Generally the larger the peak pressure developed upon a surface the larger the amplitude of the ultrasound which is generated. Thus, neglecting attenuation of the ultrasound, the compression wave generated in mild steel should have a larger amplitude than a compression wave generated in aluminium by this mechanism.

The initial rate at which the pressure pulse develops is obtained by differentiating the pressure profile with respect to time for small values of time. These are shown in Figs. 3. 9b and 3. 10b for aluminium and mild steel respectively. It is observed that the pressure pulse rises rapidly in a time ~ 10^{-11} s (from Table 3. 2) and then decays at a slower rate down to zero over the duration of the laser pulse. The rate of decay from the peak pressure is greater for aluminium than for mild steel. As a consequence of this the ultrasonic compression wave generated in aluminium will be expected to have a smaller width than a compression wave generated in mild steel.

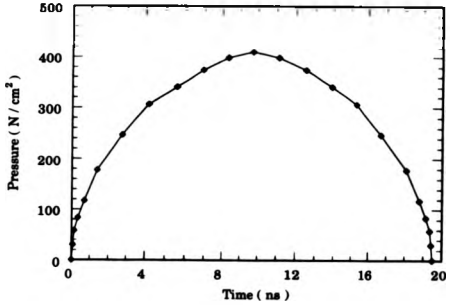

Figure 3. 9a : Pressure due to highly condensed gas region in aluminium as a function of time.

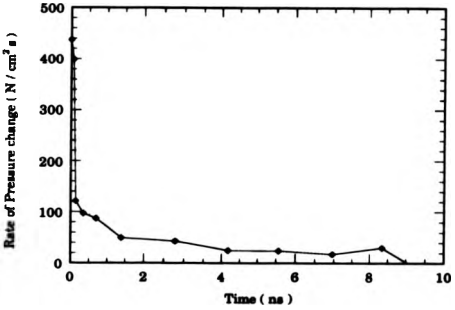

Figure 3. 9b : Rate of pressure change in aluminium over the duration of the laser pulse.

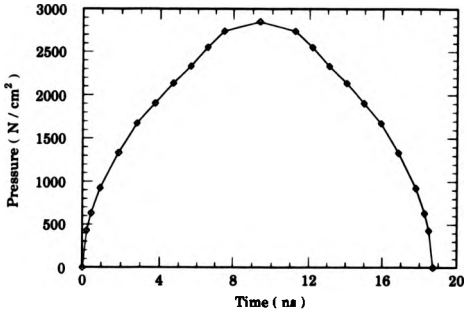

Figure 3. 10a : Pressure due to highly condensed gas region in mild steel as a function of time.

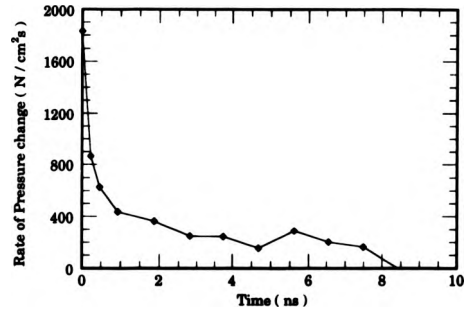

Figure 3. 10b : Rate of pressure change in mild steel over the duration of the laser pulse.

3. 2. 5 : Effects of the plasma on the ultrasonic generation process

This section derives the pressure developed upon the solid surface by the formation of a plasma. The vapourisation of the ions and electrons contained within the superheated region results in the formation of a plasma above the irradiated surface with almost solid state number density. For aluminium the solid state number density is 6.05×10^{22} cm^{-3} whilst for mild steel it is 8.47×10^{22} cm^{-3}. Light of frequency ω approaching a uniform semi - infinite plasma in which the electron density, n_{elec}, exceeds the critical value given by (Hughes (1975))

$$n_{elec} = \frac{\omega^2 m_{elec} \varepsilon_o}{e^2} \qquad (3.39)$$

where m_{elec} is the mass of the electron ($= 9.11 \times 10^{-31}$ kg),
ε_o is the vacuum permittivity ($= 8.85 \times 10^{-12}$ F / m),
and e is the charge of an electron ($= 1.6 \times 10^{-19}$ C),

will be reflected. For Nd:YAG laser light (1.06 μm wavelength) $n_{elec} = 10^{21}$ cm^{-3} and thus the initial plasma formed above the aluminium and mild steel surfaces will reflect most of the incident laser energy. Most of the laser radiation is absorbed via inverse bremsstrahlung in a thin layer of the plasma in front of the material surface where the plasma frequency is close to the laser frequency. The absorbed laser energy tends to increase the rate of expansion of the plasma (Hughes (1975)) thereby decreasing the number density and thus allowing more laser light through to the solid surfaces. It is possible for a self - regulating plasma to develop if enough material is vapourised

upon subsequent laser heating of the solid to increase the number density beyond the critical value again (10^{21} cm^{-3} for Nd:YAG laser light). Laser heating of the surface is suspended and instead used to heat the plasma causing further expansion until once again the number density reduces to below the critical value. Further heating of the solid commences and the process is repeated. This has been considered in more detail by Hughes (1975) and is not considered here. The aim of this section is to derive the order of magnitude contribution of the plasma pressure upon the solid surface to the total pressure developed.

Initially the plasma is assumed to expand towards the laser away from the surface. Streak photographs by Cooper (1985) of the plasma produced by a Nd:YAG laser irradiating aluminium illustrated plasma expansion towards the laser occurring during the first ~ 0.2 μs from plasma formation. Thus the plasma is assumed to be cylindrical in shape with a diameter of 0.2 cm and a thickness which increases with increasing time at a rate determined by the expansion velocity.

The mean velocity of expansion, V_{exp}, of the plasma may be taken to be equal to the isothermal velocity and is given by

$$V_{exp} = \sqrt{\frac{3KT_{plasma}}{m_{AV}}} \qquad (3.40)$$

where T_{plasma} is the average temperature of the plasma,

and m_{AV} is the mass of an ion and electron within the plasma.

The average plasma temperature was calculated in the following manner. For a particular time, the r.m.s. average temperature above the vapourisation temperature is calculated and this temperature is assumed to be the temperature of the plasma. After the initial

vapourisation the temperature of the additional ions and electrons will be more than the plasma temperature. Thermal equilibrium occurs which for the purposes of this calculation is taken to be the average of the different temperatures. Extending this calculation for both aluminium and mild steel materials over the duration of the laser pulse and until vapourisation ceases results in an average plasma temperature of 2990 ^{o}K for aluminium and 4020 ^{o}K for mild steel.

If the ions and electrons within the plasma are assumed to be non - interacting than there will be effectively two expansion velocities corresponding to the different masses of the ions and electrons. For aluminium these expansion velocities will be 1.66×10^{6} cm / s for ion and 3.69×10^{7} cm / s for electron expansion. The corresponding expansion velocities for a plasma formed above mild steel are 1.34×10^{6} cm / s (ion expansion) and 3.69×10^{7} cm / s (electron expansion). These velocities are not dissimilar to the plasma expansion velocity above aluminium determined by Krehl et al. (1975) of 1.1×10^{7} cm / s. To enable an order of magnitude calculation for the plasma pressure, and taking into account some interaction between the ions and electrons in the plasma, an average velocity is calculated. Thus for aluminium the expansion velocity is considered to be 1.85×10^{7} cm / s whilst for mild steel it is 1.91×10^{7} cm / s. It is assumed that this velocity remains constant over twice the duration of the laser pulse i. e. when new material is continuing to be added to the plasma.

Assume, for convenience, that at a time $\tau = 0.5$ (3.48×10^{-10} s for aluminium and 2.34×10^{-10} s for mild steel) the plasma has expanded so that the critical density, n_{elec}, of 10^{21} cm^{-3} is obtained. The thickness of the plasma expanding towards the laser at this critical density, assumed cylindrical in shape, may be calculated. With further vapourisation of the material surface and a constant velocity of

expansion it is possible to calculate the thickness of the plasma and the number density, n (in cm^{-3}), as a function of time over the duration of the laser pulse and until vapourisation ceases. These are shown in Fig. 3. 11 for aluminium and mild steel. It is appreciated that the diameter of the plasma will also increase though at a slower rate. This, however, is not taken into account in this calculation. Note that the number density of the plasma decays rapidly, within ~ 3 ns for aluminium and ~ 2 ns for mild steel, to a stabilised number density of ~ 4 x 10^{19} cm^{-3} for aluminium and ~ 2 x 10^{20} cm^{-3} for mild steel which is below the critical value of 10^{21} cm^{-3}. Thus the surface is not shielded by the plasma to any great extent over the duration of the laser pulse.

The pressure, P_{plasma}, upon the solid surface owing to the expanding plasma may be calculated using

$$P_{plasma} = \frac{1}{3} n \, m_{AV} \, V_{exp}^2 \qquad (3.41)$$

where n is the number density (in cm^{-3})

which, by using equation (3. 40) for V_{exp}, becomes

$$P_{plasma} = 100 \, n \, k \, T_{plasma} \qquad (N / cm^2) \qquad (3.42)$$

As for the previous section, the units of pressure are given in N / cm^2 so that direct comparison with the source dimensions may be made. Using the data in Fig. 3. 11, the plasma pressure produced by the expanding plasma upon the aluminium and mild steel surface is calculated and shown as a function of time over twice the duration of the laser pulse in Fig. 3. 12. A stabilised plasma pressure of ~ 200 N / cm^2 for aluminium

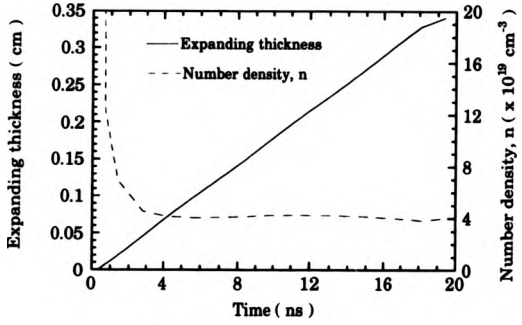

Figure 3. 11a : Thickness of expanding plasma and number density, n, as a function of time for aluminium

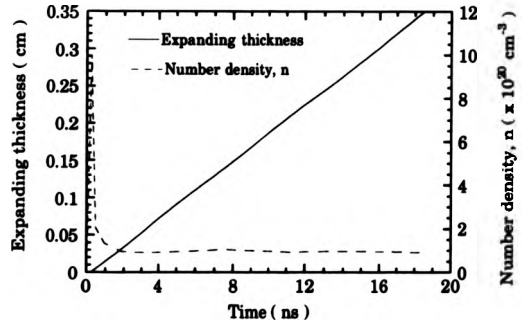

Figure 3. 11b : Thickness of expanding plasma and number density, n, as a function of time for mild steel

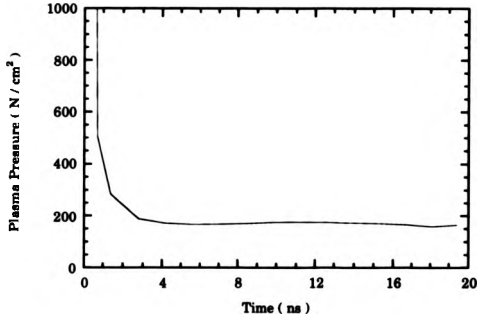

Figure 3. 12a : Pressure on aluminium surface owing to expanding plasma as a function of time over twice the duration of the laser pulse

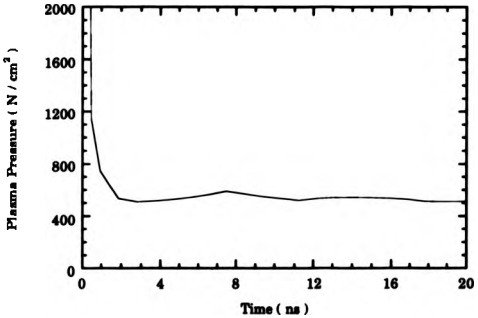

Figure 3. 12b : Pressure on mild steel surface owing to expanding plasma as a function of time over twice the duration of the laser pulse

and ~ 500 N / cm^2 for mild steel is obtained after approximately 3 ns from the onset of the laser pulse which exists over a longer time period than the pressure developed as a result of vapourisation. These pressures correspond to a force acting over the 0.2 cm diameter source size of ~ 6 N for aluminium and ~ 16 N for mild steel. The time over which the plasma pressure remains significant, i. e. more than atmospheric pressure, may be estimated by considering the free expansion of an ideal gas for which there is no temperature change (Reif (1981)). For aluminium, atmospheric pressure is reached when the number density, n, becomes 2.5 x 10^{18} cm^{-3} which corresponds to a thickness of (assuming the same type of expansion of the plasma) 5.6 cm. As the expansion velocity remains constant, by virtue of a constant plasma temperature, a thickness of 5.6 cm is obtained in 0.3 μs. For mild steel, atmospheric pressure is reached when the number density becomes 1.8 x 10^{18} cm^{-3} corresponding to a thickness of 18 cm which is obtained in 0.9 μs. When the plasma pressure reduces to below atmospheric pressure it is destroyed. If the plasma is formed in a vacuum then the pressure will act over an even longer timescale. The time duration of the plasma formed above the aluminium surface compares favourably to streak photograph measurements of the plasma duration by Cooper (1985).

3. 2. 6 : Discussion

The previous sections have described the various stages involved in the production of a pressure (stress) pulse in a solid when irradiated with a laser pulse of sufficient power density to eventually cause vapourisation. This plasma regime ultrasonic generation process

results in relatively large amplitude compression waves with fast (~ ns) risetimes which tend to follow the incident laser pulse profile. Quantitative assessments of the contribution of each process involved in the production of the resulting stress were made. These investigations indicated that, in addition to the incident laser pulse profile, the properties of the irradiated solid also affect the properties of the ultrasound generated. The main results from the previous sections are summarised in an attempt to ascertain the best type of material required to produce a fast risetime, broadband, ultrasonic compression wave pulse for a particular incident laser pulse profile.

The first stage in the ultrasonic generation process is the absorption of the incident photon energy by the conduction electrons to the electromagnetic skin depth. This absorption increases with increasing photon energy and occurs in ~ (10^{-12} - 10^{-13}) s. The absorbed energy increases the temperature of the solid. The temperature variation with distance into a solid, before vapourisation occurs, has been determined by Dabby and Paek (1972) using the heat conduction equation with appropriate boundary conditions. This was calculated for aluminium and mild steel and it was observed that the temperature rise extended to a greater depth in aluminium owing to its larger thermal conductivity.

The time for a solid to reach its vapourisation temperature in terms of its thermal and mechanical properties was also derived by Dabby and Paek (1972). This time was calculated by the author for a variety of solids (Equation 3. 13 and Table 3. 2) and was typically ~ 10^{-11} s for a laser pulse power density of 10^9 W / cm^2. The solid with the lowest time to reach vapourisation was soft solder which is characterised by having relatively low valued thermal properties. From a qualitative viewpoint a solid with a low specific heat capacity and

thermal conductivity will have a fast rate of temperature rise up to its vapourisation temperature. If the vapourisation temperature and latent heat of vapourisation are also relatively low then the explosive removal of material will commence more quickly. Qualitative analysis of equations (3. 13), (3. 14) and Fig. 3. 1 indicates that small times to reach vapourisation will be attained for a particular power density, I, for low values of the thermal conductivity, optical absorption coefficient and vapourisation temperature in association with low values of the density and specific heat capacity. A solid with these properties will absorb more of the incident laser pulse energy to a greater depth. The absorbed energy within this larger volume will have a small mass of material to heat owing to its low density. A low mass and specific heat capacity will result in a large temperature rise which will not conduct to a larger volume as its thermal conductivity is low. The temperature increases up to the solids vapourisation temperature more quickly and, if this temperature and the latent heat of vapourisation is also low, vapourisation commences more quickly.

The time a particular solid takes to reach its vapourisation temperature is much less than the risetime of the assumed incident laser pulse which has a rise and fall time of 1 ns and duration of 10 ns. Thus the solid can be considered to attain vapourisation immediately upon the onset of the laser pulse. Using laser pulses with risetimes $\sim 10^{-11}$ s, it would be possible to investigate more fully the variation of time to reach vapourisation and its effect on the generated ultrasound.

It was assumed in the derivation of the temperature profile before vapourisation occurs that the optical absorption coefficient of the solid remained unchanged. Hughes (1975) considered the liquid stage in the heating of a solid up to its vapourisation point. Studies indicated that a marked increase in the rate of heating by a laser pulse of constant

irradiance occurs when surface melting takes place. This may be accounted for in the heat conduction model followed by replacing the optical absorption coefficient, b, with a temperature dependant optical absorption coefficient, e. g. b (θ), which increases during the liquid phase. Other possible changes in the properties of the solid as a function of temperature have been considered by Ready (1971).

The heat conduction model was extended by Dabby and Paek (1972) to include vapourisation of the front part of the solid surface. The temperature variation as a function of time and distance into the solid was derived and calculations performed by the author for aluminium and mild steel. It was shown that a region, in which the temperature was above the vapourisation temperature, existed extending from the irradiated surface into the solid. This superheated region, which may be modelled as a highly condensed gas with solid state density, is explosively removed owing to the large pressures produced. Further heating of the solid by the laser pulse continues resulting in another superheated region of increased thickness and thus further vapourisation. The velocity with which the vapourisation front moves into the solid was calculated and it was shown that the thickness of this region increases with increasing time over the duration of the laser pulse. When laser heating of the solid ceased the material cools down at a rate which was assumed to be the same as the rate at which it heated up. Vapourisation of material continues after the cessation of the laser pulse with the thickness of the superheated region decreasing at a rate equivalent to the rate at which it increased. An assumption which is supported by the experimental investigations of Fairand and Clauer (1979). A small ablation pit, whose depth can be estimated by integrating the distance the vapourisation front extends into the solid over twice the duration of the laser pulse, results from the explosive

removal of material. The variation of the thickness as a function of time for aluminium and mild steel is shown in Fig. 3. 13. The depth of material removed is 2.7 μm for aluminium and 3.9 μm for mild steel and is not at variance with a depth of 5 μm determined by Cooper (1985).

The pressure developed as a result of this superheated region was derived by the author and calculations performed for aluminium and mild steel over twice the duration of the laser pulse. Peak pressures of 400 N / cm^2 for aluminium and 2800 N / cm^2 for mild steel were achieved which are very much greater than the atmospheric pressure of 10.1 N / cm^2. The rate at which this pressure (stress) pulse develops was also calculated and it was observed to have a risetime of ~ 10^{-11} s followed by a slower rate of decay back down to zero. The rate of decay from the peak pressure is greater for aluminium than for mild steel. Assuming that large rates of decay from the peak pressure produce higher frequency ultrasound implies that ultrasound generated in aluminium will contain higher frequency components than ultrasound generated in mild steel as the pressure pulse more closely resembles that of a δ - function. Large rates of decay are achieved for solids in which the velocity of the vapourisation front is large. This, in turn, implies that solids with large thermal conductivities and low specific heat capacities would support fast risetime, broadband ultrasound. The low specific heat capacity also results in the solid attaining higher temperatures and hence larger pressures.

The effect of the plasma formed above the surface of the solid upon the pressure (stress) generation process was also considered. The plasma pressure developed was found to be significant and to extend over a much longer timescale than the laser pulse duration. The plasma formed above the aluminium surface existed for approximately 0.3 μs whilst above a mild steel surface it existed for approximately 0.9 μs. The

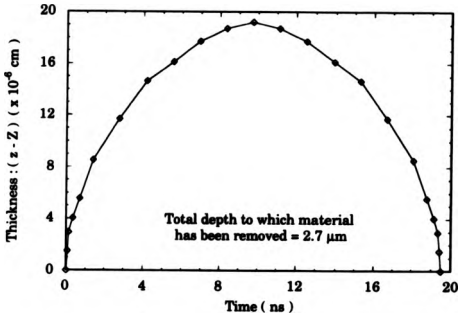

Figure 3. 13 a : Thickness of superheated region as a function of time for aluminium

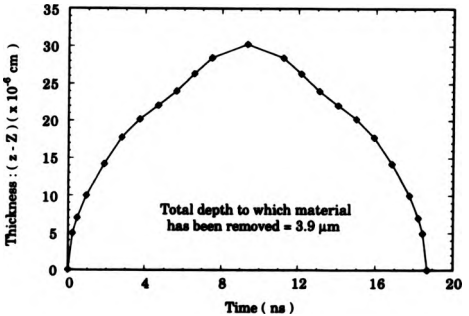

Figure 3. 13b : Thickness of superheated region as a function of time for mild steel

rate of decay of the plasma pressure is required to be fast if the resulting pressure profile acting on the solid is to have δ - function characteristics. The major factor affecting the rate of decay of the plasma is the average temperature of the plasma which is required to be large if the rate of decay is to be large. This, in turn, requires the irradiated solid to have a large vapourisation temperature.

The total pressure profile may be obtained by adding the contributions of the pressure developed as a result of vapourisation and the plasma pressure. The total pressure profile for aluminium and mild steel are shown in Fig. 3. 14. Depending upon the properties of the plasma, the pressure profile consists of a relatively large amplitude spike for approximately twice the duration of the incident laser pulse followed by a slower rate of decay to zero pressure after this time owing to the plasma pressure. By using an appropriate laser pulse and solid it may be possible to tailor the pressure profile to suit a particular need. Similar shaped pressure profiles and the resulting ultrasonic epicentral displacement have been considered by Dewhurst et al. (1982) using a Green' s function formalism.

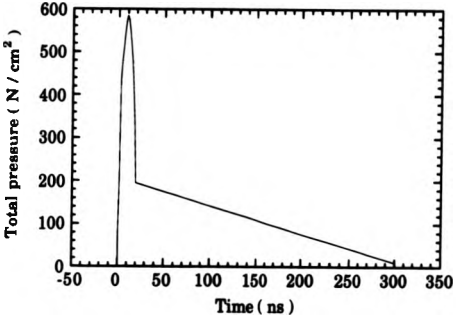

Figure 3. 14a : Total pressure profile developed upon aluminium surface by plasma regime mechanisms

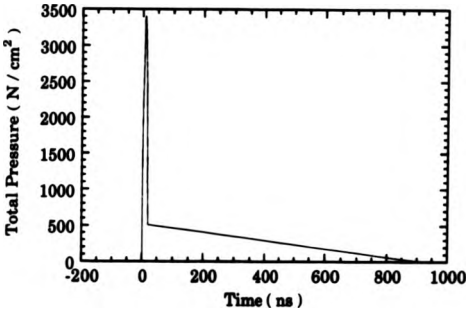

Figure 3. 14b : Total pressure profile on mild steel surface owing to plasma regime mechanisms

3. 3 : MEASUREMENT OF ULTRASONIC EPICENTRAL DISPLACEMENTS

This section describes the experimental investigations into the properties of the ultrasound generated in various solids using lasers with different pulse profiles and wavelengths in the plasma regime.

3. 3. 1 : Arrangement of experimental parameters

The experimental arrangement used to record the ultrasonic epicentral displacements in various solids is shown in Fig. 3. 15. The arrangement was the same for each laser used to generate ultrasound and the properties of the lasers used are summarised in Table 3. 3. The pulse profiles, detected using a BPX 65 photodiode (risetime – 0.5 ns) except for the picosecond laser which has been measured by the staff at the Laser Support Facility, Rutherford - Appleton Laboratories, are shown in Fig. 3. 16.

Each laser pulse was focussed to obtain a power density at the sample surface sufficient to create a plasma, i. e. $\geq 10^7$ W / cm^2. For the picosecond laser, situated at the Laser Support Facility, Rutherford - Appleton Laboratories, the laser pulse had to be focussed down, using a short (5 cm) focal length lens, to obtain the required power density. With the other lasers it was possible to attenuate, using neutral density filters, the energy in the pulse to obtain a power density with the same order of magnitude, approximately 10^9 W / cm^2. Another reason for focussing the laser pulse to as small a spot size as possible was to enable the source to approximate as a point source which is assumed in some

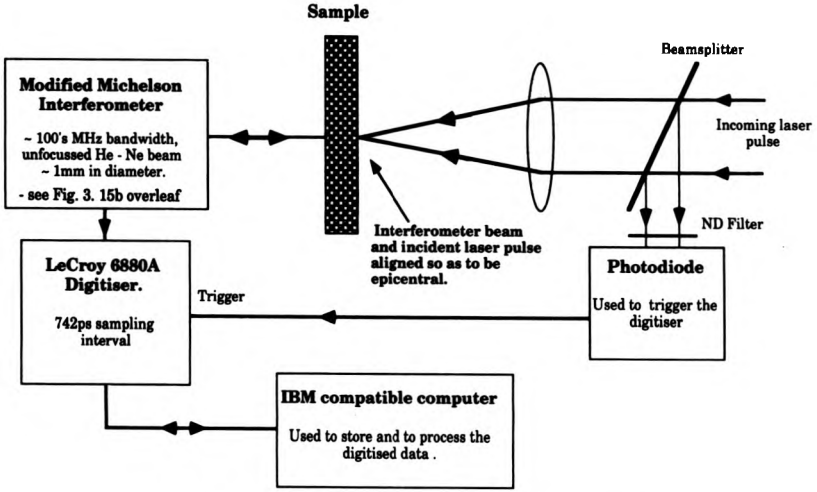

Fig. 3. 15a:Experimental arrangement used to record the ultrasonic epicentral displacement in various solids.

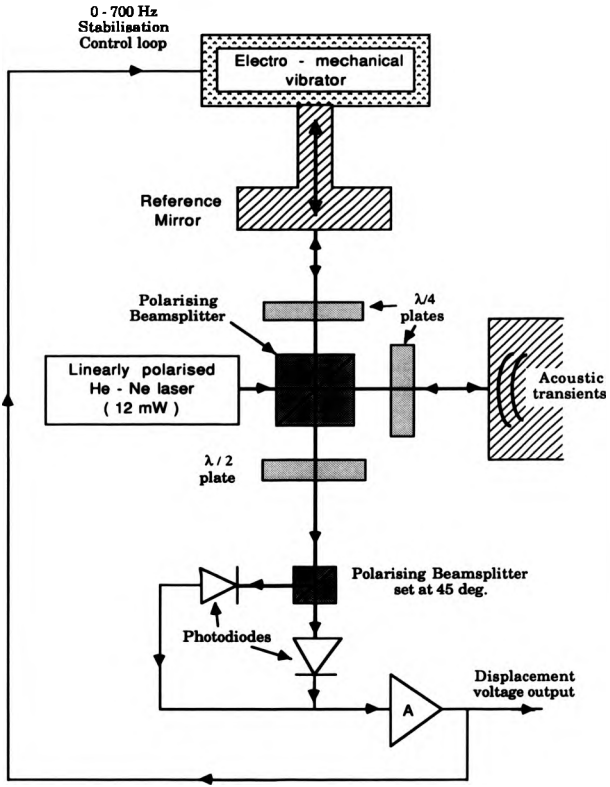

Fig. 3. 15b : Schematic diagram of the modified Michelson Interferometer

Laser	Wavelength (nm)	Pulse Risetime (ns)	FWHM	Energy / pulse	Focussed spot size	Power Density (W / cm^2)
Picosecond (Dye)	600	~ 0.1 ps	0.3 ps	0.2 mJ	0.5 mm diameter	3.4×10^{11}
Excimer (KrF)	308	4.5 ± 0.7	17 ns	36 mJ	~ 5 mm x ~ 0.1 mm	$\sim 0.3 \times 10^{9}$
Spectron Nd : YAG	1060	5.2 ± 0.7	14 ns	~ 100 mJ	~ 2 mm diameter	$\sim 0.9 \times 10^{9}$
HyperYag Nd : YAG	1060	6.2 ± 0.7	14 ns	~ 40 mJ	~ 2 mm diameter	$\sim 0.4 \times 10^{9}$

Table 3.3 : Summary of the relevant properties of the laser pulses used in this investigation

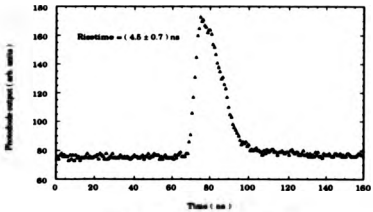

Figure 3. 16a : Eximer laser pulse profile

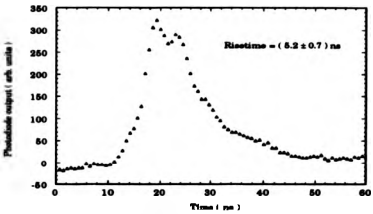

Figure 3. 16b : Spectron Nd-YAG laser pulse profile

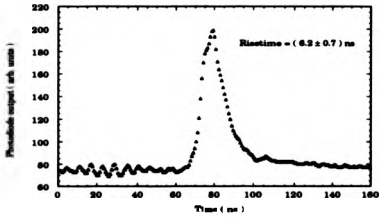

Figure 3. 16c : HyperYag Nd YAG laser pulse profile

modelling of the laser source (e. g. Cooper (1985)). A point source will also minimise path differences which would lead to a geometrical increase in the risetime of the ultrasonic compression wave pulse (Fig. 3. 17).

Two modified Michelson interferometers with wide bandwidths were used to detect the ultrasound generated in samples which varied in thickness from 1 mm to 5 mm. One face of each sample was polished to a mirror finish to allow sufficient reflection of the interferometer He - Ne beam. The interferometers had the same basic design but differed in that one interferometer had two avalanche photodiodes connected to a 430 MHz bandwidth amplifier whilst the other interferometer had slower (~ 0.5 ns) risetime photodiodes connected to a 130 MHz bandwidth amplifier. It was possible to calculate the ultrasonic displacement (in nm) from the recorded output signal voltage using this latter interferometer (McKie (1987)). The ultrasonic displacement, x, is given by

$$x = \frac{V}{V_o}\frac{\lambda}{4\pi} \qquad (\text{nm}) \qquad (3.43)$$

where V is the ultrasonic output signal voltage,
V_o is the unstabilised output voltage,
and λ is the wavelength of the He - Ne laser (= 632.8 nm).

Ideally a point source and a point detector directly opposite one another are required to correctly measure the risetime of the ultrasonic pulse. The laser source has been focussed down to as small a source size as possible using the optics available. The He - Ne beam of both interferometers has a diameter ~ 1 mm. The diameter of the detecting

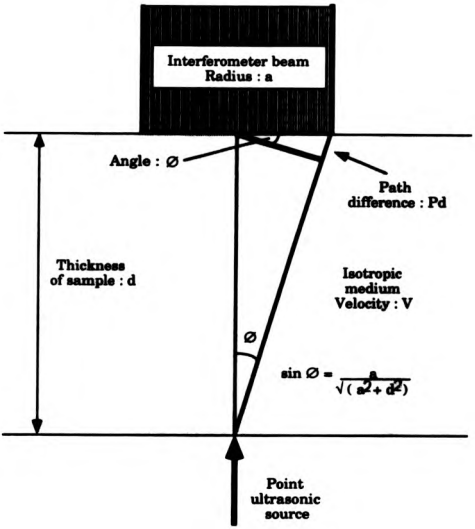

Path difference : Pd = a sinØ

$$= \frac{a^2}{\sqrt{(a^2 + d^2)}}$$

Time difference :Td = $\frac{a^2}{V \sqrt{(a^2 + d^2)}}$

Fig. 3. 17 : Diagram to illustrate the effect of interferometer beam diameter on the risetime of the detected ultrasound.

beam affects the risetime of the output signal from the interferometer and this is exacerbated if the source and detector are not directly opposite one another and may be understood by referring to Fig. 3. 17.

The interferometer will sense a risetime associated with the traverse of the ultrasonic wave front across the He - Ne beam. For a typical interferometer beam diameter of ~ 1 mm and a sample thickness of 1 mm the time difference, assuming a velocity of 6 mm / μs, is 37 ns. If the interferometer beam is focussed down to 0.1 mm the time difference becomes 0.42 ns. Thus the error owing to the finite size of the detecting beam is reduced if its sensing area is reduced. In practice, the He - Ne beam was not focussed down as the sensitivity was decreased owing to losses in beam intensity on propagating through the focussing lens. Note also that the path difference error is also increased if the source and detector are misaligned. To reduce this, the source and detector laser beams were aligned as accurately as possible so that they coincided in the region where the sample was to be placed.

The other factor affecting the path difference error is the distance the ultrasound has propagated to the detector. Analysis of Fig. 3. 17 indicates that thicker samples will result in smaller path difference errors. However if the sample is too thick then significant attenuation will result which will degrade the risetime of the ultrasonic pulse. The waveforms recorded in this investigation contained up to three compression and shear wave signals and the fastest risetime was often observed on the second or third compression wave signal. This is a result of the increased path length of the ultrasound in reflecting back and forth between the faces of the sample. For example, the second ultrasonic wave arrival, propagating at a velocity of 6 mm / μs through a 1 mm thick sample and incident upon the 1 mm diameter detecting beam of the interferometer, has an effective path length of 3 mm. The

time difference now becomes 14 ns whilst the third ultrasonic arrival has a time difference of 8 ns. Compression wave signals after the third arrival were not considered in this investigation as their amplitudes were diminished owing to attenuation.

The risetime of an ultrasonic pulse, t_r, detected by an interferometer with an associated risetime, t_{det}, owing to the active sensing region of the interferometer and the bandwidth of the electronic circuitry, results in a recorded output pulse with a risetime, t_{out}, given by

$$t_{out} = \sqrt{(t_r^2 + t_{det}^2)} \qquad (3.44)$$

and

$$t_{det}^2 = t_{sens}^2 + t_{elec}^2 \qquad (3.45)$$

where t_{sens} is the risetime associated with the active sensing region of the interferometer,

and t_{elec} is the risetime associated with the electronic circuitry of the interferometer. This is evaluated in the next section.

In effect the output signal recorded is the convolution of the ultrasonic pulse with the frequency response of the detecting region and the detector electronics. A similar analysis has been described by Sullivan and Tam (1984) and Tam (1984). Using equations (3. 44), (3. 45) and the recorded risetime, t_{out}, it is possible to estimate the risetime of the ultrasonic pulse, t_r. However these calculations were not performed in this investigation as an accurate determination of the necessary variables was not obtainable. For example, the interferometer detecting beam is considered to have a flat response to surface displacements over

the diameter of the beam. In reality the beam intensity from the He - Ne laser has a Gaussian distribution resulting in a greater sensitivity at its centre than on the fringes of the beam. Account must be made of this variation which is beyond the scope of this investigation. In addition the source is a finite size and this too would have to be taken into account. Use of equations (3. 44) and (3. 45) would be more beneficial if a source and detector size of ~ μm were employed in the recording of the ultrasonic risetime.

3. 3. 2 : Evaluation of Interferometer Bandwidth

It was possible to determine the bandwidths of the two interferometers using the picosecond laser. The picosecond laser pulse was directed onto the photodiodes within each interferometer in turn. Neutral density filters were used to attenuate the intensity of light so that the photodiodes were not damaged. The amplifier outputs were recorded using the LeCroy 6880A digitiser operated under software control using an IBM - PC compatible computer and are shown in Fig. 3. 18.

Fig. 3. 18a illustrates the output pulse from the interferometer containing the ~ 0.5 ns risetime photodiodes connected to the 130 MHz bandwidth amplifier. The risetime of the pulse is (4.5 ± 0.7) ns which, using the relation between bandwidth, B, and pulse risetime, t_{elec}, given by

$$B = \frac{1}{\pi t_{elec}}, \qquad (3.46)$$

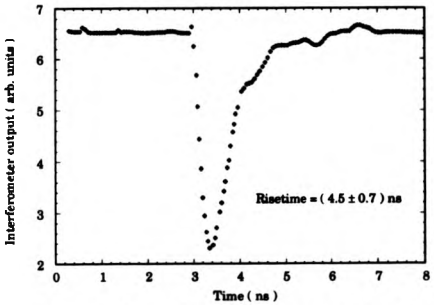

Figure 3. 18a : Output pulse from interferometer containing ~ 0.5 ns risetimes photodiodes with picosecond laser light input.

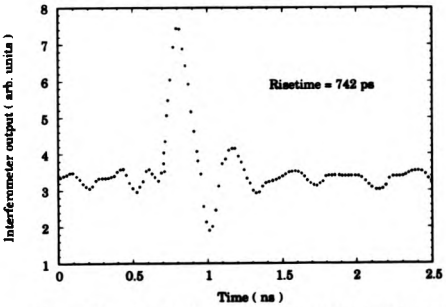

Figure 3. 18b : Output pulse from interferometer containing avalanche photodiodes with picosecond laser light input.

gives a bandwidth of (72 ± 14) MHz. A 0.3 ps pulse width would be expected to contain frequency components up to ~ 10^{12} Hz. The limit on the maximum frequency detectable using this interferometer is a combination of the type of photodiodes used, the matching of the photodiodes to the amplifier and the characteristics of the amplifier.

Fig. 3. 18b illustrates the output pulse from the interferometer containing the avalanche photodiodes connected to the 430 MHz amplifier. The risetime of this pulse is 742 ps (Bandwidth 430 MHz) which is on the limits of the digitisation rate of the LeCroy 6880A. It could be possible for this interferometer to detect faster risetimes but a digitiser with a sampling interval ~ 0.1 ps and a corresponding wideband interferometer amplifier would be required. These results indicate that the fastest risetimes that could be detected are (4.5 ± 0.7) ns for the 72 MHz bandwidth interferometer and 742 ps for the 430 MHz bandwidth interferometer.

3. 3. 3 : Ultrasound detected using the 430 MHz bandwidth interferometer

The ultrasonic epicentral displacements generated by the Excimer and the two Nd:YAG lasers are illustrated in Figs. 3. 19 - 3. 22 for aluminium, mild steel, copper and silicon respectively. The waveforms shown are for those samples in which the fastest risetimes were recorded. These were primarily the 1 mm and 2 mm thick samples and the ultrasound propagated at the compression and shear wave velocities characteristic of a particular solid and are given by, for example, Kaye and Laby (1989). All of the waveforms, except to some

(a) EXCIMER LASER

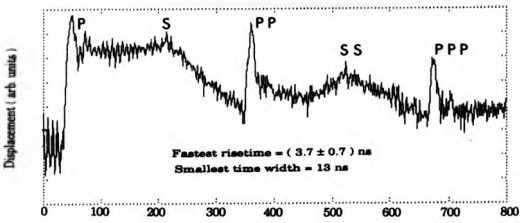

(b) SPECTRON Nd:YAG LASER

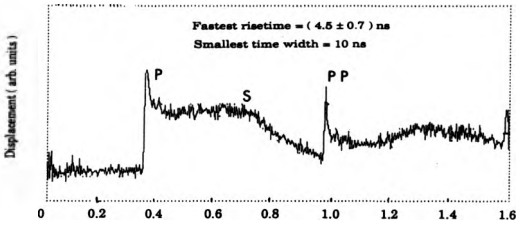

(c) HYPERYAG Nd:YAG LASER

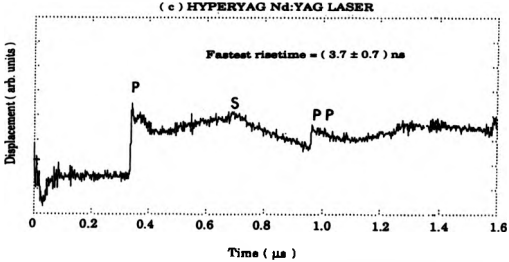

Figure 3. 19 : Ultrasonic epicentral displacement waveforms recorded on aluminium for various incident laser pulses

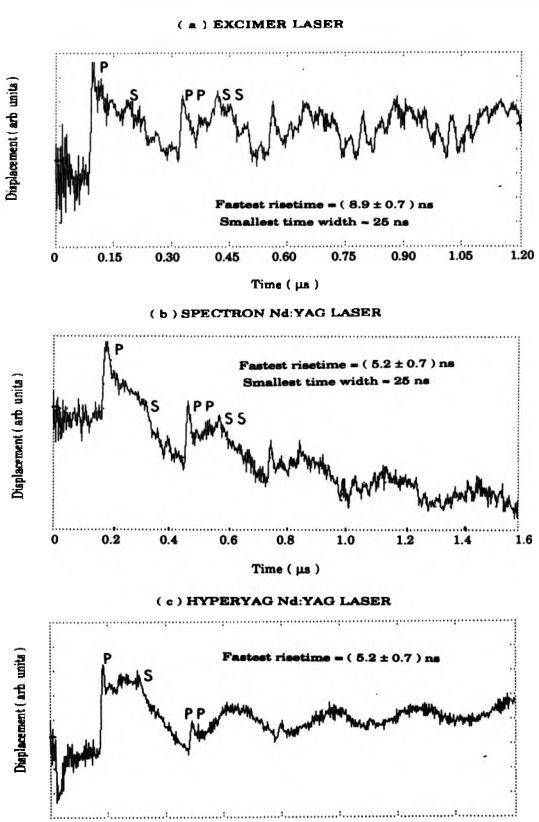

Figure 3. 20 : Ultrasonic epicentral displacement waveforms recorded on mild steel for various incident laser pulses

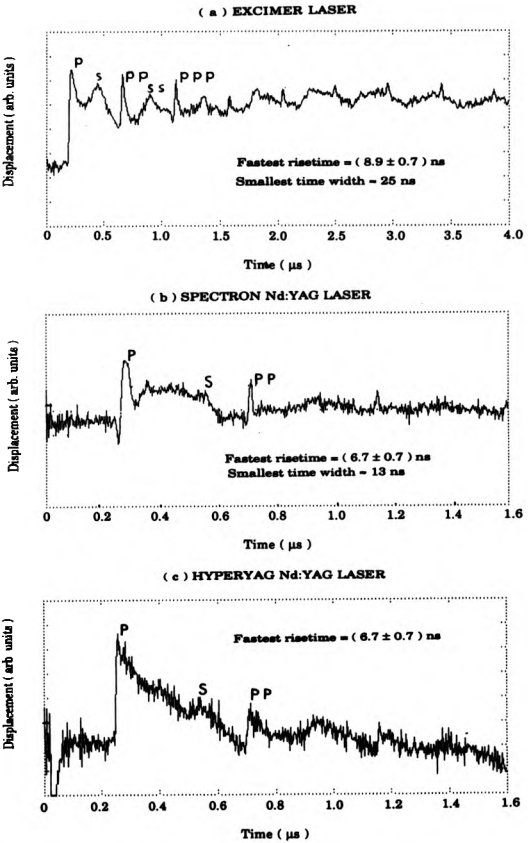

Figure 3. 21 : Ultrasonic epicentral displacement waveforms recorded on copper for various incident laser pulses

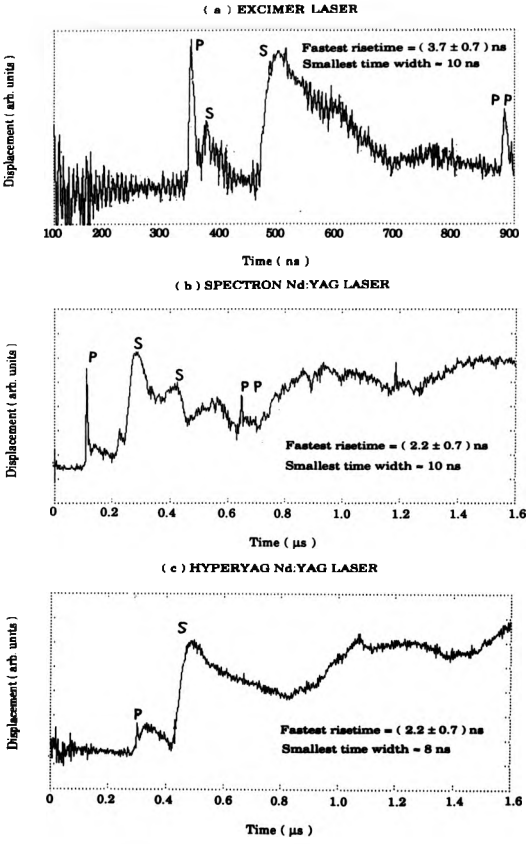

Figure 3. 22 : Ultrasonic epicentral displacement waveforms recorded on silicon for various incident laser pulses

extent silicon, have the typical profile of ultrasound generated by a plasma regime source of ultrasound.

It was also intended to use this interferometer to detect the ultrasound generated by the picosecond laser. However the picosecond laser - generated ultrasonic displacements on the opposite face of 1 mm thick samples were ~ 30 pm when detected using the 72 MHz bandwidth interferometer. This was beyond the detection resolution of the 430 MHz bandwidth interferometer when used in a single shot capture mode. The interferometer has an inherent noise level of ~ 100 mVpp and no ultrasonic signal is output if its amplifier output voltage is below 100 mVpp. Once its amplitude is above the noise level then large amplification occurs and the signal - to - noise level ratio becomes large (~ 20). Subsequent measurements have indicated that the displacement resolution of this interferometer is ~ 500 pm at full bandwidth. Signal averaging tended to increase the risetime of the ultrasonic pulse as the 10 Hz repetition rate of the picosecond laser resulted in pitting of the sample surface producing a progressively decreasing source to detector distance. This effect was much reduced when the other lasers were used as they could be operated in single shot mode.

3. 3. 4 : Ultrasound detected using the 72 MHz bandwidth interferometer

In addition to recording the ultrasonic epicentral displacements generated by the Excimer and Nd:YAG lasers, this interferometer was able to detect the corresponding displacements generated in various solids by the picosecond laser pulse. The investigations conducted using the picosecond laser have been described elsewhere (Davies et al. (1990)). The ultrasonic epicentral displacements generated by each

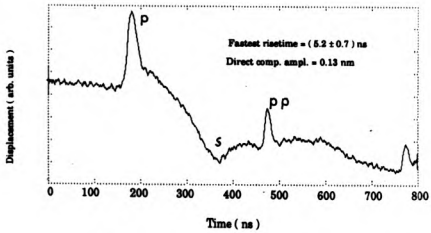

Figure 3. 23a: Ultrasonic epicentral displacement waveforms recorded on aluminium for picosecond laser pulse

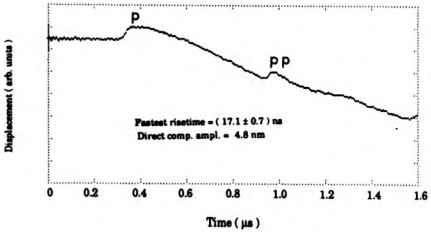

Figure 3. 23b : Ultrasonic epicentral displacement waveforms recorded on aluminium for Excimer laser pulse

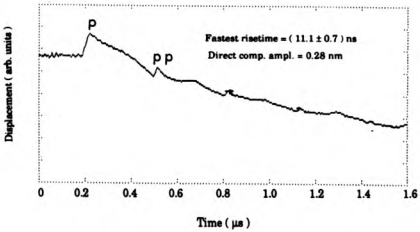

Figure 3. 23c : Ultrasonic epicentral displacement waveforms recorded on aluminium for Spectron Nd:YAG laser pulse

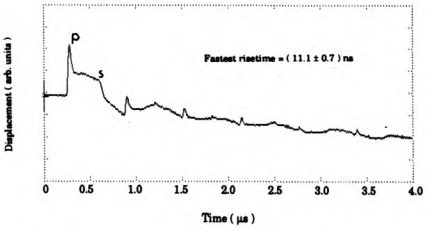

Figure 3. 23d : Ultrasonic epicentral displacement waveforms recorded on aluminium for HyperYag Nd:YAG laser pulse

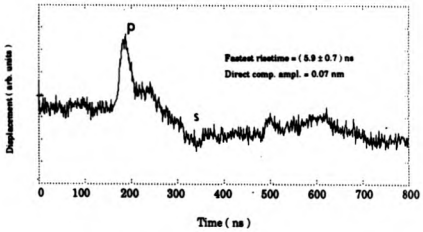

Figure 3. 24a : Ultrasonic epicentral displacement waveform recorded on mild steel for incident picosecond laser pulse

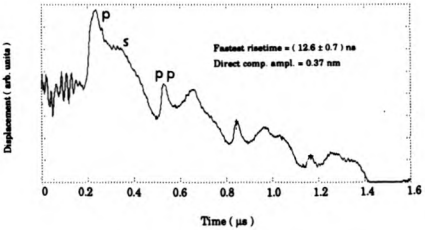

Figure 3. 24c : Ultrasonic epicentral displacement waveform recorded on mild steel for incident Spectron Nd:YAG laser pulse

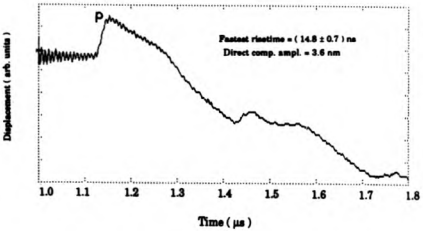

Figure 3. 24b : Ultrasonic epicentral displacement waveform recorded on mild steel for incident Excimer laser pulse

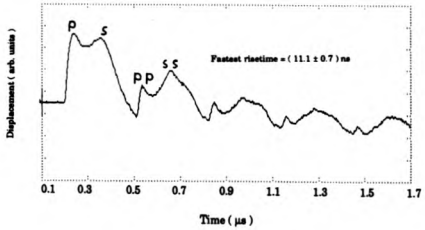

Figure 3. 24d : Ultrasonic epicentral displacement waveform recorded on mild steel for incident HyperYag Nd:YAG laser pulse

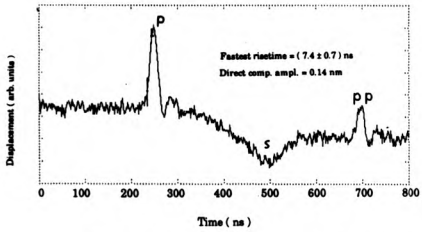

Figure 3. 25a : Ultrasonic epicentral displacement waveform recorded on copper for incident picosecond laser pulse

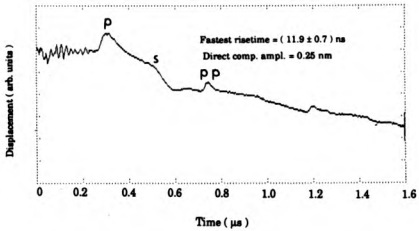

Figure 3. 25c : Ultrasonic epicentral displacement waveform recorded on copper for incident Spectron Nd:YAG laser pulse

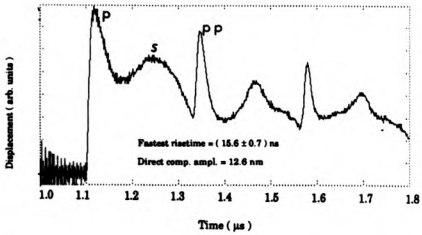

Figure 3. 25b : Ultrasonic epicentral displacement waveform recorded on copper for incident Excimer laser pulse

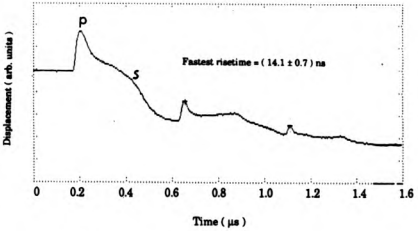

Figure 3. 25d : Ultrasonic epicentral displacement waveform recorded on copper for incident Nd:YAG laser pulse

laser used and detected using the 72 MHz bandwidth interferometer are shown in Figs. 3. 23 - 3. 25 for aluminium, mild steel and copper only.

3. 3. 5 : Discussion

The properties of the compression wave (e. g. the risetime, amplitude and time width) generated in the various solids by the different laser pulses are discussed with relevance to the theoretical modelling described previously.

The fastest risetimes recorded on the different solids by the 430 MHz and 72 MHz bandwidth interferometers are summarised in Tables 3. 4 and 3. 5 respectively. The risetimes of the ultrasonic compression wave pulses exhibited significant variation on different solids for the various incident laser pulses used in this investigation. Indicating that the properties of the irradiated solid also affects the profile of the ultrasonic compression wave pulse. The fastest recorded risetimes were ~ 2 ns for silicon and ~ 3.7 ns for aluminium and mild steel detected using the 430 MHz bandwidth interferometer. These risetimes are less than the risetime of the incident laser pulses and is not unexpected as the power density, I, sufficient to cause vapourisation is obtained immediately upon the onset of the laser pulse. It then takes, from Table 3. 2, ~ 10^{-11} s (~ 10^{-10} s for silicon) for the irradiated solid to reach its vapourisation temperature and hence for the ablation of material to commence. This time is very much less than the risetime of the Excimer and Nd:YAG lasers. The picosecond laser pulse transferred a proportion of its energy to the solid in approximately 0.3 ps which is on a similar time scale to the relaxation times of photon absorption by conduction electrons. It is thus possible for electrons to be

Material	Fastest recorded risetimes for the various lasers used (in ns)		
	Excimer laser	Spectron Nd : YAG laser	HyperYag Nd : YAG laser
	(Pulse risetime = (4.5 ± 0.7) ns)	(Pulse risetime = (5.2 ± 0.7) ns)	(Pulse risetime = (6.2 ± 0.7) ns)
	Error = ± 0. 7 ns	Error = ± 0. 7 ns	Error = ± 0. 7 ns
Aluminium	3.7	4.5	3.7
Mild Steel	3.9	5.2	5.2
Soft solder	8.2	-	4.5
Stainless Steel	9.6	8.2	5 9
Copper	8.9	6.7	6 7
Brass	9.6	6.7	8.9
Silicon	3.7	2.2	2.2

Table 3. 4 : Summary of the fastest risetimes recorded on various solids using the lasers listed to generate and the 430 MHz bandwidth Interferometer to detect the ultrasound.

Material	Fastest recorded risetimes for the various lasers used (in ns)			
	Picosecond laser (Pulse risetime ~ 0.1 ps) Error = ± 0.7 ns	Excimer laser (Pulse risetime = (4.5 ± 0.7) ns) Error = ± 0. 7 ns	Spectron Nd : YAG laser (Pulse risetime = (5.2 ± 0.7) ns) Error = ± 0. 7 ns	HyperYag Nd:YAG laser (Pulse risetime = (6.2 ± 0.7) ns) Error = ± 0. 7 ns
Aluminium	5.2	17.1	11.1	11.1
Mild Steel	5.9	14.8	12.6	11.1
Soft solder	-	21.5	-	21.5
Stainless Steel	8.2	11.1	10.4	11.9
Copper	7.4	15.6	11.9	14.1
Brass	10.4	17.1	17.1	14.1
Silicon	11.1	6.7	11.1	11.1

Table 3. 5 : Summary of the fastest risetimes recorded on various solids using the lasers listed to generate and the 72 MHz bandwidth Interferometer to detect the ultrasound.

ejected from the surface by the photoelectric effect (Tipler (1983)) in addition to the thermal processes described.

The fastest risetime detected using the 72 MHz bandwidth interferometer was ~ 5 ns for aluminium and mild steel which is on the limits of the risetime detectability for this interferometer. Ultrasonic compression wave risetimes recorded on the other solids were typically ~ (6 ± 1) ns when detected by the 430 MHz bandwidth interferometer and ~ (10 ± 1) ns when detected by the 72 MHz bandwidth interferometer.

The difference between the recorded risetimes for the same laser / solid but different detector is accounted for by the respective bandwidths of the two interferometers, assuming that the error owing to the finite size of the detecting He - Ne beam is the same for both interferometers. Combining equations (3. 44) and (3. 45), the output risetime for a particular arrangement is given by

$$t_{out} = \sqrt{t_r^2 + t_{sens}^2 + t_{elec}^2} \qquad (3.47)$$

Assuming, for a particular solid and laser, that t_r and t_{sens} remain constant and only t_{elec} is different, corresponding to the different bandwidths of the two interferometers, results in a recorded output pulse risetime difference, t_{out} (diff), given by

$$t_{out}(\text{diff}) = \sqrt{t_{elec}^2(72\text{MHz}) - t_{elec}^2(430\text{MHz})} \qquad (3.48)$$

where t_{elec}(72 MHz / 430 MHz) is the risetime associated with the electronic circuitry of the 72 MHz / 430 MHz bandwidth interferometer.

Thus the recorded output pulse risetime difference for data recorded using the 72 MHz and 430 MHz bandwidth interferometers is

~ (4.4 ± 0.8) ns. In practice the risetime associated with the active sensing region of the interferometer will differ owing to the different He - Ne lasers used in each interferometer.

Comparison of the risetimes detected using each interferometer for a particular laser (Tables 3. 4 and 3. 5) indicates that generally the difference is of the order of (4.4 ± 0.8) ns. The difference in the risetime of the ultrasound generated by the Excimer laser is significantly larger than (4.4 ± 0.8) ns particularly for the aluminium, mild steel and soft solder samples. The profile of the recorded ultrasonic displacements (Fig. 3. 19a and 3. 23b (aluminium), 3. 20a and 3. 24b (mild steel)) indicates that a slightly different source was used. Further examination of the source characteristics when the 72 MHz bandwidth interferometer was used has shown that the source was slightly larger than the source used for the ultrasound detected with the 430 MHz bandwidth interferometer.

Ultrasonic displacements detected in the silicon sample exhibited features which were not found in the metallic samples. The waveforms illustrate an initial compressive pulse with a recorded risetime of ~ 2 ns for the incident Nd:YAG lasers. Other ultrasonic arrivals are observed between the direct compression pulse and the backwall reflected compression arrival. The signal corresponding to the shear wave arrival (~ 0.3 μs in Fig. 3. 22) is characterised by a unipolar pulse with a risetime ~ 15 ns. Laser - generated ultrasound in silicon has also been described by Harada et al. (1989).

The relatively low optical absorption coefficient for silicon at the Nd:YAG wavelength results in a weak cylindrically shaped ultrasonic source. Such a source has been investigated for laser light absorption by liquids (Berthelot (1989)) and for CO_2 laser light absorption by plastics (Taylor (1990)). Such an acoustic source tends to produce compression

waves whose maximum amplitude emanates from the sides of the source with the epicentral compression wave amplitude smaller. The fast (~ 2 ns) risetime compression waves produced by the Nd:YAG laser is a result of the non - linear absorption of the incident laser energy. Non - linear absorption occurs once a certain intensity is reached and effectively results in an incident energy pulse with reduced risetime. In the initial stages of the onset of the laser pulse, absorption similar to absorption in the metallic samples occurs. At a certain laser intensity the non - linear absorption threshold is reached resulting in a much increased absorption of the remainder of the laser energy. The laser intensity reaches its peak and decreases to the non - linear absorption threshold. Further absorption of the laser energy is then significantly reduced. In effect the silicon has acted as a filter reducing the incident laser pulse profile to a much reduced risetime generating pulse which, in turn, produces a much reduced ultrasonic compression wave pulse risetime.

An interesting shear wave profile is also observed in this silicon sample. Musgrave (1970) has considered the propagation of ultrasound in crystals with various symmetries. Crystals with cubic symmetry, such as silicon, exhibit cusp points in the shear wave surfaces offering the possibility of observing two or more shear wave arrivals for ultrasound propagated in a particular direction. The existence of two shear wave arrivals is illustrated in Figs. 3. 22 b and c especially. Unfortunately the orientation of the crystal axes of this particular silicon sample was unknown. Accurate measurement of the shear wave velocities as a function of angle would enable a determination of the orientation of the crystal to be made.

The amplitude of the ultrasonic displacements were calculated using the data recorded with the 72 MHz bandwidth interferometer and

equation (3. 43). Thus the variation in the surface displacement as a function of laser wavelength and the irradiated solid could be determined. To make a comparison between the lasers used in this investigation, the ultrasonic displacement per incident mJ of laser energy was calculated for each laser and solid used. These data are given in Table 3. 6.

Aindow et al. (1980) proposed that, as the absorption of laser energy increased with decreasing wavelength, the ultrasonic amplitude would also increase with decreasing wavelength. Their investigations, conducted using CO_2, Nd:YAG and KrF Excimer lasers, confirmed this prediction. Consideration of the ultrasonic displacement per mJ values in Table 3. 6 for the Excimer and Spectron Nd:YAG lasers illustrates that the ultrasonic displacement increases with decreasing wavelength. A dichotomy arises when the picosecond laser is also considered. Although the picosecond wavelength implies that the amplitude of the ultrasonic displacement per mJ of incident energy should lie between the values given in the other two columns for a particular solid, consideration must be given to its time width. The Excimer and Spectron Nd:YAG laser pulse profiles have time widths of 17 ns and 14 ns respectively whilst the time width of the picosecond laser pulse is 0.3 ps. As mentioned previously, absorption of the picosecond laser energy also occurs through the photoelectric effect. Thus there is an increased proportion of absorbed energy relative to the other laser pulses and this would result in the larger ultrasonic displacement per mJ values. No laser with a wavelength ~ 600 nm and time width ~ 15 ns was available to confirm this postulate.

The pressure developed as a result of vapourisation on mild steel was predicted to be an order of magnitude greater than for aluminium (section 3. 2. 4). This would result in larger amplitude ultrasound

Material	Ultrasonic displacement per mJ for the lasers used (in nm / mJ)		
	Excimer laser	Picosecond laser	Spectron Nd:YAG laser
	Energy / pulse = 36 mJ	Energy / pulse = 0.2 mJ	Energy / pulse = 100 mJ
	(λ = 308 nm)	(λ = 600 nm)	(λ = 1060 nm)
Aluminium	0.13 ± 0.02	0.65 ± 0.03	0.003 ± 10 %
Mild Steel	0.10 ± 0.02	0.35 ± 0.03	0.004 ± 10 %
Stainless Steel	0.14 ± 0.02	0.35 ± 0.03	0.004 ± 10 %
Copper	0.35 ± 0.03	0.70 ± 0.04	0.003 ± 10 %
Brass	0.20 ± 0.02	0.65 ± 0.03	0.010 ± 10 %

Table 3. 6 : Values of the ultrasonic displacement produced per incident mJ of energy of the lasers used in this investigation to illustrate the effect of the laser wavelength upon the amplitude of the ultrasound produced.

propagating within mild steel when compared to ultrasound propagating within aluminium. Table 3. 6, neglecting the values for the picosecond laser, indicates that the amplitude of the ultrasound is of the same order of magnitude within both solids. A major factor in the comparability of the displacements within aluminium and mild steel is the magnitude of the attenuation. Typical values for the attenuation at 10 MHz are (Kaye and Laby (1989)) 0.4 Np / m for aluminium and ~ 5 Np / m for mild steel (1 Np / m = 0.12 dB / m). Attenuation is strongly dependent on frequency and can vary as high as (frequency)^4 which is the Rayleigh scattering regime. Thus attenuation in mild steel is at least a factor of ten more than in aluminium and this accounts for the compatibility of the displacements for the two metals.

The width of the ultrasonic compression wave pulse in the solids investigated was also determined from the data recorded using the 430 MHz bandwidth interferometer. Typical time widths for compression wave signals detected in aluminium were ~ 10 ns and for mild steel ~ 25 ns. This represented the approximate range of the time widths recorded. The difference in the time widths for aluminium and mild steel is in agreement with the theoretical prediction of section 3. 2. 4 which suggested that the resulting ultrasonic pulse produced in aluminium would have a smaller time width than an ultrasonic pulse in mild steel.

3. 4 : CONCLUSIONS

The pressure developed upon a solid surface when irradiated with a laser of sufficient power density to eventually cause vapourisation

has been derived. The pressure profile consisted of two contributions corresponding to the vapourisation of ions and electrons from the solid and the effect of the subsequent plasma. The pressure profile has a relatively large amplitude spike with a risetime of ~ 10^{-11} s and a fall time which depends upon the magnitude of the mechanical and thermal properties of the irradiated solid. The pressure developed as a result of vapourisation lasts for approximately twice the duration of the laser pulse. After this time the pressure owing to the formation of the plasma becomes dominant and lasts for 0.3 μs for the plasma above aluminium and 0.9 μs for the plasma above mild steel.

To generate broadband ultrasound the pressure profile is required to approach a δ - function form. Qualitative analysis of the pressure developed as a result of vapourisation implies that such a pressure profile will be developed if the solid has a relatively large thermal conductivity with the remaining relevant mechanical and thermal properties relatively low. For the plasma to decay rapidly a large vapourisation temperature is required. The incident laser pulse is required to have a power density sufficient to eventually cause vapourisation which is $\geq 10^7$ W / cm^2. Therefore both the properties of the incident laser pulse and the irradiated solid affect the properties of the ultrasound generated in the plasma regime. This prediction was verified from the data obtained in the experimental investigations which showed a significant variation in the risetimes of the ultrasonic compression wave pulse for different solids.

3.5 : REFERENCES

Aindow, A. M. (1986) PhD Thesis, University of Hull (1986)

Aindow, A. M. et al. (1980) SPIE, **236**, 478 (1980)

Aussel, J. D. et al. (1988) Ultrasonics, **26**, 245 (1988)

Berthelot, Y. H. (1989) J. A. S. A., **85**, 1173 (1989)

Bleaney, B. I. and B. (1978) ' Electricity and Magnetism ', 3rd Ed., (OUP) (1978)

Bourkoff, E. and Palmer, C. H. (1985) Appl. Phys. Lett., **46**, 143 (1985)

Cooper, J. A. (1985) PhD Thesis, University of Hull (1985)

Dabby, F. W. and Paek, U. C. (1972) IEEE QE - **8**, 106 (1972)

Davies, S. J. et al. (1990) Report submitted to Laser Support Facility, Rutherford - Appleton Laboratories (1990)

Dewhurst, R. J. et al. (1982) J. Appl. Phys., **53**, 4064 (1982)

Dewhurst, R. J. and Al' Rubai, W. S. (1989) Ultrasonics, **27**, 262 (1989)

Fairand, B. P. and Clauer, A. H. (1979) J. Appl. Phys., **50**, 1497 (1979)

Fassbender, S. et al. (1989) Mat. Sci. Eng., **A122**, 37 (1989)

Harada, Y. et al. (1989) — J. Phys. D : Appl. Phys., **22**, 569 (1989)

Hughes, T. P. (1975) — ' Plasmas and Laser Light ', (Adam Hilger) (1975)

Jones, E. D. (1971) — Appl. Phys. Lett., **18**, 33 (1971)

Kaye, G. W. C. and Laby, T. H. (1989) — ' Tables of Physical and Chemical Constants ', 15th Ed., (1989)

Krehl, P. et al. (1975) — J. Appl. Phys., **46**, 4400 (1975)

McKie, A. D. W. (1987) — PhD Thesis, University of Hull (1987)

Musgrave, M. J. P. (1970) — ' Crystals Acoustics ', (Holden - Day) (1970)

Peercy, P. S. et al. (1970) — Appl. Phys. Lett., **16**, 120 (1970)

Ready, J. F. (1963) — Appl. Phys. Lett., **3**, 11 (1965)

Ready, J. F. (1971)	' Effects of High Power Laser Radiation ', (Academic Press) (1971)
Reif, F. (1981)	' Fundamentals of Statistical and Thermal Physics ', (McGraw - Hill) (1981)
Sullivan, B. and Tam, A. C. (1984)	J. A. S. A., **75**, 437 (1984)
Tam, A. C. (1984)	Appl. Phys. Lett., **45**, 510 (1984)
Tam, A. C. and Coufal, H. (1983)	Appl. Phys. Lett., **42**, 33 (1983)
Taylor, G. S. (1990)	PhD Thesis, University of Warwick (1990)
Tipler, P. A. (1983)	' Modern Physics ', 6th print (Worth) (1983)

Chapter Four

PHASE CHARACTERISTICS OF BULK DEFECTS

4. 1 : INTRODUCTION

This chapter outlines the investigations into the characterisation of defects using the phase information contained within an ultrasonic pulse scattered from a defect. Ultrasonic data were recorded with the source and detector in the Time - of - Flight Diffraction arrangement. The properties of the laser ultrasonic source were used in this investigation, in particular the wide bandwidth nature of the laser - generated ultrasound. The advantages in using laser - generated ultrasound and interferometric detection over conventional piezoelectric probes have been highlighted in Chapter Two. The methods of operation and the advantages and disadvantages in using piezoelectric probes can be found elsewhere (Krautkramer (1977), Sharpe et al. (1984) and Silk et al. (1987)).

A brief description of the Time - of - Flight Diffraction technique is given along with the advantages in using remote generation and detection. The associated mathematical modelling of the interaction of ultrasound with embedded defects is also described. Experimental investigations into the phase behaviour of the scattered ultrasound were conducted and used to verify some of the results of this modelling.

4. 2 : THE TIME - OF - FLIGHT DIFFRACTION TECHNIQUE

The basic arrangement for the Time - of - Flight Diffraction (TOFD) defect detection technique, developed at the National Non - Destructive Testing centre, Harwell, under the guidance of Dr. M. G. Silk, is illustrated in Fig. 4. 1. The technique will soon become a British Standard (BS DD : 174 (1988)) for the non - destructive testing of materials. Other ultrasonic non - destructive testing techniques, which may be used with any type of ultrasonic transducer in a variety of configurations, are illustrated in Fig. 4. 2.

The tips of defects such as cracks provide the sources for the diffracted signals. By timing their arrival at the detector and knowing the geometry of the source and detector configuration, the depths of the tips can be calculated. The technique is useful in that it can both search for and size defects after one scan.

The main advantage of this technique over other ultrasonic techniques such as pulse - echo detection, is that the technique does not rely on the amplitude of the received signal to size the defect. The amplitude of the diffracted signal is required to be above the noise level (achieved in practice by suitable averaging) so that accurate timing measurements can be made. The amplitude of the ultrasound propagating within a material is affected by several factors other than the scattering from a defect. These include variations in the coupling medium between a piezoelectric probe and the sample surface (this affect is negated if a laser pulse is used to generate ultrasound), beam skewing, attenuation, wave interference and grain boundary scattering. The orientation of the defect also affects the returned signal amplitude

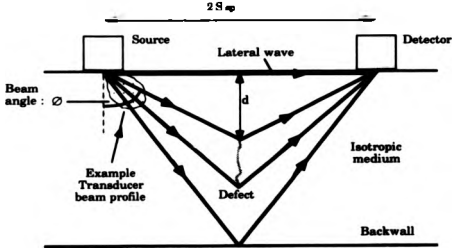

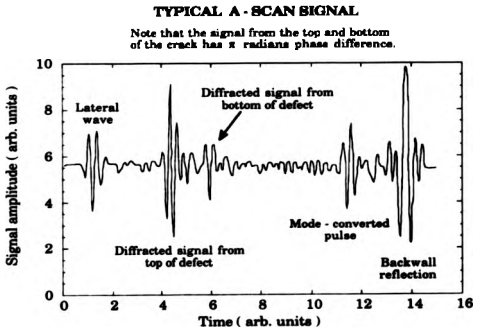

Figure 4. 1 : Probe arrangement and typical A - scan signal for the Time - of - Flight Diffraction Technique.

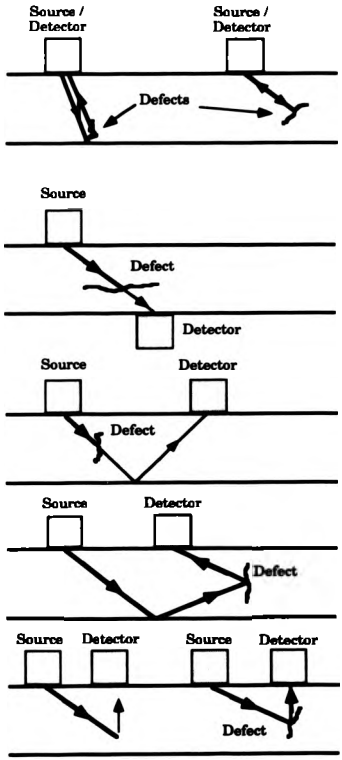

Figure 4. 2 : Common inspection geometries for the ultrasonic testing of materials (after Silk et al. (1987)).

and its effect on the TOFD signal has been discussed by Toft (1986) and Charlesworth and Temple (1989).

Using the probe arrangement shown in Fig. 4. 1, the transit time, t (in μs), from a crack tip at a depth d (in mm) below the surface is given by (ignoring any time delay which occurs if piezoelectric probes are used)

$$t = \frac{2\sqrt{S_{ep}^2 + d^2}}{c} \qquad (\mu s) \qquad (4.1)$$

where S_{ep} is half the source to detector distance (in mm),

d is the depth of the defect (in mm),

and c is the ultrasonic wave velocity within the material (in mm / μs).

Rearranging (4. 1) gives the depth, d, of the defect as

$$d = \sqrt{(\frac{ct}{2})^2 - S_{ep}^2} \qquad (mm) \qquad (4.2)$$

It is possible to determine the velocity of the ultrasonic wave mode used knowing the lateral and backwall wave transit times (Carter (1984)).

The source and detector may be scanned over the sample surface in either a **Parallel** scan, where the line joining the source and detector is parallel to the direction of the scan, or a **Transverse** scan, where the line joining the source and detector is perpendicular to the direction of the scan. Highmore and Rogerson (1987) have reported on a variation of these scans wherein they twisted the piezoelectric probes with respect to the scanning direction and, in another scan, they increased the source to detector distance about a central point.

The TOFD studies conducted so far have used angled piezoelectric transducers to generate and detect the ultrasound. The angle of beam entry into the material was chosen to be 60° from the normal of the sample surface in most cases. This proved to be near to the optimum angle necessary for defect detection when the theory was fully developed. By choosing an appropriate source to detector separation and considering the beam spread of each transducer, different regions of the material under test could be scanned. By using more transducers with different source to detector distances it is possible to probe all of the material in one scan (Curtis and Hawker (1983), Temple (1983)). This, however, introduces further data processing and interpretation can be difficult. The normal practice is to focus the ultrasound to a depth at which a defect is likely to occur and to scan, at a fixed separation, over the sample surface. If data are to be collected over a three - dimensional half - space then four or more transducers in a two - dimensional array may be used (Temple (1983), Mak (1989a)).

An immediate advantage in using laser - generated ultrasound for TOFD studies is the potential resolution of the tips of a defect or of defects which are close together. The wavelength range in aluminium is typically ~ 6 mm to ~ 0.3 mm whilst a piezoelectric probe has a typical wavelength in aluminium of 1.2 mm (G5KB piezoelectric probe). The higher frequency (lower wavelength) components and narrow temporal width of laser - generated ultrasound has the potential to sense smaller scale changes within the material in which it propagates, compared to the relatively large wavelength of ultrasound generated by a piezoelectric transducer.

Another advantage is the ability of the laser source and interferometric detector to scan, using appropriate optics, the surface of

the material under test rapidly without contact. Using a high (≥ 100 Hz) repetition rate laser as generator it would be possible to take a large number of averages at a particular location, thus increasing the signal - to - noise ratio.

4. 3 : SOURCES OF ERROR IN TOFD MEASUREMENTS

The possible sources of error in TOFD timing measurements, which are eliminated or reduced when remote laser generation and detection is used, are listed below. Further details are given by Lidington et al. (1976) and Charlesworth and Temple (1989).

Changes in the couplant thickness,
Refraction at the sample surface,
Errors due to the finite size of the source and detector,
Errors in the measurement of source to detector distance.

Other sources of error in TOFD timing measurements which are independent of the type of ultrasonic transducer used are described in more detail below.

4. 3. 1 : Lateral error

If a defect tip is considered to be a point scatterer and the source and detector to be omnidirectional within the material, then its location can be anywhere on an ellipse of constant travel time with the source

and detector as focal points. This can introduce a lateral error to the location of the defect if it is assumed to be midway between the source and detector as shown in Fig. 4. 3a. This problem is overcome if another source or detector is used or if the source and detector are scanned over the sample surface.

Using another source or detector results in two ellipsi, the intersection of which indicates the location of the scatterer. Use of more transducers results in further intersections which achieves greater accuracy in locating the scatterer. An example is shown in Fig. 4. 3b which is one of the defects within the plates from the Defect Detection Trials (Hawker (1983), Curtis and Hawker (1983)).

If a source and detector, at a fixed separation, is scanned over a surface then the point scatterer will produce a hyperbola when the A - scan signals are viewed as a function of distance and time. The apex of the hyperbola indicates the position when the point scatterer is midway between the source and detector.

4. 3. 2 : Error in sizing near surface defects

The accuracy in determining the defect depth, d, is also determined by the depth of the defect in connection with the angle of incidence of the ultrasound upon the defect. Differentiating (4. 2) with respect to t gives

$$\Delta d = \frac{c}{2d}\sqrt{d^2+S_{sp}^2}\,\Delta t \qquad (4.3)$$

which, using

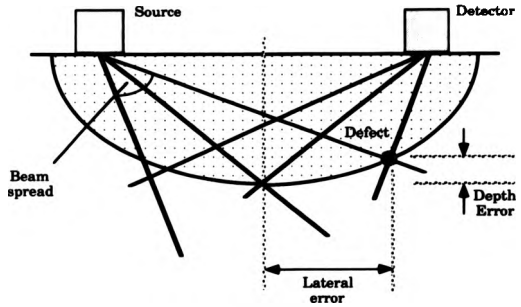

Figure 4. 3a : Explaination of the lateral error, defect tip at a constant transit time may be located on any point of the ellipse

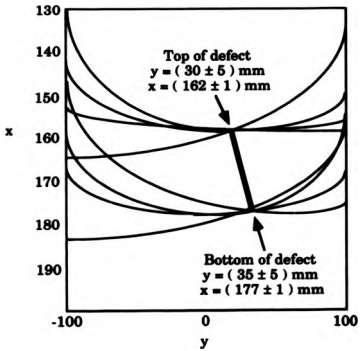

Figure 4. 3b : Ellipsi from several combinations of source and detector combined to collectively locate the top and bottom of a defect (after Hawker (1983))

$$\cos\varnothing = \frac{d}{\sqrt{d^2+S_{sp}^2}} \qquad (4.4)$$

becomes

$$\Delta d = \frac{c}{2\cos\varnothing}\Delta t \qquad (4.5)$$

Using a digitiser with a sampling interval of 10 ns and a source to detector distance of 30 mm, the error in the depth as a function of the defect depth and the beam angle can be calculated, using (4. 3) and (4. 5), and this is shown in Fig. 4. 4. This shows that the best resolution is obtained for defect depths of $\geq$ 15 mm and for beam angles of $\geq$ 65°. In a later section, the amplitude of the diffracted ultrasound as a function of angle around a defect tip is illustrated. Fig. 4. 4 and the results from this section are used to determine the optimum angles for the detection of defects.

The other problem encountered in sizing near surface defects, using piezoelectric probes, results from the diffracted wave signals overlapping those of the lateral wave which has a lower frequency. Silk (1979) concluded that these lower frequency components were contributions from low frequency enhancement in directions away from the piezoelectric probe beam centre line and, to a lesser extent, from grain boundary scatter. The lateral wave typically lasts for ~ 1 μs which corresponds to a depth of ~ 6 mm in aluminium. Thus any diffracted signal from a defect will be lost in the higher amplitude, lower frequency lateral wave.

A similar problem occurs when a laser is used to generate ultrasound. As stated in Chapter Two, a laser source produces simultaneously compressional, shear and Rayleigh (surface) waves on

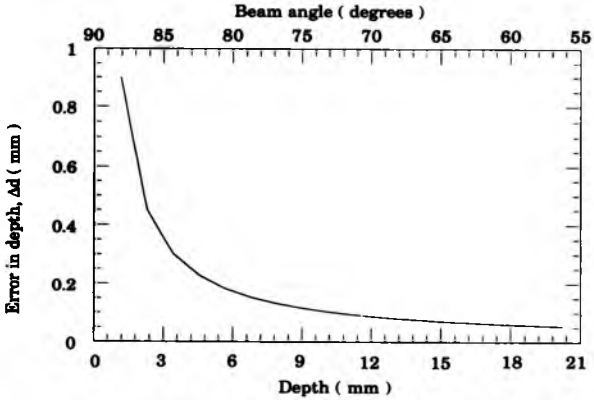

Figure 4. 4 : Error in defect depth as a function of the defect depth and the beam angle.

thick samples. The Rayleigh waves, which have a much larger amplitude than the bulk waves and are very much larger than the bulk waves scattered from defects, penetrate to a depth ~ 5 mm. Any compression or shear wave diffracted from a defect in this near surface region may be obscured if its arrival time corresponds to the arrival time of the Rayleigh wave. In association with its large amplitude, the Rayleigh wave time width, which is a function of the source and detector size, is long compared to the time width of the diffracted compression wave signal. For a 1 mm diameter source and detector the time width of the Rayleigh wave would be ~ 700 ns. Typical time widths of laser - generated compression wave pulses are ~ 20 ns (from Chapter Three) which corresponds to a travel distance of ~ 0.1 mm in aluminium. A near surface defect would be expected to alter the shape of the Rayleigh wave (Aindow et al. (1984)) but for the purpose of this investigation this effect is ignored.

The source to detector separation must be chosen so that the Rayleigh wave arrives either much before or much after the expected arrival time of the diffracted compression or shear wave pulse. It must also satisfy the requirement of sufficient resolution (Fig. 4. 4). Consider the TOFD arrangement (Fig. 4. 1) with a laser source and interferometer detector. In Fig. 4. 5 are graphs of the travel time of the Rayleigh wave and of the diffracted compression wave pulse in aluminium and the difference in the travel time as a function of source to detector distance for a defect at a depth of 3 mm. The signals from the two wave modes will become separated when the time difference between the two paths is $\geq$ 700 ns. Referring to Fig. 4. 5b this occurs for source to detector distances of $<$ 2 mm and $>$ 25 mm in aluminium. Using equation (4. 4) implies beam angles, $\varnothing$, of $\leq 18°$ and $> 76.5°$. From Fig. 4. 4 the error in the depth increases with increasing angle of

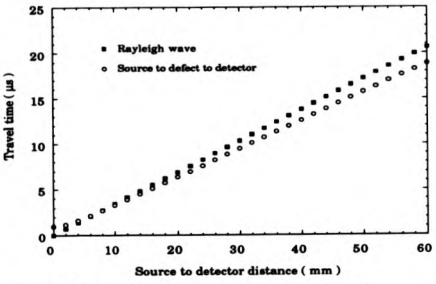

Figure 4. 5a : Travel times of the direct Rayleigh wave and the compression wave diffracted from a defect 3 mm below the surface.

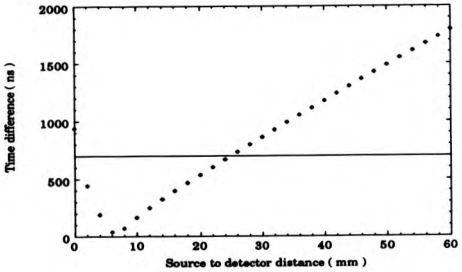

Figure 4. 5b : The difference in the travel times for the direct Rayleigh wave and the diffracted compression wave

incidence. The error in the depth for $\varnothing \leq 18°$ is ≤ 0.05 mm whilst for $\varnothing > 76.5°$ it is ≥ 0.15 mm. Clearly the smaller beam angle will result in potentially better resolution. However, the directivity of the diffracted amplitude around the crack tip must also be taken into account and this will be discussed in section 4. 6.

4. 3. 3 : Errors due to surface irregularities

Consider a local rise in the surface height of the sample under test. The ensuing error in timing due to this change in path length can be determined (Lidington et al. (1976)). Typically this gives an error of 70 ns / mm or an error of 0.8 mm in crack depth measurement for a 1 mm variation in surface height. This implies that it is not possible to locate the crack extremities to an accuracy better than the surface finish of the material under test regardless of the technique or source and detector used.

4. 4 : EXPERIMENTAL STUDIES AND ACCURACY OBTAINABLE USING PIEZOELECTRIC PROBES IN THE TOFD ARRANGEMENT

Various groups have conducted studies on defective samples using the TOFD technique. Naturally most of the investigations were conducted by the National Non - Destructive Testing Centre at Harwell. The technique was firmly established as an accurate sizing technique after its success in locating and sizing defects in the round robin PISC

and Defect Detection Trials (Nichols and Crutzen (1986), Curtis and Hawker (1983)). The various errors associated with the TOFD technique culminate in an accuracy of better than 0.5 mm (~ 0.2 λ) when sizing fatigue cracks at ≥ 10 mm depths in steel using compression waves (Lidington et al. (1976), Carter (1984)). This accuracy decreases for defects near to the scanning surface and also depends on the surface roughness. Curtis and Hawker (1983) reporting on Defect Detection Trial Plates One and Two obtained an accuracy on the defect through - thickness size of ± 1.5 mm for defects of length ≥ 2 mm.

Mackiewicz et al. (1986) used the TOFD technique to size artificial slits in steel at depths ranging from 0.5 mm to 10 mm. Good agreement was obtained between the measured and calculated slit depth for slits > 1.5 mm deep. The authors concluded that the error in the measurement of crack sizes ranging from 2 mm to ~ 40 mm was ± 0.15 mm.

Paradis et al. (1986a) used focussed ultrasonic probes, which produced plane wave fronts in the vicinity of their focus, in a TOFD arrangement. The travel time of the signal diffracted by the edge of a cracklike defect varied linearly with the position of the transducer in the incidence plane. The error on depth measurement and sizing was ± 0.5 mm for crack lengths of 3.5 mm to 7.5 mm.

Murgatroyd et al. (1988) reported on a series of defect detection trials using the TOFD technique on samples with deep and near surface defects. They accurately located and sized the deep defects (> 10 mm from the surface) but were less successful with the near surface defects. These trials highlighted the disadvantage of the TOFD technique using piezoelectric probes to locate and size near surface defects and indicated that more research into this particular problem was necessary.

Other articles on the general properties of the TOFD technique which includes discussions on the various methods of data presentation (e. g. B -, C - scan) and signal processing (e. g. Synthetic Aperture Focussing Technique) can be found elsewhere (Slessenger and Hesketh (1985), Charlesworth and Temple (1989), Lilley (1989) and DeVadder et al. (1989)). Mak (1989b) used error analysis to determine the accuracy in locating a point scatterer using the TOFD technique. It was concluded that the errors in the location of a point scatterer could be calculated from uncertainties in the measurement of transit time, velocity and the location of the transducer scan positions. The maximum through thickness error was about 0.2 mm whilst the lateral error was much larger.

A current application for the TOFD technique is in the monitoring of defect size to aid in the prediction of the lifetime of a particular component (Terpstra et al. (1989), Silk et al. (1989)). Regular monitoring of defect size provides a check on the defect stability. Silk et al. (1989) presented a method for obtaining the error in flaw growth from TOFD data and obtained precisions of 0.25 mm or better.

4. 5 : THEORETICAL MODELLING OF THE INTERACTION OF ULTRASOUND WITH EMBEDDED DEFECTS

The theoretical modelling of the interaction of ultrasound with various types of embedded defects is undertaken by numerous research groups. The various methods used have been reviewed recently (Thompson and Wadley (1989)). The first stage in the modelling process is concerned with determining the scattered elastic

displacement field for a particular defect. This aids in the development of a solution for the inverse problem of characterising an unknown defect using the recorded scattered displacement field.

A good starting point for the development of an ultrasonic scattering theory is to consider the total displacement field recorded at some point as the superposition of the incident and scattered displacement fields. For flaws with all the dimensions finite, the scattered far field may be written as

$$\underline{u}^{scat}(\text{far field}) = \underline{a}(\theta,\phi)\,A(\theta,\phi)\,\frac{\exp(-i(\omega t - kR))}{kR} \qquad (4.6)$$

where $\underline{a}(\theta,\phi)$ is the polarisation as a function of the angles θ and ϕ,
$A(\theta,\phi)$ is known as the scattering amplitude,
R is the distance from the flaw,
and $k = \omega / c = 2\pi / \lambda$ and is the ultrasonic wavenumber.

The scattered fields from simple defects such as cylinders and spheres may be obtained by the solution of (4. 6). Exact solutions, which show good agreement with experiment, have been obtained using this method (e. g. Pao and Mow (1973), Tittman (1983), Sato et al. (1987)).

This method of solution does not, however, generalise to more complex flaw shapes. The scattered displacement field now becomes represented by an integral equation containing a time - harmonic Green's displacement tensor (Mura (1968)) and numerical techniques have to be employed. The integral expression representing the scattered displacement field consists of two terms in this formulation : one which represents the scatter from density changes in the medium and the other one which represents the scattering from elastic constant changes.

It is the development of a general solution to the time - harmonic Green's displacement tensor that is difficult. Approximate solutions have been developed in some special cases of significant practical interest using the Born approximation (e. g. Mal and Knopoff (1967), Gubernatis et al. (1977)). In this approximation, the flaw is assumed to have properties close to those of the medium and the scattered field is considered to be small with respect to the incident field. More sophisticated generalisations of these methods may also be used to determine the scattered displacement field (Thompson and Wadley (1989)).

An alternative procedure is to obtain a surface formulation of the integral equation which can be written in terms of the displacement fields, their derivatives and the elastic constants. The integral expression for the scattered displacement field includes the Green's displacement tensor, a stress tensor and a quantity known as the Crack Opening Displacement (C. O. D.). This is defined as (Achenbach et al. (1982))

$$\Delta \underline{u} = \underline{u}^{+} - \underline{u}^{-} \qquad (4.7)$$

where $\underline{u}^{+}$ ($\underline{u}^{-}$) is the displacement on the upper (lower) crack face. To solve the expression for the scattered displacement field an approximate solution for the dynamic C. O. D. is used.

Various approximations to the dynamic C. O. D. may be substituted in the scattered displacement field integral depending on the frequency of the ultrasound. At low frequencies, $ka << 1$, a quasi - static solution exists in which the C. O. D. is derived from the static deformation of the crack (e. g. Datta (1977), Teitel (1978)). At high frequencies, $ka \geq 1$ and near specular angles, the elastodynamic

Kirchhoff approximation is used (Achenbach et al. (1982)). In this approximation, the shadow side of the crack is assumed to be motionless while the illuminated side is assumed to move locally as it would if it were a planar surface illuminated by a plane wave of amplitude equal to that of the local illuminating radiation.

The Kirchhoff theory breaks down away from specular geometries and the signals become dominated by diffraction from the crack tips. The mathematical reason is that a systematic error develops in the assumed form for the C. O. D. near the crack edges (Coffey and Chapman (1983)). The tip diffracted signals are predicted much more accurately by the elastodynamic geometrical theory of diffraction (GTD), which is explicitly formulated to correctly treat the edge diffracted waves in the high frequency limit, $ka \geq 1$ (Keller (1962)).

Solutions for the two - dimensional and three - dimensional scattering of ultrasound by cracks using the GTD have been obtained by Maue (1953), Golan et al. (1980, with corrections to the mathematics), Chapman (1981), Achenbach et al. (1982), Ogilvy and Temple (1983), Vopilkin (1985a, 1985b) and Georgiou et al. (1989). It is the theory most relevant to the TOFD technique for the determination of the scattered displacement field.

Chapman (1981) and Ogilvy and Temple (1983) considered the two - dimensional scattering of monochromatic plane elastic waves with a time dependence of exp (- $i\omega t$) from a semi - infinite crack embedded in a homogeneous isotropic elastic solid. This is illustrated in Fig. 4. 6. Exact solutions for the scattered displacement field for incident compression, shear (vertically polarised with respect to the crack edges) and Rayleigh waves were expressed in terms of the C. O. D. The derivation may also be used for a broadband ultrasonic pulse simply by

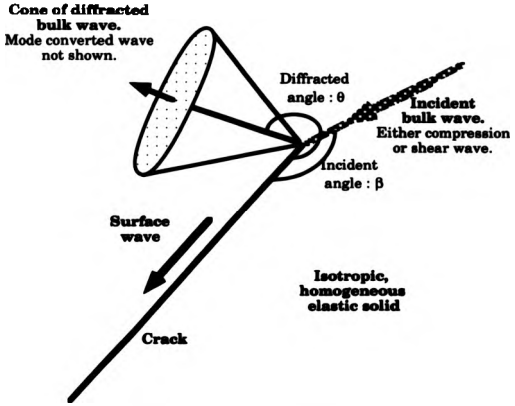

Figure 4. 6 : Diffracted wave produced by the incidence of a bulk wave upon a crack

splitting the incident ultrasound into its individual frequency components (Coffey and Chapman (1983)).

The integral expressions for the two - dimensional scattered displacement and stress fields, in terms of the C. O. D. and the Green's displacement tensor, were Fourier transformed into the frequency domain using the convolution theorem. The frequency domain stress fields were expressed in terms of the frequency domain scattered displacement fields and the equations were rearranged to be in the form

$$F^{-}(\Omega) = G^{+}(\Omega) \qquad (4.8)$$

where F^{-} (containing the Fourier transform stress term) is regular in some lower half - plane of the complex Ω - plane,

and G^{+} (containing the Fourier transform C. O. D. term) is regular in some upper half - plane such that there is a region of overlap within which both functions are regular.

This region of overlap was assumed to exist and shown a posteriori when the Fourier transform of the C. O. D. and the stress field had been evaluated.

The Wiener - Hopf technique (Noble (1958), Pilant (1979)) could then be used to obtain the required solution for the Fourier transform of the C. O. D. The Fourier transform of the stress field may also be obtained. The C. O. D. was obtained by calculating the inverse Fourier transform of the derived expression and used to determine the scattered displacement field for large kR (i. e. in the far field region). This was determined using the method of steepest descents (Jeffreys and Jeffreys (1966)).

The scattered displacement field can be written in terms of scalar (ϕ) and irrotational vector (ψ) potentials, i. e.

$$\underline{u}^{diff} = \nabla \phi^{diff} + \nabla \wedge \psi^{diff} \qquad (4.9)$$

and

$$\nabla \cdot \psi = 0 \qquad (4.10a)$$

$$(\nabla^2 + k^2)\,\phi = 0 \qquad (4.10b)$$

$$(\nabla^2 + K^2)\,\psi = 0 \qquad (4.10c)$$

where k, K are the wavenumbers for the compression and shear waves respectively.

For compression waves, $\psi = 0$, ϕ is finite whilst for shear waves, $\phi = 0$ and ψ is finite. The scalar and vector potentials for the diffracted displacement field derived by Chapman (1981) and Ogilvy and Temple (1983) are

$$\phi^{diff} = \begin{Bmatrix} F_P(\theta, \beta) \\ G_P(\theta, \beta) \end{Bmatrix} \sqrt{\frac{\lambda_P}{R}} \exp(i k_P R) \qquad (4.11)$$

for diffracted compression waves, and

$$\psi^{diff} = \begin{Bmatrix} F_S(\theta, \beta) \\ G_S(\theta, \beta) \end{Bmatrix} \sqrt{\frac{\lambda_S}{R}} \exp(i k_S R) \qquad (4.12)$$

for diffracted shear waves.

where R is the distance from the crack tip to the observation point, $k_{p,s}$ and $\lambda_{p,s}$ are the wavevectors and wavelengths for the compression and shear waves respectively, and the complex diffraction coefficients (or scattering amplitudes) $F_{p,s}(\theta, \beta)$ and $G_{p,s}(\theta, \beta)$ are given by Ogilvy and Temple (1983).

Taking account of the range to the crack and attenuation, Ogilvy and Temple (1983) determined the optimum incident compression and shear wave angles for the maximum diffracted amplitude directed towards the scanned surface. Although the TOFD technique does not use the amplitude to size defects it must be ensured that the received amplitude for a given arrangement will be large enough to be detected. For a defect placed symmetrically between source and detector, the optimum angle for maximising the signal from both ends of the defect is ~ 65° for compression waves depending on attenuation and on the crack depth. Thus the use of 60° probes for the TOFD technique proved to be an optimum choice. For incident vertically polarised shear waves the optimum angles are 45° for the top and 57° for the bottom of a buried vertical crack. With reference to section 4. 3. 2 and Fig. 4. 5, a source to detector distance of ~ 30 mm would result in angles of incidence at which the maximum diffracted amplitude from the top and bottom of a defect occurs and sufficient resolution is obtained to accurately size the defect.

Other methods for the determination of the scattered displacement fields are numerical techniques such as the finite element and finite difference approach (Bond (1982)), T - matrix (Waterman (1976)), boundary element method or boundary integral approach (Hirose and Achenbach (1989), Beskos (1987)) and the method of

moments (Varadan and Varadan (1986)). These numerical approaches can predict the scattered displacement fields for specific flaw geometries with high accuracy. The disadvantage is that they, in general, provide less physical insight to the scattering process.

The faces of the defect used in the techniques described above are assumed to be smooth, infinitely close and non - contacting i. e. they do not transmit tractions. Real cracks, however, particularly fatigue and stress corrosion cracks, have rough faces which may contact each other (Achenbach et al. (1989)). Sometimes there is not a single crack but a configuration of a principal crack and an adjoining satellite crack e. g. a macrocrack and a neighbouring microcrack. It is common also for smaller scatterers, such as voids and inclusions, to be located near a crack. The secondary scattering from these inhomogeneities will affect the overall scattered field. Another complication is introduced if small zones of different material properties are present at the crack tips. The effects of ' real ' cracks on the scattered displacement field have been described by Ro et al. (1988), Ogilvy (1989a), Nagy and Adler (1987), Mashashvili (1987), Buck et al. (1984), Mikita and Achenbach (1988) and Sotiropoulous and Achenbach (1988). Temple (1985) considered the effects of stress and crack morphology on TOFD signals.

Defects located within a region of a solid whose velocity is highly anisotropic, such as in welded sections of a structure, also complicate the modelling. The direction dependent velocity must be taken into account when the various modelling techniques are employed. Ultrasonic scattering from defects within anisotropic materials has been considered by, for example, Norris (1983) and Ogilvy (1988).

4. 6 : SCATTERED DISPLACEMENT FIELD PATTERNS

The scattered displacement field patterns from various defects derived using the modelling theories discussed have been shown in papers by, for example, Langenburg (1986), Schmitz and Langenburg (1987) and Sato et al. (1987). Ludwig and Lord (1988) used a finite element formulation to predict the A - scan signals obtained after propagation of ultrasound around a cylindrical hole defect. Photoelastic visualisations are a useful aid to the understanding of the interaction of ultrasound with defects. The scattered ultrasonic fields observed using this technique have been shown in papers by, for example, Ying et al. (1984) and Harumi et al. (1987, 1989a, 1989b).

The diffraction coefficients (or scattering amplitudes) have been plotted over a 2π scattering angle as a function of incident angle and wave type by Ogilvy and Temple (1983), Golan et al. (1980) and Temple (1983). Discontinuities in the diffraction coefficients arise for angles of incidence of 0, $\pi / 2$ and π radians corresponding to a changeover of diffraction from the top / bottom to the bottom / top of the defect (Chapman (1981)). Experimental verification of the diffracted amplitudes and phase change using various types of source and detector have been reported by Chapman and Toft (1987), Burch et al. (1988) and Ravenscroft et al. (1989). Three dimensional diffraction coefficients have been calculated (Ogilvy (1989b)) for the incident and scattered displacement fields in different planes.

Laser - generated ultrasound has specific directivities for the compression and shear waves dependent on the particular type of source used (Figs. 2. 5 and 2. 6 in Chapter Two). The two - dimensional diffraction coefficients (both amplitude and phase change) for angles of

incidence corresponding to the maximum in each directivity pattern can be calculated using data supplied by Temple (1989). The thermoelastic source has its maximum compression wave amplitude at an angle of ~ 60° from the surface normal which corresponds to an angle of incidence, β, defined in Fig. 4. 6, upon the top of a defect of 120°. The reradiated compression and shear wave profiles for a compression wave incident upon a defect in aluminium at β = 120° are shown in Fig. 4. 7. Both the thermoelastic and plasma regime sources have the maximum vertically (relative to the irradiated surface) polarised shear wave amplitude at an angle of ~ 30° from the surface normal corresponding to an angle of incidence, β, upon the top of a defect of 150°. The corresponding diffraction coefficients in aluminium for a vertically polarised shear wave incident at this angle are shown in Fig. 4. 8. The plasma regime source has its maximum compression wave amplitude normal to the irradiated surface. For convenience, an angle of 20° from the surface normal is chosen to represent this maximum amplitude and the diffraction coefficients for the compression wave incident upon the top (β = 160°) and bottom (β = 20°) of a defect in aluminium are shown in Figs. 4. 9 and 4. 10 respectively. Note that, for all the reradiated profiles shown, the amplitude of the diffracted component of the scattered ultrasonic field is very much less than the specularly reflected and straight through ultrasonic components. As the angle of incidence approaches 0 or π radians the cross - section of the defect available to interact with the incident ultrasound diminishes. Most of the incident ultrasound propagates past the defect. The largest scattered ultrasonic amplitude would occur when the incident ultrasound is specularly reflected from the sides of the defect. Although this would provide information on the depth of the defect it would not enable a determination of the defect length to be made. The phase change of the

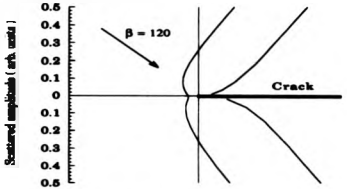

Figure 4. 7a : Reradiated compression wave pattern for compression wave incident at an angle of 120°

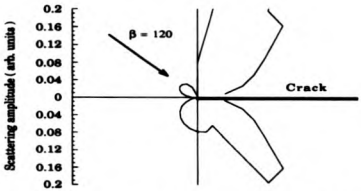

Figure 4. 7c : Reradiated shear (SV) wave pattern for compression wave incident at an angle of 120°

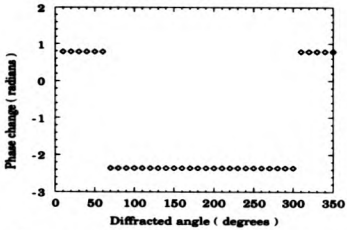

Figure 4. 7b : Phase change of diffracted compression wave for compression wave incident at 120°

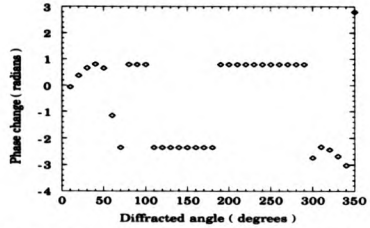

Figure 4. 7d : Phase change of diffracted shear (SV) wave for compression wave incident at 120°

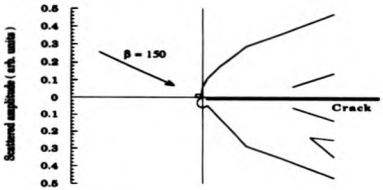

Figure 4. 8a : Reradiated shear wave pattern for shear wave incident at an angle of 150°

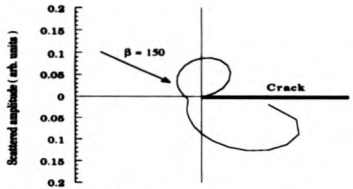

Figure 4. 8c : Reradiated compression wave pattern for a shear wave incident at an angle of 150°

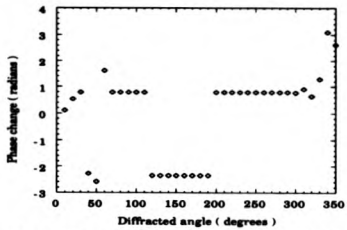

Figure 4. 8b : Phase change of reradiated shear waves for shear wave incident at an angle of 150°

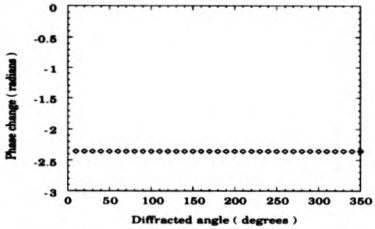

Figure 4. 8d : Phase change of diffracted compression waves for shear wave incident at an angle of 150°

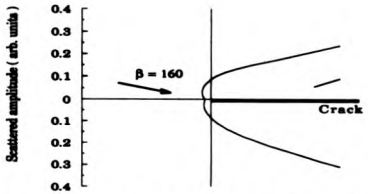

Figure 4. 9a : Reradiated compression wave pattern for compression wave incident at an angle of 160°

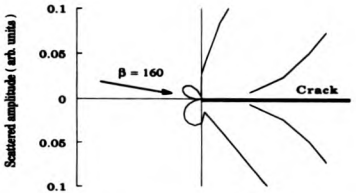

Figure 4. 9c : Reradiated shear wave pattern for compression wave incident at an angle of 160°

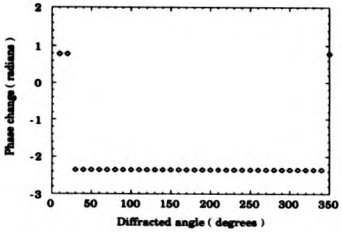

Figure 4. 9b : Phase change of diffracted compression wave for compression wave incident at an angle of 160°

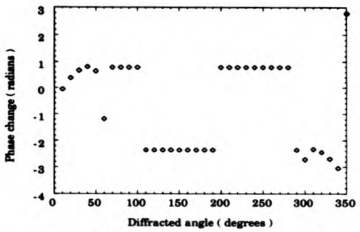

Figure 4. 9d : Phase change of diffracted shear wave for compression wave incident at an angle of 160°

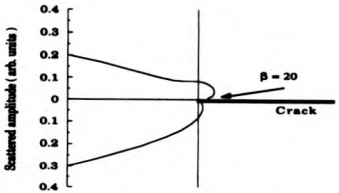

Figure 4. 10a : Reradiated compression wave pattern for compression wave incident at an angle of 20°

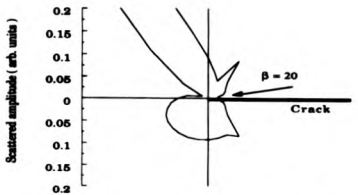

Figure 4. 10c : Reradiated shear wave pattern for compression wave incident at an angle of 20°

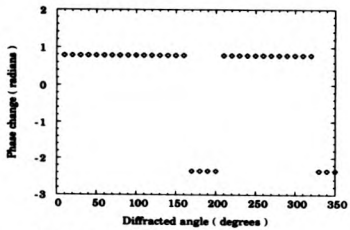

Figure 4. 10b : Phase change of diffracted compression wave for compression wave incident at an angle of 20°

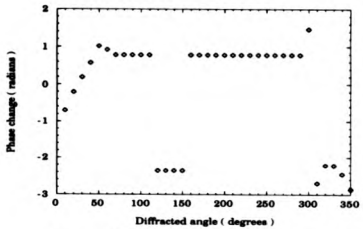

Figure 4. 10d : Phase change of diffracted shear wave for compression wave incident at an angle of 20°

reradiated compression waves tends to be either $\pi / 4$ or $- 3 \pi / 4$ radians whereas the reradiated shear wave phase change exhibits a greater variability. The displacement of the elastic waves, produced by the thermoelastic and plasma regime sources of ultrasound, diffracted from defects has also been considered by Scruby et al. (1986).

The experimental reradiated compression wave amplitude as a function of angle for a compression wave incident upon a 0.6 mm wide slot in aluminium at $\beta = 120°$ was obtained and compared to the theoretical profile. The ultrasound was generated, using a Nd:YAG laser pulse, in the plasma regime so as to obtain sufficient signal. The source was offset, with respect to the 0.6 mm wide slot, so that the maximum compression wave amplitude from this type of source was incident at an angle of 120° upon the defect tip. The scattered displacements were detected using a modified Michelson interferometer which was scanned around the diameter of the cylindrically shaped slotted sample thus maintaining a constant ultrasonic path length. It was possible to calculate the resulting surface displacement using the output voltage from this interferometer and equation 3. 43 (from Chapter Three).

The experimental amplitude of the compression wave as a function of angle around a 0.6 mm wide slot, for a compression wave incident at $\beta = 120°$, is shown in Fig. 4. 11a, along with a representative diagram of the experimental arrangement, and the theoretical reradiated compression wave profile, for the same angle of incidence, is shown in Fig. 4. 11b. The agreement between the experimental and theoretical reradiated profiles is generally good in the regions in which it was possible to record the scattered compression wave. There were, however, regions around the sample where it was not possible to record the ultrasonic signal scattered from the slot tip. For angles $\theta \leq 90°$, the

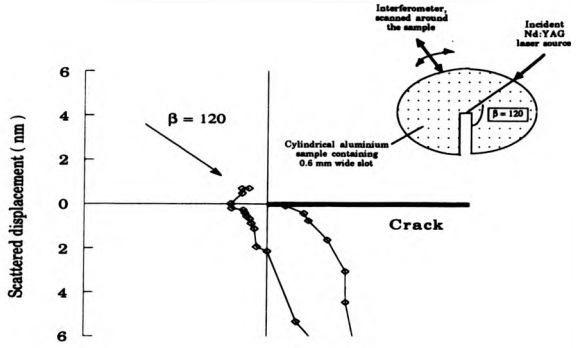

Figure 4. 11a : Experimental reradiated compression wave amplitude for compression wave incident at an angle of 120°

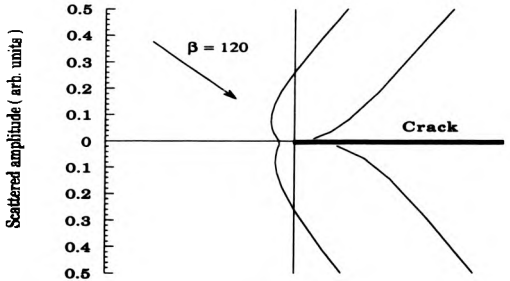

Figure 4. 11b : Reradiated compression wave pattern for compression wave incident at an angle of 120°

compression wave signals were essentially reflections from the side of the slot. This resulted in larger amplitude (~ 6 nm) displacements which arrived at progressively smaller travel times and increasing time width. It was not possible to distinguish the scattered component from the slot tip. For angles $110° \leq \theta \leq 130°$ the incident Nd:YAG laser pulse and He - Ne interferometer detecting beam were essentially coincident. For angles $180° \leq \theta \leq 190°$ the travel time of the compression wave scattered from the slot tip was the same as the Rayleigh wave arrival time. Thus, for reasons cited earlier, the compression wave signal was shrouded within the Rayleigh wave signal. At angles $\theta \sim 300°$ the direct compression wave from source to detector was recorded and it was necessary to discriminate between this ultrasonic signal and the scattered ultrasonic signal.

4. 7 : PHASE CHARACTERISTICS OF DEFECTS

Determination of the phase change in the ultrasonic pulse scattered from a particular defect may aid in its characterisation. Little attention has been paid to the phase behaviour of ultrasound scattered from a defect owing to the apparent difficulty in obtaining phase information from the recorded signal. An example of the use of phase information in NDT has been given by Barna and Johnson (1983) who determined the phase change of the specular echo from three different cracks. The method used to determine the phase was not described but their results indicated that smaller cracks show larger phase shifts. Hull et al. (1985) calculated both the power and phase spectra of a reference signal and a backwall echo. The spectra were used to

determine the ultrasonic velocity. Paradis et al. (1986b) and Mak (1988) describe techniques for separating the resulting overlapping echoes from near surface defects and the lateral wave using phase information and convolution in the frequency domain.

A method for determining the phase change which occurs when ultrasound is scattered from a defect has been described by Burch and Ramsey (1989). Observations of the A - and B - scan images of compression wave signals diffracted from the top and bottom of a crack have a phase difference of π radians between the two signals (Fig. 4. 1). Analysis of the complex diffraction coefficients for diffracted compression waves predicts a phase change of π / 4 radians for the bottom of the defect ($0° < \beta < 90°$ and $0° < \theta < 90°$, $270° < \theta < 360°$) and $-3\pi / 4$ for the top of the defect ($90° < \beta < 180°$ and $90° < \theta < 270°$). The phase change has discontinuities at $\beta = 0°$, 90° and 180°. These angles correspond to the changeover of diffraction from the top and bottom of the defect.

Burch and Ramsey (1989) described an algorithm, based on Fourier transform techniques, which was capable of determining any angle of phase difference between two similar pulses. The algorithm was independent of the arrival time of the signal and thus independent of the flaw location. The Fourier transform (Brigham (1974)) of the incident time domain signal x (t) may be given by

$$X(f) = \frac{1}{2\pi} \int_{-\infty}^{+\infty} x(t) \exp(-2\pi i f t) dt \qquad (4.13)$$

where f, t are the frequency and time variables respectively.

The Fourier transform function X (f) is complex and can be expressed as

$$X(f) = A_x(f) \exp(i\phi_x(f)) \qquad (4.14)$$

where $A_x(f)$ and $\phi_x(f)$ are the amplitude and phase spectra of the function X (f) respectively.

The interaction of ultrasound with a defect can be assumed to be described by a transfer function H (f) so that the Fourier transform of the scattered signal is given by

$$S(f) = H(f)X(f) \qquad (4.15)$$

Note that this is akin to the convolution operator ' * '. The scattered signal in the time domain, s (t), is a result of the convolution of the incident pulse with a transfer function, h (t), unique to the defect. So that

$$s(t) = x(t) * h(t) \qquad (4.16)$$

In the frequency domain this is given by (4. 15) above.

Rearranging (4. 15) and using (4. 14) gives the transfer function, H (f), as

$$H(f) = \frac{A_s(f)}{A_x(f)} \exp[i(\phi_s(f) - \phi_x(f))] \qquad (4.17)$$

The phase of the flaw transfer function is obtained by subtracting the phase spectra of the incident and scattered pulses.

In practice the incident pulse is taken as the reflected signal from a backwall with a travel time distance the same as the scattered signal from a defect. The same travel time distance ensures that any frequency dependent dispersion effects can be neglected. The phase of the transfer function at a particular frequency, f, is now only dependent on

- any difference between the arrival times of the two pulses. This time difference, Δt, has a linear phase variation with frequency and is given by $2\pi f \Delta t$.

- any phase changes introduced by the flaw.

At zero frequency the phase of the transfer function is unaffected by arrival time differences. However the phase at zero frequency can not be measured directly since at zero frequency the spectral amplitudes of the ultrasonic pulses are zero and the corresponding phase spectra are undefined. A linear extrapolation of the phase values at higher frequencies can be used to estimate the phase of the transfer function at zero frequency. In making this extrapolation it is assumed that the phase change due to the flaw is independent of frequency as predicted for the diffracted signals from crack tips (Coffey and Chapman (1983)).

Burch and Ramsey (1989), using a piezoelectric transducer in pulse - echo mode, recorded the signal diffracted from a crack tip, grown in a high grade mild steel sample, for incident and scattered angles $\beta = \theta = 180°$. For the reference signal the backwall echo with the same travel time distance and in the same material was used. The peak amplitudes in each pulse were aligned so as to occur at the same relative point in the digitised record. Each waveform was Fourier transformed into the frequency domain using an FFT algorithm and the

power and phase spectra calculated. These are shown in Fig. 4. 12a and b. Where the spectral amplitudes are low (< 10 % of peak amplitude) noise causes the phase spectrum to oscillate rapidly between ± π. The Phase Difference spectrum defined as

$$\text{Phase difference } (f) = \text{Phase of defect signal } (f) - \text{Phase of reference signal } (f) \qquad (4.18)$$

was calculated over a frequency range at which a significant amplitude on the power spectrum (≥ 10% of peak value) was present. This range extended from 1 MHz to 4 MHz using the piezoelectric transducer. The phase difference spectrum obtained in this way is shown in Fig. 4. 12c. The phases are plotted such that a positive sign corresponds to a phase lag of the diffracted wave from the incident pulse. Extrapolating the best fit straight line to zero frequency gives an intercept of - (40 ± 3)° or - (0.70 ± 0.05) radians. Burch and Ramsey (1989) corrected the measured phases for the 180° change in phase that occurs for a backwall reflection and thus obtained a phase difference of (40 ± 3)° or (0.70 ± 0.05) radians. This phase difference is equivalent to - (140 ± 3)° or - (2.44 ± 0.05) radians if a negative sign is taken to correspond to a phase lag of the diffracted wave from the incident pulse. This is in good agreement with the theoretical value of - 135° or - 3 π / 4.

Burch and Ramsey (1989) proceeded to determine the phase difference for incident and scattered angles $10° \leq (\beta, \theta) < 180°$ using compression and shear (SV) waves. The amplitudes of the diffraction coefficients for these orientations are relatively small and thus the signals received must have had a small signal - to - noise ratio. This introduces an element of scatter in the phase difference data which is illustrated in their graphs. Also for $(\theta, \beta) < 90°$ there will be a

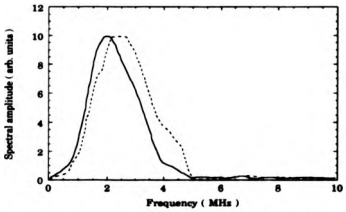

Figure 4. 12a : Spectral amplitude spectra of the crack tip and reference waveforms (after Burch and Ramsey (1989))

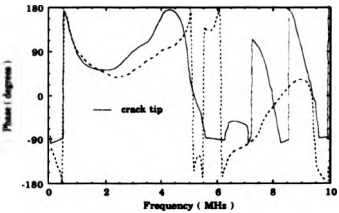

Figure 4. 12b : Phase spectra of the crack tip and reference waveforms (after Burch and Ramsey (1989))

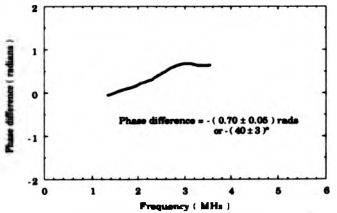

Figure 4. 12c : Phase difference spectrum obtained for fatigue crack (after Burch and Ramsey (1989))

component within the received signal which is a direct reflection from the side of the crack. The broader the ultrasonic pulse the more likelihood that the signal received is a reflection from the crack side at these angles (Section 4. 6). A preliminary investigation of the diffracted amplitude from a 1 mm wide slot in aluminium as a function of angle using laser generation and interferometric detection in effective pulse - echo mode was conducted by the author. For angles { θ, ß } < 90° no signal from the slot tip was received only a reflection from the slot side directly below the source and detector.

Other experimental verifications of the amplitude and phase of the diffraction coefficients as a function of the incident angle ß and diffracted angle θ have been reported by Chapman and Toft (1987), Burch et al. (1988) and Ravenscroft et al. (1989). Chapman and Toft (1987) measured the amplitude and phase of the diffraction coefficient for a straight edged crack and a straight edged 270° vertex. Burch et al. (1988) used three smooth straight edged fatigue cracks and determined the diffraction coefficients for incident and diffracted compression and shear (SV and SH) waves. Again good agreement with the theoretical values was obtained but some statistically significant variability was observed to occur. Ravenscroft et al. (1989) used a variety of sources and detectors to record the diffracted amplitudes and phase at various angles around machined defects and fatigue cracks. The phase difference values were observed to be significantly different from the theoretical predictions and this was probably owing to the small signal - to - noise ratio of the recorded waveforms. The diffracted amplitude and phase was also observed to vary significantly from the theoretical predictions depending upon the crack morphology. A smooth crack with non - contacting faces showed close agreement to the theory. Whereas the diffracted amplitude and phase values for a crack with contacting faces showed significant differences. This is to be expected as the theory assumes a crack with smooth, non - contacting faces. A crack with contacting faces allows the transmission of ultrasound from one face to the other. In effect the dynamic C. O. D. has been altered.

4. 8 : INVESTIGATION OF THE PHASE CHARACTERISTICS OF VARIOUS DEFECTS USING LASER ULTRASONICS

An investigation of the phase characteristics of laser - generated ultrasonic interactions with various defects was undertaken. The aim of the study was to determine whether a particular type of defect produces a unique phase change to the incident ultrasound. Scattered signals from defects are similar when viewed in the time domain and it is hard to determine from the signal what type of defect it is. By looking at the phase characteristics of a particular reflector it may be possible to characterise a defect as a crack / slot, as a pore hole or as a slag defect.

The investigations were intended to complement the work already described. The frequency range over which the phase difference was calculated was extended from ~ 4 MHz (Burch and Ramsey (1989)) to ~ 20 MHz by using the wide bandwidth property of laser - generated ultrasound. The phase characteristics of various sized slots and holes were determined.

4. 8. 1 : Procedure

Initially the source and detector were positioned directly above the slot top or hole in an effective pulse - echo mode at $\beta = \theta = 180°$ (Fig. 4. 6). The incident Nd:YAG laser pulse was focussed to ~ 2 mm diameter burn spot size on the aluminium surface. No grease or other surface constraints were used to enhance the generation of ultrasound as a repeatable source, from shot to shot, was required. The distance between the source and the detecting He - Ne beam of the interferometer was

(5 ± 1) mm, thus the source and detector could be considered to be operating in pulse - echo mode. The Nd:YAG laser was used to generate ultrasound in the plasma regime so that sufficient signal was obtained using the 72 MHz bandwidth interferometer. As the plasma expands outwards it passes over the volume illuminated by the He - Ne laser. The plasma changes the refractive index of the air and thus changes the velocity of the He - Ne laser light. This is detected as a low frequency, high amplitude oscillation, illustrated in Fig. 4. 13, upon which the signals corresponding to the ultrasonic arrivals are superposed. To remove this disturbance a plasma shield was inserted between the source and detector.

Data were recorded for three incident laser pulse energies for each slot / hole size. This was in an attempt to determine whether the characteristics of the source would affect the value obtained for the phase change. The reference signal used was a reflection from the plane backwall of a semi - cylindrical block. The range from the source / detector to the backwall was the same as the range of the source / detector to the defect. Fig. 4. 14a is the reference compression wave reflection obtained using a laser pulse energy of (301 ± 9) mJ. The risetime of the ultrasonic pulse detected using the interferometer in this arrangement was ~ 15 ns which implies frequency components up to ~ 20 MHz are present within the ultrasonic pulse. Fig. 4. 14 b and c are the corresponding power and phase spectra obtained using an FFT algorithm which will be described later. The power spectrum illustrates that significant frequency components up to ~ 20 MHz are present within the ultrasonic pulse detected in this arrangement. The phase spectrum has a linear variation in the frequency range (2 - 24) MHz. Values of the power and phase for frequencies of < 2 MHz represent the d. c. and low frequency components contained within the recorded

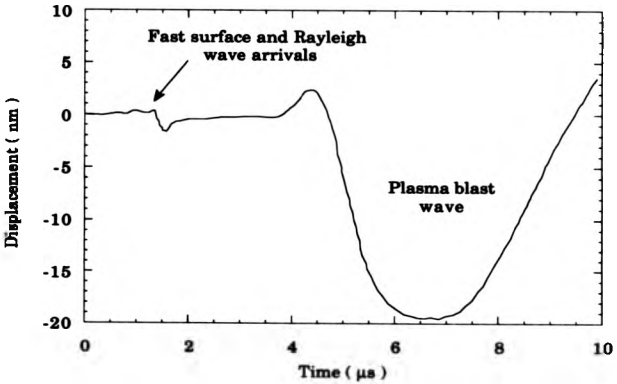

Figure 4. 13 : Plasma blast wave detected as the plasma expands across the He - Ne beam of the interferometer

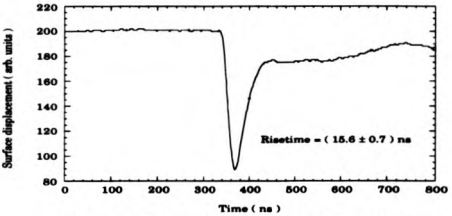

Figure 4. 14a : Reference compression wave signal for incident laser pulse energy of (301 ± 9) mJ

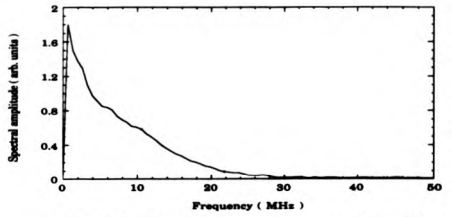

Figure 4. 14b : Power spectrum of reference compression wave above

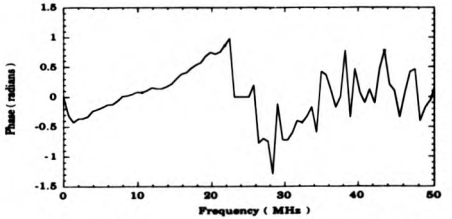

Figure 4. 14c : Phase spectrum of reference compression wave above

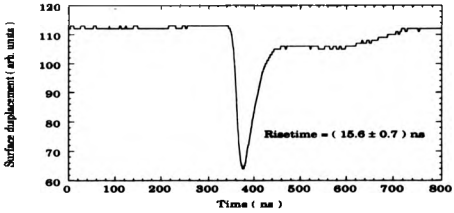

Figure 4. 15a : Reference compression wave signal for incident laser pulse energy of (190 ± 5) mJ

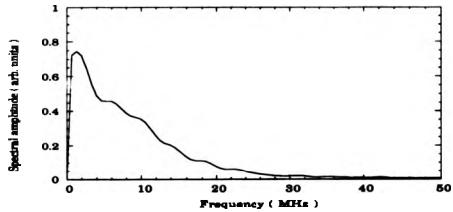

Figure 4. 15b : Power spectrum of the reference compression wave above

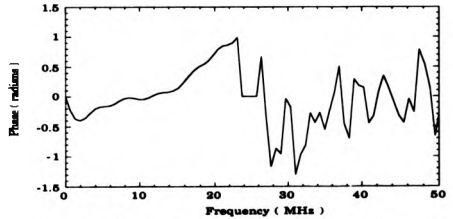

Figure 4. 15c : Phase spectrum of the reference compression wave above

signal. These low frequency variations upon which the ultrasonic pulse is superposed are due to other factors (e. g. rising of the sample surface back to its equilibrium position after the source laser pulse, mechanical vibrations in the laboratory environment) not associated with the ultrasonic interaction with the backwall or defect. For frequencies of > 24 MHz the spectral amplitude is within the noise level and any small variation in the real and imaginary components of the Fourier transformed signal is augmented when the phase is calculated. Thus the phase varies rapidly over ± π radians.

Fig. 4. 15 illustrates the corresponding compression wave, power and phase spectra when the ultrasound is generated by the Nd:YAG laser pulse with an energy of (190 ± 6) mJ. Again significant frequency components up to ~ 20 MHz are present within the pulse. Note the similarity between the phase spectra over the range (2 - 24) MHz for the two laser energies - Figs. 4. 14 c and 4. 15 c.

The defects, for which the phase characteristics were investigated, were slots, ranging in width from 1 mm to 20 mm, and cylindrical holes, ranging in diameter from 1 mm to 5 mm, in aluminium cylindrical blocks. The range from the source / detector to the defect was the same for all defects. The data processing used to determine the phase difference spectra for each defect is illustrated in Fig. 4. 16. The delay and time window on the digitiser was chosen so as to obtain the compression wave pulse and as much of the waveform which remained at a constant level as possible. The minimum point on the waveform was positioned at the centre of the window.

The minimum value of a particular 2048 point waveform was positioned at the centre + 1. If the dataconverted waveform did not contain 2048 points then it was effectively zero filled up to 2048. A Gaussian window was applied to the waveform to ensure that the first

For each slot / hole size the following data processing was undertaken :

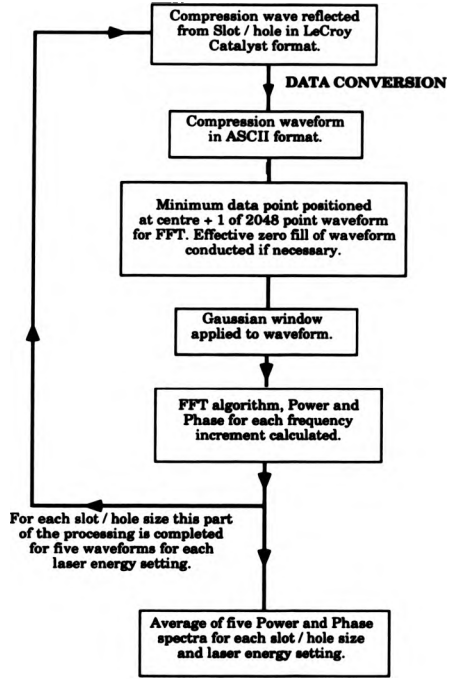

Figure 4. 16 : Flowchart illustrating the data processing conducted to obtain phase difference spectra.

and last point of the waveform was at the same level. If these points were not at the same level, the FFT output had superimposed upon the output a low amplitude, high frequency component. Fourier transform theory assumes a periodic waveform, thus the dataconverted waveform is seen as a single cycle in a periodic train. The first and last point of the waveform occurring at different levels implies a fast (one sampling point) transition from one level to the other. This introduces a high frequency (1 / (2 x sampling interval)) component to the FFT output. By applying a window to the waveform the beginning and end occur at the same level and thus this effect is negated. The central portion of the waveform remains unaffected by the windowing operation. Various windows (e. g. Triangle, Hanning, Gaussian (Harris (1978))) were applied to the dataconverted waveform to assess the effect each window had on the output. The Gaussian window defined as

$$w(n) = \exp\{ -0.5 * (\frac{7n}{N})^2 \} \qquad (4.19)$$

where n is the number variable of the waveform,

and N is the total number of points within a waveform,

did not significantly alter the shape of the ultrasonic pulse and it was decided that this was the best, most practicable window to use for this investigation.

The sampling interval of the LeCroy 6880A digitiser is 742ps. Thus the frequency increment (= 1 / N Δt where N is the number of points contained in a waveform digitised at a sampling interval Δt) for a 2048 point waveform is 0.66 MHz. Using the five power and phase spectra for each defect and for each laser energy setting, the phase difference were

calculated and an average phase difference spectrum obtained. The 180° phase shift on reflection at the backwall was inherently taken into account by the experimental arrangement. The ultrasonic signal scattered from the defect had a 180° phase shift plus the phase change owing to the defect. The phases are plotted such that a positive sign corresponds to a phase lag of the scattered wave from the incident pulse. Thus for each defect there were three averaged phase difference spectra corresponding to the three laser energy settings used in recording the data. These phase difference spectra were plotted and are shown for the laser energy setting of (301 ± 9) mJ / pulse only.

4. 8. 2 : Results

Figs. 4. 17a and 4. 18a show the ultrasonic compression wave pulses after interacting with a 1 mm wide slot and a 1 mm diameter hole respectively. Note the similarity in the shape of the pulses, it would be difficult to decide whether a particular signal was reflected from a slot / crack or a hole defect. Also shown are the corresponding power and phase spectra for the two waveforms. There is a difference between the phase spectra for the two defects especially at the higher frequencies in the useful frequency range. Fig. 4. 19 illustrates the corresponding phase difference spectra for the 1 mm wide slot and the 1 mm diameter hole. The difference between the two spectra is obvious. A best fit straight line using the least - squares method is fitted to the phase difference spectrum of the 1 mm wide slot and extrapolated to zero frequency. The intercept is (0.62 ± 0.05) radians. Note also the existence of a modulation upon the phase difference spectra. No attempt has been

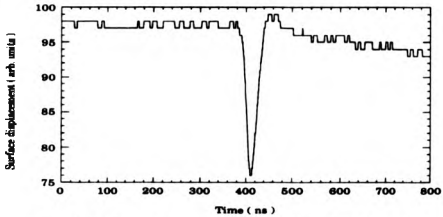

Figure 4. 17a : Compression wave signal after reflection from a 1 mm wide slot

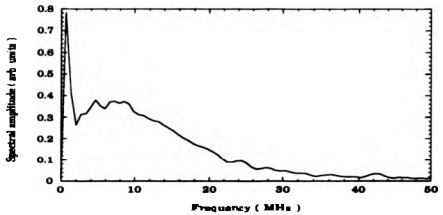

Figure 4. 17b : Power spectrum of the compression wave signal above

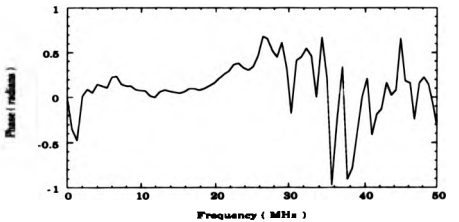

Figure 4. 17c : Phase spectrum of the compression wave signal above

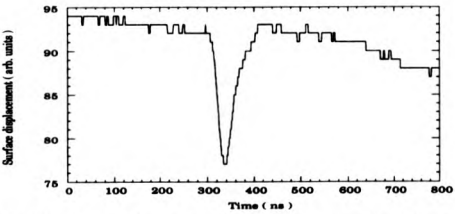

Figure 4. 18a : Compression wave signal after reflection from a 1 mm diameter hole

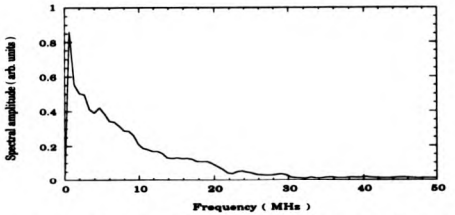

Figure 4. 18b : Power spectrum of the compression wave signal above

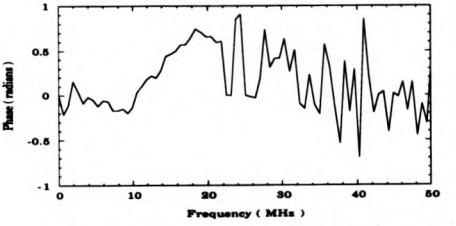

Figure 4. 18c : Phase spectrum of the compression wave signal above

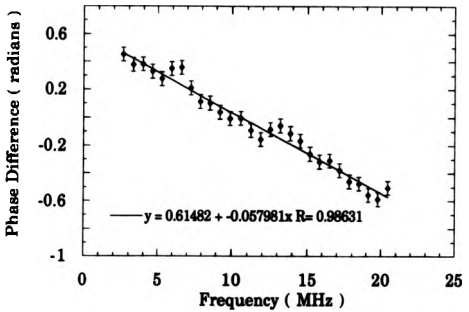

Figure 4. 19a : Phase Difference spectrum for 1mm wide slot

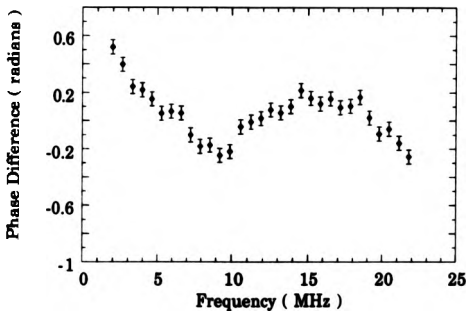

Figure 4. 19b : Phase Difference spectrum for 1 mm diameter hole

made to fit a polynomial expression to the data contained in the phase difference spectrum for the 1 mm diameter hole.

Figs. 4. 20 - 4. 22 compares the waveforms and the phase difference spectra for a 1.3 mm wide slot / 1.5 mm diameter hole, 2 mm wide slot / 2 mm diameter hole and a 4 mm wide slot / 4 mm diameter hole respectively. Once again there is a clear difference in the phase difference spectra for the slots and holes. Note that as the width of the slot increases the compression wave pulse becomes more bipolar whereas the compression wave signal from a hole remains unipolar. The time difference between the minimum and maximum points on these slot scattered compression waveforms is ~ 50 ns for the 2 mm and 4 mm wide slots. It was observed on the scattered ultrasonic signals from wider slots that the bipolarity reduced, the waveform becoming more unipolar and similar in shape to the reference waveform. As with the phase difference spectra for the 1 mm wide slot and hole, a modulation upon the phase difference spectra for these slot widths is also observed. To some extent it also exists on the phase difference spectra for the holes implying that it is an artefact of the data processing. Burch and Ramsey (1989) noticed a similar effect on their phase difference spectra and it was accounted for by the slightly different arrival times of the crack scattered and reference pulses. Owing to the sampling interval of the digitiser it was not possible to align the two pulses exactly in the time domain.

Fig. 4. 23 illustrates the remaining phase difference spectra for slots ranging from 6 mm to 20 mm. An interesting effect is observed for the 6 mm and 8 mm wide slots. The phase difference spectra have finite gradient with intercept at the lower frequencies (larger wavelengths) and zero phase difference at the higher frequencies (smaller wavelengths). An explanation for this effect is given in a later section.

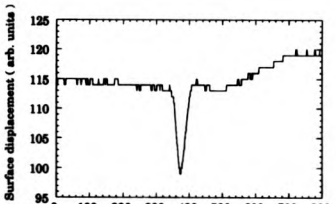

Figure 4. 20a : Compression wave signal after reflection from a 1.3 mm wide slot

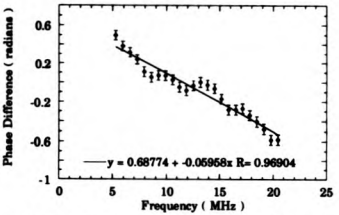

Figure 4. 20b : Phase Difference spectrum for 1.3 mm wide slot

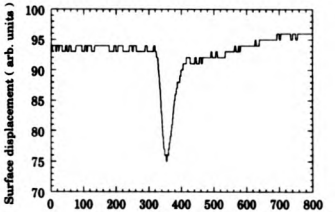

Figure 4. 20c : Compression wave signal after reflection from a 1.5 mm diameter hole

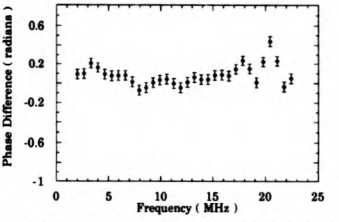

Figure 4. 20d : Phase difference spectrum for 1.5 mm diameter hole

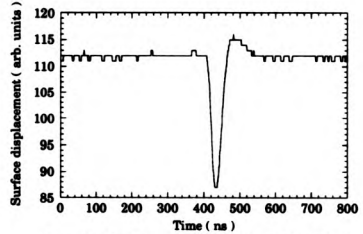

Figure 4. 21a : Compression wave signal after reflection from a 2mm wide slot

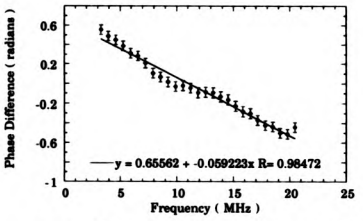

Figure 4. 21b : Phase Difference spectrum for 2mm wide slot

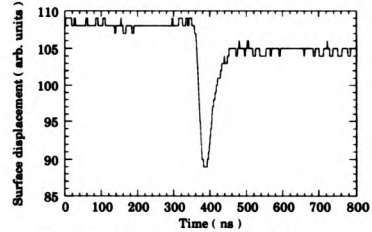

Figure 4. 21c : Compression wave signal after reflection from a 2 mm diameter hole

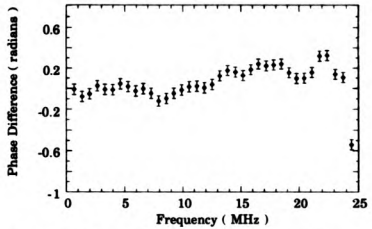

Figure 4. 21d : Phase Difference spectrum for 2mm diameter hole

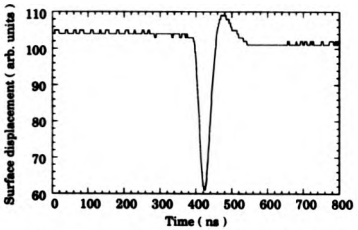

Figure 4. 22a : Compression wave signal after reflection from a 4 mm wide slot

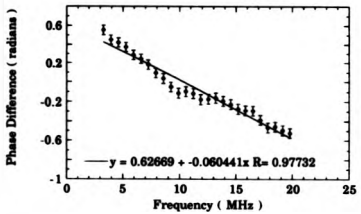

Figure 4. 22b : Phase Difference spectrum for 4 mm wide slot

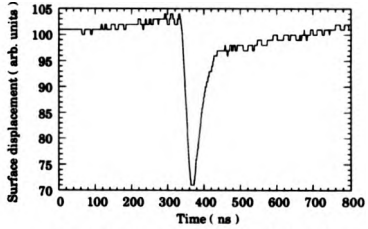

Figure 4. 22c : Compression wave signal after reflection from a 4mm diameter hole

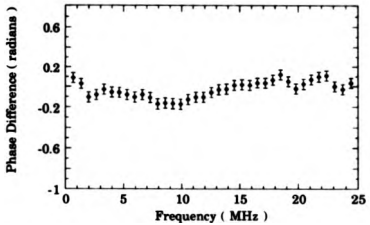

Figure 4. 22d : Phase Difference spectrum for 4 mm diameter hole

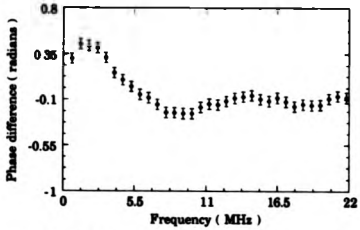

Figure 4. 23a : Phase difference spectrum for 6 mm wide slot

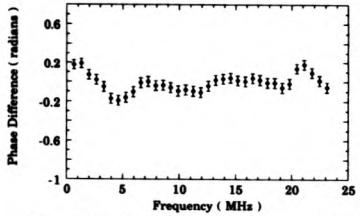

Figure 4. 23b : Phase Difference spectrum for 8mm wide slot

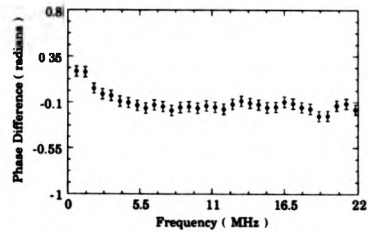

Figure 4. 23c : Phase Difference spectrum for 10 mm wide slot

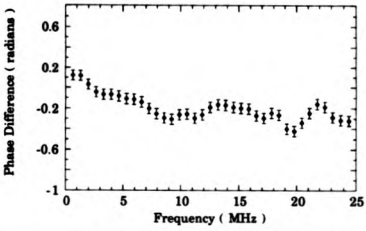

Figure 4. 23d : Phase Difference spectrum for 20 mm wide slot

For slot widths ≥ 10 mm the phase difference spectra are essentially zero, implying that there is little difference in the reflected compression wave signal from these wide slot tops and the backwall reflections.

Fig. 4. 24 illustrates the phase difference spectra for the remaining cylindrical hole samples ranging from (2.5 - 5) mm in diameter. There is essentially zero phase difference over the useful frequency range which is not dissimilar to the theoretical predictions by, for example, Sato et al. (1987) using their DITSO model. The difference between the phase difference spectra for the slots and for the holes is clear. The original intention of the investigation of the phase difference for ultrasonic interactions with holes was to assess whether some feature within the phase difference spectra could be used as an aid to its sizing. Unfortunately, as evident in the phase difference spectra, there is no feature which could be used.

An evaluation of the sensitivity required by the interferometer to detect diffracted signals from ' real ' cracks (~ 0.1 mm wide) was also undertaken. Fig. 4. 25 is the amplitude of the compression wave, for an incident laser pulse energy of (301 ± 9) mJ, as a function of both the slot width and hole diameter. Extrapolating the compression wave amplitude as a function of slot width (Fig. 4. 25a) down to zero implies that a slot width of ~ 0.1 mm results in a displacement of ~ 0.1 nm. The modified Michelson interferometer has a displacement resolution of ~ 30 pm. This implies that it is possible to detect surface displacements of ~ 0.1 nm but it requires a large (~ 10 Vpp) unstabilised output voltage and sufficient averaging, as the signal - to - noise ratio required for the data processing is ~ 30. Fig. 4. 25b implies that a similar sized hole results in a displacement of ~ 0.4 nm. The difference in the amplitudes of the compression waves scattered from these slots and holes may be used as an indicator to the type of defect.

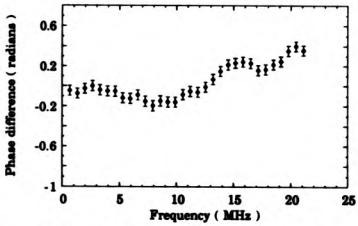

Figure 4. 24a : Phase difference spectrum for 2.5 mm diameter hole

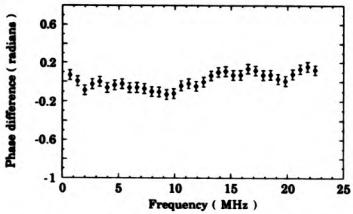

Figure 4. 24b : Phase difference spectrum for 3 mm diameter slot

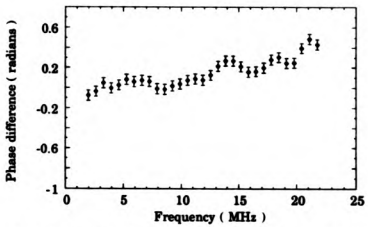

Figure 4. 24c : Phase difference spectrum for 4.5 mm diameter hole

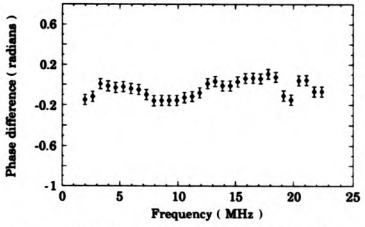

Figure 4. 24d : Phase difference spectrum for 5 mm diameter hole

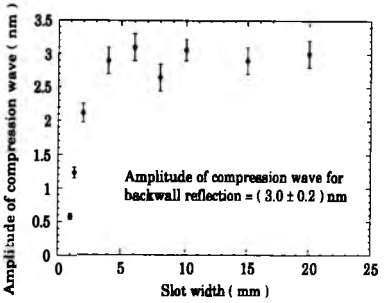

Figure 4. 25a : Amplitude of the scattered compression wave as a function of slot width

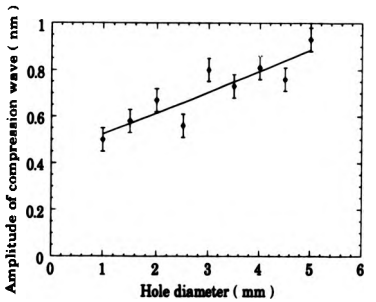

Figure 4. 25b : Amplitude of the scattered compression wave as a function of cylindrical hole size

4. 8. 3 : Discussion

The average phase change of the ultrasound upon interacting with the slots used in this investigation, determined from the phase difference spectra for all slot widths up to 6 mm and the three laser pulse energies used, was (0.64 ± 0.05) radians or (37 ± 3)°. If a negative sign is taken to correspond to a phase lag then the average phase change is - (2.50 ± 0.05) radians or - (143 ± 3)°. This compares favourably with the value obtained by Burch and Ramsey (1989) of (0.70 ± 0.05) radians / (40 ± 3)° (phase lag taken as positive) or - (2.44 ± 0.05) radians / - (140 ± 3)° (phase lag taken as negative). Also it is in general agreement with the theoretically predicted value of - 2.36 radians / - 135° of Chapman (1981) and Ogilvy and Temple (1983). The phase change for slot widths of > 6 mm tended to zero implying that the slot scattered compression wave was similar in form to the reference compression wave. The phase difference spectra for these slot sizes were similar to the spectra for all the cylindrical hole sizes used in this investigation in that they had essentially zero gradient and intercept over the useful frequency range.

A useful analysis may be conducted by modelling the laser - generated ultrasound as the superposition of ultrasonic waves with frequencies up to ~ 20 MHz. In aluminium this corresponds to wavelengths in the range (6.4 - 0.32) mm and is defined as the distance between successive wavefronts perpendicular to the axis of the slot or hole. In broad terms, it is only possible to perceive the average structure over an area the size of the first Fresnel zone defined as

$$\text{Fresnel Radius } R = \sqrt{\frac{\lambda h}{2}} \qquad (4.20)$$

where h is the distance from the source to the object of interest as shown in Fig. 4. 26. For h = 20 mm, R = (8 - 1.8) mm

As the width of a slot increases a gradual changeover from a slot scattered signal to a backwall reflection occurs. Owing to the wide bandwidth nature of the laser - generated ultrasound this changeover in the scattered signals is observed in the phase difference spectra. For a particular slot width, w, two mechanisms are possible :

(i) For $w > 2R$ the ultrasound ' sees ' the slot top as an effective infinite plane and a π - phase change results. Hence the phase difference tends to zero.

(ii) For $w \leq 2R$ the ultrasound interacts with the corners of the slot resulting in two secondary sources in association with the reflection from the slot top. Interference of the ultrasound emanating from these two secondary sources results in a non - zero phase difference.

This changeover from slot to backwall occurs in the slot width range (6 - 8) mm. The phase difference spectra for these slot sizes (Fig. 4. 23 a and b) has two regions. At the lower frequencies (larger wavelengths), $\leq$ 8 MHz, the phase difference spectra has finite gradient with finite intercept. At the higher frequencies (smaller wavelengths) the phase difference is essentially zero with zero intercept implying there is little difference in the slot reflected and the reference backwall ultrasound at these frequencies. Frequencies of > 8 MHz correspond to Fresnel diameters of < 5.6 mm. Thus the corners of slots of width

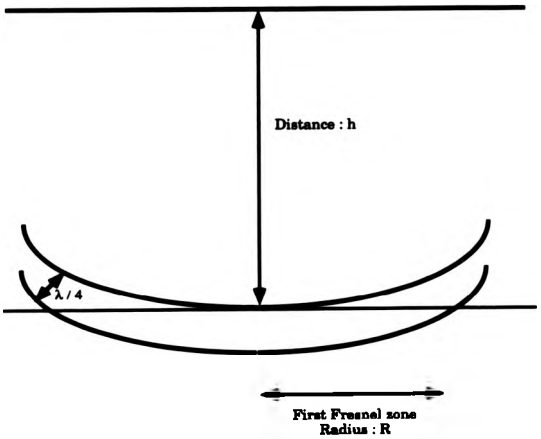

Figure 4. 26 : Diagram to illustrate the first Fresnel zone radius and its relation to the lateral resolution.

> 5.6 mm will not participate in the scattering of the laser - generated ultrasound at frequencies of > 8 MHz. In effect a backwall reflection occurs and hence the phase difference is zero. Conversely, laser - generated ultrasound with frequencies of ≤ 8 MHz, corresponding to Fresnel diameters of > 5.6 mm, will interact with the slot corners resulting in the phase change which is observed.

The changeover from finite gradient with finite intercept to zero gradient and zero intercept on the phase difference spectrum occurs at approximately 8 MHz for the 6 mm wide slot and at approximately 4 MHz for the 8 mm wide slot. The Fresnel diameter for a frequency of 8 MHz in aluminium at a range of 20 mm is, from above, 5.6 mm whilst a frequency of 4 MHz in aluminium at a range of 20 mm has a Fresnel diameter of ~ 8 mm. In accordance with this analysis, a 10 mm wide slot would be expected to show a change in gradient in its phase difference spectrum at a frequency of 2.5 MHz and a 20 mm wide slot at a frequency of 0.6 MHz. There is some evidence to suggest the existence of this change in gradient in the 10 mm and 20 mm phase difference spectra but the expected frequencies lie within the low frequency noise band of the recorded data.

If the frequency components within the ultrasonic pulse could be extended by using a laser pulse with a faster risetime (from Chapter Three) then it would be possible to observe this change in gradient at larger frequencies indicative of smaller slot widths. The frequency at which the gradient changes is illustrated in Fig. 4. 27 as a function of slot width. A 2 mm wide slot, for example, would be expected to have a change of gradient in its phase difference spectrum at a frequency of ~ 64 MHz. Thus using the phase difference spectrum it would be possible to characterise a particular defect scattered signal as a slot (or crack) from the value of the intercept and, if high enough frequency

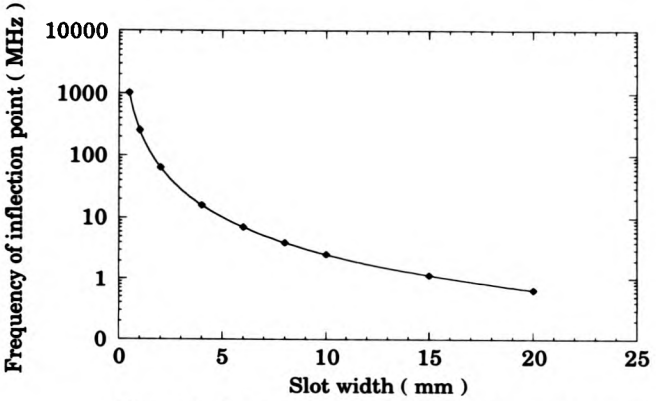

Figure 4. 27 : Frequency of expected change in gradient as a function of slot width

components exist, obtain an estimate of the defect width from the frequency at which a change in the gradient of the phase difference spectrum occurs.

The difference between the phase difference spectra for the slots and the holes is due to the corners of the slots which act as secondary sources when irradiated with ultrasound. The contribution to the scattered ultrasonic signal from these slot corners is superimposed upon the specularly reflected component from the slot tops. This is observed upon the recorded compression wave signals as a slightly positive contribution occurring after the displacement minimum in Figs. 4. 21a and 4. 22a especially. As the slot width increases the contribution from the corners is reduced and the scattered compression wave is similar in form to the reference compression wave. It is anticipated that as the slot width decreases, the time difference between the signal minimum and the maximum of this small positive contribution will decrease. Sufficient signal - to - noise ratios for the smaller slot widths were not obtained however to enable the positive contribution to be observed. This is also illustrated in the phase difference spectra for the smaller slot widths which display more scatter than the other spectra.

Ultrasound incident upon the cylindrical holes does not encounter the same abrupt change in defect profile as for the slots. Ultrasound with a particular Fresnel diameter tends to be specularly reflected from a tangential region of the hole surface of length equal to this Fresnel diameter. Thus a π radians phase change occurs resulting in a phase difference which is essentially zero over the useful frequency range. With decreasing radius, the larger Fresnel diameter ultrasound (lower frequencies) is scattered by a smaller tangential cross section. Thus these lower frequency components would be expected to have a smaller

interaction with the hole than the higher frequency components and to propagate through the hole. The smaller cross section for scattering of the holes considered in this investigation is illustrated in the amplitude of the scattered compression wave from holes, Fig. 4. 25b, which is an order of magnitude smaller than the compression wave amplitude scattered by the slots, Fig. 4. 25a.

4. 9 : PHASE INVESTIGATIONS FOR TOFD ARRANGEMENT OF SOURCE AND DETECTOR.

The phase behaviour of ultrasound incident upon and scattered from a defect at acute angles was investigated. The phase change of compression waves scattered from slots, ranging in width from 1 mm to 20 mm, for various angles of incidence were determined. The aim of this investigation was to demonstrate the potential usefulness of phase information determined from data recorded with the source and detector in a TOFD arrangement.

4. 9. 1 : Procedure

A procedure similar to that outlined in the previous section was repeated with the source and detector at different locations around the cylindrical sample containing a slot defect. The source and detector laser beams were positioned in the same plane parallel to the normal of the slot top and such that the slot top was symmetrically between the source and detector.

The angles used were 10°, 30°, 50° and 60° or, in terms of the reference frame of the theoretical modelling (Fig. 4. 6), the angle sets

$$\{ \beta, \theta \} = \{ (170, 190), (150, 210), (130, 230), (120, 240) \} \quad (4.21)$$

The experiments were not conducted on the cylindrical hole defect samples as the phase difference is zero regardless of the location of the source and detector in this arrangement. The ultrasound is reflected from a tangent to the hole of length given by the first Fresnel zone for the resultant wavelength perpendicular to the slot axis, dependent upon the angle of incidence. This radius of curvature is approximately constant at all angles of inspection of the hole. Thus if the phase difference is zero after reflection from one part of the cylindrical hole then this will be true for the other angles of inspection used in this investigation (Eringen and Shububi (1975)).

Reference compression wave signals were obtained for each angle using the same reference sample. Angles greater than 60° were not considered as the direct compression wave and the reflected compression wave signals became indistinguishable. For each angle, five waveforms were collected and the FFT algorithm used to calculate the power and phase spectra for each waveform. The five sets of spectra were then averaged. To determine whether a phase change other than 180° occurred at these angles the phase spectra of the reference compression wave signal obtained in the pulse - echo mode was subtracted from the phase spectra for a particular angle. The resulting phase difference spectra were plotted for each of the three laser energy settings and are shown, Fig. 4. 28, for the laser energy setting of (301 ± 9) mJ / pulse only. Also shown are the average phase changes for each angle determined from the phase difference spectra for each laser

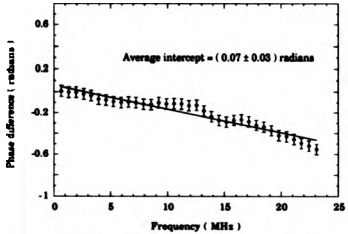

Figure 4. 28a : Phase difference spectrum of reference reflection and 10° offset reference reflection

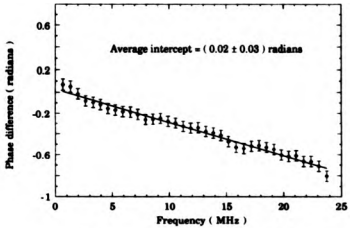

Figure 4. 28c : Phase difference spectrum of reference reflection and 50° offset reference

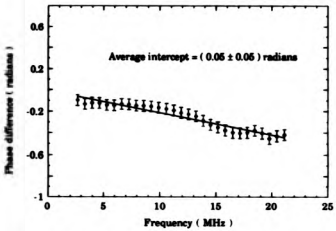

Figure 4. 28b : Phase difference spectrum of reference reflection and 30° offset reflection

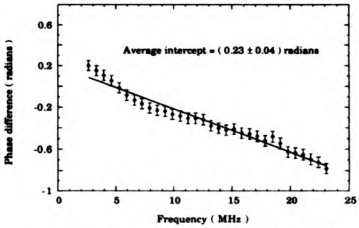

Figure 4. 28d : Phase difference spectrum for reference and 60° offset reference

energy used. These data indicate that, except for the 60° angle of incidence, there is little zero phase change between the reference pulse - echo pulse and the reference reflections for the other angles of incidence. The 60° angle of incidence has an average phase change of (0.23 ± 0.04) radians or (13 ± 2)° if a phase lag is taken as positive or - (2.91 ± 0.04) radians or - (167 ± 2)° if a phase lag is taken as negative. The amplitudes of the 10°, 30°, 50° and the 60° angle of incident reflected compression waves expressed as a ratio relative to the reference pulse - echo compression wave amplitude were ~ 1, (0.68 ± 0.07), (0.51 ± 0.07) and (0.42 ± 0.07) respectively. These values are not dissimilar to the theoretically predicted ratios of 0.96 (10°), 0.77 (30°), 0.52 (50°) and 0.45 (60°) for a Poisson' s ratio of 0.345 (aluminium) given by, for example, Achenbach (1987).

4. 9. 2 : Results

Compression waves incident and scattered from the various slot widths at the particular angles of incidence cited above were used, in conjunction with the reference reflection for the same angle of incidence, to determine the phase difference spectrum and hence the phase change. The phase difference spectra obtained as a function of the angle of incidence for a 1 mm, 2 mm, 4 mm and 8 mm wide slot are shown in Figs. 4. 29 - 4.32 respectively. Similar features discussed in the previous section are shown on these spectra. For slot widths of < 8 mm the phase difference has a finite gradient and finite intercept. The phase difference spectra as a function of angle for the 8 mm wide slot (Fig. 4. 32) is of interest. At angles of incidence of ≤ 30° the phase difference spectra have essentially zero gradient and intercept. As the

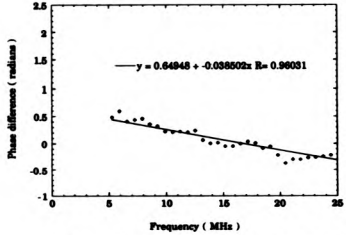

Figure 4. 29b : Phase difference spectrum of 1 mm wide slot for 30° angle of incidence

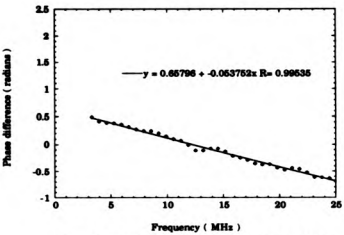

Figure 4. 29a : Phase difference spectrum of 1 mm wide slot for 10° angle of incidence

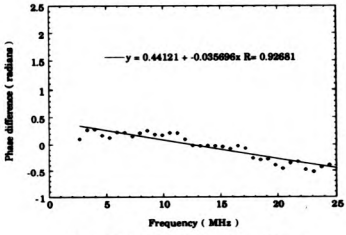

Figure 4. 29c : Phase difference spectrum of 1 mm slot for 50° incident compression wave

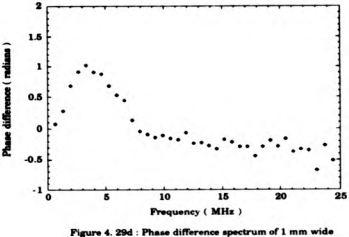

Figure 4. 29d : Phase difference spectrum of 1 mm wide slot for 60° angle of incidence

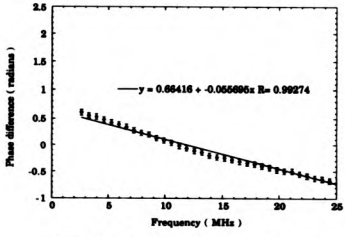

Figure 4. 30a : Phase difference spectrum of 2 mm wide slot for 10° angle of incidence

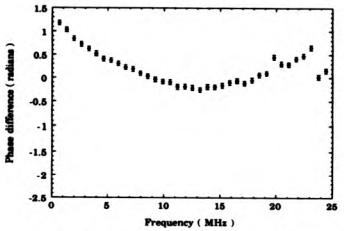

Figure 4. 30b : Phase difference spectrum of signal scattered from 2 mm wide slot for 30° angle of incidence

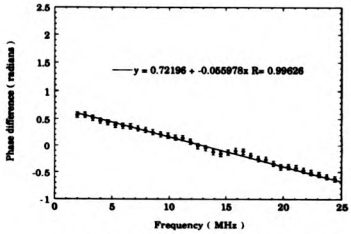

Figure 4. 30c : Phase difference spectrum of signal scattered from 2 mm wide slot for 50° angle of incidence

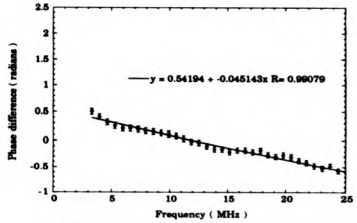

Figure 4. 30d : Phase difference spectrum of signal scattered from 2 mm wide slot for 60° angle of incidence

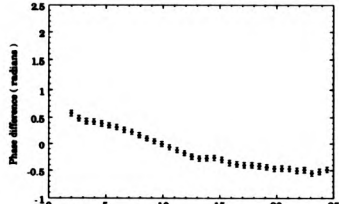

Figure 4. 31a : Phase difference spectrum of signal scattered from 4 mm wide slot for 10° angle of incidence

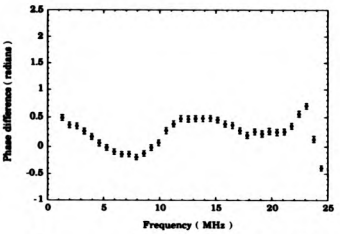

Figure 4. 31b : Phase difference spectrum of signal scattered from 4 mm wide slot for 30° angle of incidence

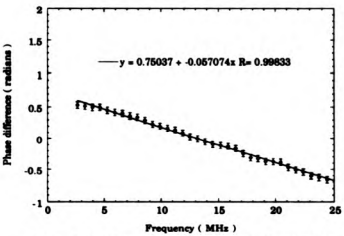

Figure 4. 31c : Phase difference spectrum of signal scattered from 4 mm wide slot for 50° angle of incidence

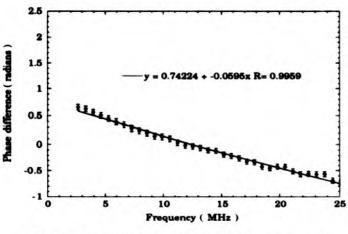

Figure 4. 31d : Phase difference spectrum of signal scattered from 4 mm wide slot for 60° angle of incidence

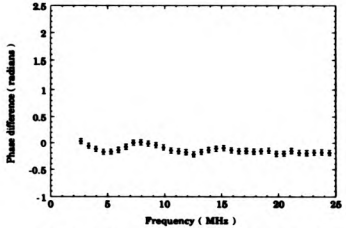

Figure 4. 32a : Phase difference spectrum of signal scattered from 8 mm wide slot for 10° angle of incidence

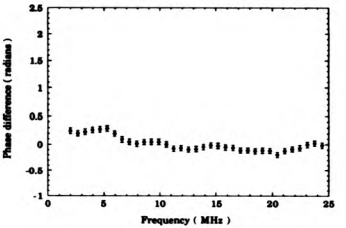

Figure 4. 32b : Phase difference spectrum of signal scattered from 8 mm wide slot for 30° angle of incidence

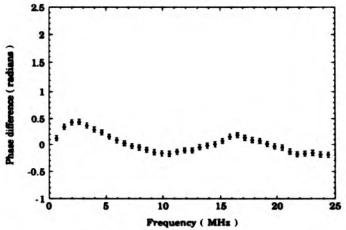

Figure 4. 32c : Phase difference spectrum of signal scattered from 8 mm wide slot for 50° angle of incidence

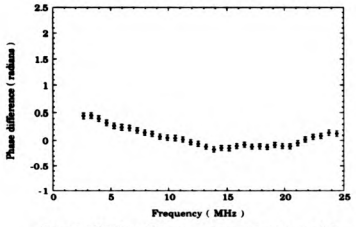

Figure 4. 32d : Phase difference spectrum of signal scattered from 8 mm wide slot for 60° angle of incidence

angle of incidence increases further it is observed that the spectra has finite gradient with intercept of ~ 0.6 radians. The average phase change determined from the phase difference spectra for these and the other slots for all the laser energies used are listed in Table 4. 1.

4. 2. 3 : Discussion

The magnitudes of the phase change of the ultrasonic compression waves scattered from slots of widths of ≤ 6 mm for angles of incidence of ≤ 30° were not significantly different from the average phase change value obtained in the previous section. The exception is the phase change obtained for a 2 mm wide slot and 30° angle of incidence. This difference is thought to be due to an error in the experimental measurement. Phase change values for angles of incidence of > 30° did show a more significant difference. No general trend was apparent from the phase change data for these angles of incidence.

An analysis similar to that described in the previous section is implemented. The component of the incident ultrasonic wavelength parallel to the slot top, λ_v, is evaluated by replacing λ with $\lambda_v = \lambda \cos \varnothing$ where $\varnothing$ is the angle of incidence and λ_v decreases with increasing $\varnothing$. The Fresnel diameters, for a particular frequency, are thus reduced at the larger angles of incidence in comparison to the diameter for a pulse - echo mode of operation. For example, the wavelengths, λ, generated by the laser source are in the range (6.4 - 0.32) mm which, for an angle of incidence of 60°, results in ultrasonic wavelengths parallel to the slot top of (3.2 - 0.16) mm. The effective Fresnel diameters in the vicinity of a slot top are thus in the range (11 - 2.5) mm whilst in the pulse - echo mode of operation they are in the range (16 - 3.6) mm. Thus the

	Average phase change (radians)			
	Error = ± 0.05 radians			
Slot width (mm)	10°	30°	50°	60°
1	0.66	0.66	?	?
1.3	0.69	0.67	0.69	0.52
2	0.67	1.02	0.72	0.52
4	0.68	0.59	0.74	0.73
6	0.53	?	0.67	0.66
8	?	?	0.61	0.56
10	?	?	?	0.49

Table 4. 1 : Average phase change for various slot widths as a function of the angle of incidence

transition from a purely backwall reflection to a backwall plus slot corner interaction, for a particular angle of incidence, occurs at comparatively smaller slot widths. Correspondingly, for a particular slot width, the frequency at which the transition from finite gradient and finite intercept to zero gradient and zero intercept would be expected to occur at smaller frequencies if the incident compression wave interacts with both corners of the slot.

As the slot width increases however, there is a greater likelihood that the incident compression wave will interact with the slot corner nearest to the source. There will be less of an interaction with the slot corner nearest to the detector. Compression waves incident at angles of $\geq 50°$ upon slot widths of ≥ 6 mm would be expected to have zero phase difference over the useful frequency range if the incident ultrasound interacted equally with both corners of the slot. As stated above, the slot corner nearest to the source interacts more strongly than the other slot corner and thus a different phase change is expected to occur. This is observed in the phase difference spectra for these larger angles of incidence and slot widths illustrated in Figs. 4. 29 - 4. 32.

Analysis of the average phase change values for a particular angle of incidence and slot width (Table 4. 1), suggests that a phase change comparable to that obtained in the previous section is obtained, at all angles of incidence, for slot widths of ≤ 1.3 mm. Determination of the phase change of the ultrasonic compression wave scattered from a crack using the source and detector in the TOFD arrangement would thus be expected to result in a value in accordance with the theoretically predicted value.

It was not possible to determine the phase change for some of the slot widths and angles of incidence used in this investigation as the phase difference spectra were essentially zero over the useful frequency

range. For slot widths in which it was possible to determine the phase change significant variation was obtained especially for the larger angles of incidence, ≥ 50°. The phase change for these angles of incidence tended to reach a maximum of ~ 0.73 radians for a slot width of 4 mm and then decreased with increasing slot width in accordance with the scattered signal resembling more closely the reference signal. The larger phase difference may be accounted for by the greater interaction of the incident ultrasound with the slot corner nearest to the source. With the source and detector in a pulse - echo arrangement, equal interaction with both corners of the slot occurred. An increasing angle of incidence resulting in an asymmetric interaction with the slot corners.

4. 10 : CONCLUSIONS

An investigation of the phase characteristics of bulk defects using remote laser generation and interferometric detection was undertaken. The aim of the investigation was to provide experimental data to support theoretical predictions, complementing some previous experimental investigations, and to determine whether a particular type of defect had a unique phase characteristic. The properties of laser - generated ultrasound were employed in this investigation, in particular its wide bandwidth nature.

Data were recorded with the laser source and interferometric detector in the Time - of - Flight Diffraction (TOFD) arrangement. This defect detection and sizing technique, which does not rely on signal amplitude to characterise defects, was briefly described with specific

relevance to its application with a remote source and detector. Accuracies of better than 0.5 mm (~ 0.2 x wavelength) have been achieved using piezoelectric transducers on a variety of samples. Laser - generated ultrasound with a much greater bandwidth than piezoelectric transducers has the potential of improving the defect sizing accuracy and resolution. However there are disadvantages to using laser - generated ultrasound and interferometric detection in a TOFD arrangement and, at present, it has not been used to non - destructively test a component in an industrial environment.

Theoretical modelling of the scattering of ultrasound by defects with particular application to a source and detector in a TOFD arrangement was also undertaken by various research groups. The scattering theory most relevant to the TOFD technique utilises the elastodynamic geometrical theory of diffraction which is explicitly formulated to correctly treat the diffracted waves from crack tips. Using this theory it is possible to obtain an expression for the crack opening displacement and hence to obtain the diffraction coefficients for a defect. This is useful for determining the optimum angles of the incident and scattered ultrasound necessary to size a defect. The amplitude and phase of the diffraction coefficients for ultrasonic wave modes incident at angles corresponding to the maxima in the directivities of the thermoelastic and plasma regime sources, predicted by this theory, were shown. Experimental verification of this theory has been reported by several research groups.

The geometrical theory of diffraction predicts a phase change of the ultrasound upon interacting with the top of a crack of - $3\pi / 4$ radians or - 135°, i. e. the ultrasound is delayed - $3\pi / 4$ radians by the scattering process, and $\pi / 4$ radians or 45° for the bottom of a crack. An investigation was undertaken to determine experimentally the phase

characteristics, using a Fourier transform algorithm, of laser - generated ultrasound scattered from various sized slots and holes. The phase change was determined with the source and detector operating in pulse - echo mode and with the source and detector separated at equal angles, ranging from 10° to 60°, from the normal of a slot top.

The phase difference spectra obtained with the source and detector in pulse - echo mode were shown for various sized slots and holes. The difference between the spectra for the slots and holes was obvious in that the phase difference spectra for slots tended to have a finite gradient and finite intercept, whilst, for the holes, the spectra tended to zero gradient and zero intercept. The average intercept for slots of width ≤ 6 mm was - (2.50 ± 0.05) radians or - (143 ± 3)° when a phase lag is taken as negative. This compares favourably to the value obtained by a previous investigation (Burch and Ramsey (1989)) and with the theoretically predicted value.

A transition from finite gradient and finite intercept at low frequencies to zero gradient and zero intercept at higher frequencies was observed to occur on the phase difference spectra for slot widths ~ (6 - 8) mm. This effect is a result of the broadband nature of laser - generated ultrasound. The large wavelength (low frequency) components contained within the ultrasonic compression wave pulse tend to interact with both the slot top and corners resulting in a phase difference spectrum with finite gradient and intercept. The small wavelength (high frequency) components, on the other hand, tend to interact with the slot top only, resulting in a π radians phase change and hence zero phase difference when compared to the reference backwall reflection. It was indicated that the frequency at which this change in gradient occurs could be used to obtain an estimate of the slot width. Unfortunately there was no feature in the phase difference

spectra for the holes whereby an estimate of the hole diameter could be obtained.

The distinct discrepancy between the phase difference spectra for the slots and holes can be used to characterise such defects. The compression waves scattered from these defects are similar when viewed in the time domain and any differences are only highlighted when their phase difference spectra are determined. It is appreciated that the phase difference spectra for holes and for large ($\geq$ 10 mm) slot widths are similar. However, a scan across a defect will reveal information about the lateral extent of the defect and this information, in addition to the phase difference data, may be used to characterise the defect.

The phase difference spectra for the source and detector displaced at equal angles from a slot top normal for various slot widths were also determined. This setup simulated the TOFD arrangement and angles of incidence ranging from 10° to 60° from the slot top normal were used. For slot widths of $\leq$ 1.8 mm and angles of incidence of $\leq$ 30°, the phase change values, determined from the phase difference spectra, were not significantly different from the value obtained using the source and detector in pulse - echo mode. Larger slot widths and angles of incidence exhibited a more significant variation in the phase change values which was accounted for by the asymmetric interaction of the ultrasound with the slot corners.

This chapter has demonstrated the potential usefulness of phase information in the characterisation of defects. Using an algorithm based upon Fourier transform theory, it is possible to obtain the phase difference between two similar shaped pulses. This algorithm was implemented using signals scattered from various sized slots and holes and a reference backwall reflection signal. The phase change upon an

ultrasonic compression wave interacting with a slotted defect ≤ 6 mm wide was - (2.50 ± 0.05) radians or - (143 ± 3)° which compared favourably to the theoretically predicted value and the results from previous investigations. The corresponding phase change for holes was determined and found to be essentially zero, again in agreement with theoretical predictions. Results on slotted samples using the source and detector in a TOFD arrangement resulted in similar phase change values although there was some variation.

Having demonstrated the technique using samples which introduce little noise to the scattered signal from, for example, grain boundary scattering, the next stage would be to determine the phase change of ultrasound scattered from a defect in, for example, a welded section of a structure. The noise which will be superimposed upon the recorded scattered signal from the defect may be reduced by using signal processing techniques such as Synthetic Aperture Focussing (SAFT) and Split Spectrum Processing (SSP) for which references are given in Chapter Two. Data may be recorded by scanning the source and detector over the welded section. The SAFT may then be employed on the recorded A - scans to improve the signal - to - noise ratio. This ratio is further improved when the SSP technique is applied to the SAFT'd waveforms. The phase difference can then be determined using the Split Spectrum Processed waveforms.

Achenbach, J. D. et al. (1982)	' Ray Methods for Waves in Elastic Solids ', (Pitman) (1982)
Achenbach, J. D. (1987)	' Wave propagation in Elastic Solids', 5th print. (North - Holland) (1987)
Achenbach, J. D. et al. (1989)	Metall. Trans., 20A, 619 (1989)
Aindow, A. M. et al. (1984)	NDT Int., 17, 329 (1984)
Barna, B. A. and Johnson, J. A. (1983)	Rev. Prog. Quant. NDE, 2B, 1573 (1983)
Beskos, D. E. (1987)	Appl. Mech. Rev., 40, 1 (1987)
Bond, L. J. (1982)	Res. Tech. in NDT, Vol. VI (1982)
Brigham, E. O. (1974)	' The Fast Fourier Transform ', (Prentice - Hall) (1974)
Buck, O. et al. (1984)	J. Nondestr. Eval., 4, 203 (1984)
Burch, S. F. et al. (1988)	AERE R - 13280 (1988)
Burch, S. F. and Ramsey, A. T. (1989)	Brit. J. NDT, 31, 185 (1989)
Carter, P. (1984)	Brit. J. NDT, 26, 354 (1984)
Chapman, R. K. (1981)	CEGB Report NWR / SSD / RR / 145 / 81 (1981)

Chapman, R. K. and Toft, M. W. (1987) Proc. 4th Europ. Conf. NDT, 684 (1987)

Charlesworth, J. P. and Temple, J. A. G. ' Engineering Applications of Ultrasonic Time - of - Flight Diffraction ', (John Wiley) (1989)

Coffey, J. M. and Chapman, R. K. (1983) Nucl. Energy, **22**, 319 (1983)

Curtis, G. J. and Hawker, B. M. (1983) Brit. J. NDT, **25**, 240 (1983)

Datta, S. K. (1977) J. A. S. A., **61**, 1432 (1977)

DeVadder, D. et al. (1989) Proc. 12th World Conf. NDT, 276 (1989)

Eringen, A. C. and Shububi, E. S. (1975) ' Elastodynamics ', Vol. II (Linear Theory), (Academic Press) (1975)

Georgiou, G. A. et al. (1989) Brit. J. NDT, **31**, 551 (1989)

Golan, S. et al. (1980) J. Nondestr. Eval., **1**, 11 (1980)

Gubernatis, J. E. et al. (1977) J. Appl. Phys., **48**, 2804 (1977)

Harris, F. J. (1978) Proc. IEEE, **66**, 51 (1978)

Harumi, K. et al. (1987) IEEE Ultra. Symp., 1067 (1987)

Harumi, K. et al. (1989a) Proc. 12th World Conf. NDT, 235 (1989)

Harumi, K. et al. (1989b) Proc. 12th World Conf. NDT, 279 (1989)

Hawker, B. M. (1983) Nucl. Energy, 22, 309 (1983)

Highmore, P. J. and Rogerson, A. (1987) Proc. 4th Europ. Conf. NDT, 3, (1987)

Hirose, S. and Achenbach, J. D. (1989) Int. J. Num. Meth. Eng., 28, 629 (1989)

Hull, D. R. et al. (1985) Mat. Eval., 43, 1455 (1985)

Jeffreys, H. and B. (1966) ' Methods of Mathematical Physics ', 3rd Ed., (CUP) (1966)

Keller, J. B. (1962) J. Opt. Soc. Am., 52, 116 (1962)

Krautkramer, J. and H. (1977) ' Ultrasonic Testing of Materials', 2nd Ed., (Springer) (1977)

Langenburg, K. J. (1986) World Conf. NDT, Vol. 2, 952 (1986)

Lidington, B. H. et al. (1976) Brit. J. NDT, 18, 165 (1976)

Lilley, J. R. (1989) Proc. 12th World Conf. NDT, 1104 (1989)

Ludwig, R. and Lord, W. (1988) IEEE UFFC - 35, 809 (1988)

Mackiewicz, S. et al. (1986)	World Conf. NDT, Vol. 2, 1124 (1986)
Mak, D. K. (1988)	CSNDT J., 9, 30 (1988)
Mak, D. K. (1989a)	Nondestr. Test. Comm., 4, 121 (1989)
Mak, D. K. (1989b)	Brit. J. NDT, 31, 481 (1989)
Mal, A. K. and Knopoff, L. (1967)	J. Inst. Math. Appl., 3, 376 (1967)
Mashaahvili, E. S. (1987)	Sov. Phys. - Acoust., 33, 175 (1987)
Maue, A. W. (1953)	Z. Angew. Math. Mech., 33, 1 (1953)
Mikata, Y. and Achenbach, J. D. (1988)	J. A. S. A., 83, 38 (1988)
Mura, T. (1968)	' Advances in Mechanical Materials Research ', Vol. 3 (John Wiley) (1968)
Murgatroyd, R. A. et al. (1988)	Int. J. Press. Vess. Pip., 35, 137 (1988)
Nagy, P. B. and Adler, L. (1987)	IEEE Ultra. Symp., 1083 (1987)
Nichols, R. W. and Crutzen, S. (1986)	' Ultrasonic Inspection of Heavy Steel components : The PISC II Final Report ', (Elsevier) (1988)
Noble, B. (1958)	' Methods Based on the Wiener - Hopf Technique ', (Pergamon Press) (1958)

Norris, A. (1983) — Rev. Prog. in Quant. NDE, **2B**, 907 (1983)

Ogilvy, J. A. (1988) — Ultrasonics, **26**, 318 (1988)

Ogilvy, J. A. (1989a) — Proc. 12th World Conf. NDT, 830 (1989)

Ogilvy, J. A. (1989b) — personal communication

Ogilvy, J. A. and Temple, J. A. G. (1983) — Ultrasonics, **21**, 259 (1983)

Pao, Y. H. and Mow, C. C. (1973) — ' The Diffraction of Elastic Waves and Dynamic Stress Concentrations ', (Russak & Co.) (1973)

Paradis, L. et al. (1986a) — Mat. Eval., 44, 568 (1986)

Paradis, L. et al. (1986b) — Mat. Eval., 44, 1344 (1986)

Pilant, W. L. (1979) — ' Elastic Waves in the Earth ', (Elsevier) (1979)

Ravenscroft, F. A. et al. (1989) — AERE R - 13334 (1989)

Ro, R. et al. (1988) — IEEE Ultra. Symp., 1075 (1988)

Sato, M. et al. (1987) — Jpn. J. Appl. Phys. Suppl., **27 -1**, 99 (1987)

Schmitz, V. and Langenburg, K. J. — Proc. 4th Europ. Conf. NDT, 675 (1987)

Scruby, C. B. et al. (1986)	J. Nondestr. Eval., 5, 145 (1986)
Sharpe, R. S. et al. (1984)	' Quality Technology Handbook ', 4th Ed., (Butterworth) (1984)
Silk, M. G. et al. (1987)	' The reliability of Non - destructive Inspection ', (Adam Hilger) (1987)
Silk, M. G. et al. (1989)	Int. J. Mat. Prod. Tech., 4, 215 (1989)
Slesenger, T. A. and Heaketh, G. B.	Acoust. Imag., 14, 547 (1985)
Sotiropoulos, D. A. and Achenbach, J. D.	J. A. S. A., 84, 752 (1988)
Teitel, S. (1978)	J. Appl. Phys., 49, 5763 (1978)
Temple, J. A. G. (1983)	Nucl. Energy, 22, 335 (1983)
Temple, J. A. G. (1985)	Int. J. Pres. Ves. & Piping, 19, 185 (1985)
Temple, J. A. G. (1989)	personal communication
Terpstra, S. et al. (1989)	Proc. 12th World Conf. NDT, 176 (1989)
Thompson, R. B. and Wadley, H. N. G.	Crit. Rev. in Solid State and Mat. Sci., 16, 37 (1989)
Tittmann, B. R. (1983)	Wave Motion, 5, 299 (1983)
Toft, M. W. (1986)	Proc. 21st Brit. Conf. NDT, 193 (1986)

Varadan, V. K. and V. V. (1986) ' Handbook on Acoustic, Electromagnetic and Elastic Wave Scattering, Low and High Frequency Asymptotics', Vol. 2, (North Holland) (1986)

Vopilkin, A. Kh. (1985a) Sov. J. NDT, 21, 18 (1985)

Vopilkin, A. Kh. (1985b) Sov. J. NDT, 21, 143 (1985)

Waterman, P. (1976) J. A. S. A., 60, 556 (1976)

Ying, C. F. et al. (1984) J. Nondestr. Eval., 4, 65 (1984)

Chapter Five

CHARACTERISATION OF SURFACE - BREAKING DEFECTS USING RAYLEIGH WAVES

5. 1 : INTRODUCTION

This chapter describes the investigations into the characterisation of surface - breaking defects using laser - generated Rayleigh waves. Surface - breaking defects are potentially more important to detect than embedded defects as the likelihood of failure is greater (Sharpe et al. (1984)). Rayleigh waves are useful in the detection of such defects as they are surface sensitive displacements. The mode of oscillation of particles supporting a Rayleigh wave is a retrograde ellipse whose normal (vertical) displacement reaches its maximum amplitude at a depth of approximately 0.2 λ_R, where λ_R is the Rayleigh wavelength, and then decays to zero within two wavelengths from the surface. For a point source, the surface amplitude decays at a rate proportional to $1 / \sqrt{}$ (distance) owing to the divergence of the wave beam emitted by the source. This rate of decay is less than for bulk waves which is normally at least 1 / (distance). The usefulness of Rayleigh waves for the characterisation of surface - breaking defects has been recognised since the 1960' s (Viktorov (1967)) and it continues to be an active area of NDT research.

The first part of this chapter gives an outline of the conventional techniques used to characterise surface - breaking defects using Rayleigh waves generated and detected by piezoelectric probes. It is also

possible to use laser ultrasonics for these defect detection techniques. One aspect of the modelling of the Rayleigh wave scattering process is outlined and experimental investigations to confirm the theoretical predictions conducted. In association with this modelling, the change in the Rayleigh wave amplitude and phase on reflection from and transmission through various surface discontinuities was determined.

A technique for determining the surface - breaking defect depth from analysis of the transmitted Rayleigh waveform is also given. This technique is demonstrated for surface - breaking defects perpendicular to the surface and extended to inclined surface - breaking defects. The intention is to assess whether it is possible to determine both the length of the defect and the angle of inclination from analysis of the reflected and transmitted Rayleigh waveforms.

5. 2 : TECHNIQUES FOR CHARACTERISING SURFACE - BREAKING DEFECTS USING RAYLEIGH WAVES

The simplest technique for using Rayleigh waves to detect surface - breaking defects is to use a piezoelectric transducer, operating in pulse - echo mode, and to measure the amplitude of the reflected Rayleigh pulse (Reinhardt and Dally (1970), Viktorov (1967)). This method relies on the amplitude of the reflected pulse to characterise the defect. The larger the defect length / Rayleigh wavelength ratio the larger the reflected amplitude. The disadvantage with this method is that the amplitude of the reflected Rayleigh pulse also depends on other factors unrelated to the defect such as changes in the coupling medium thickness, roughness of the surface and residual stress. This makes

comparison with reference defect reflectors difficult. Also smaller defects, i. e. defect depth / Rayleigh wavelength ratios ≤ 0.2, will reflect little (≤ 20 %) of the incident Rayleigh wave energy and hence may be undetected.

An improvement on this technique is to use separate source and detector transducers (Hudgell et al. (1974), Hall (1976)). If a defect exists between the transducers then the Rayleigh wave travel time is increased owing to the increased path length as it travels up and down the sides of the crack. The deeper the crack the longer the transit time compared with that for transmission between the probes on a defect free surface. This technique has the advantage in that it is indifferent to amplitude fluctuations.

Lidington and Silk (1975) showed that the defect size could be obtained using the time delay between the Rayleigh wave reflected from the top and from the bottom of the defect. They noted that the technique described above could not be used when testing, for example, T - butt welds. Using a single transducer in pulse - echo mode, they demonstrated that defects ranging from 2 mm to 30 mm long could be accurately sized. Lloyd (1975) described a similar method of determining the defect depth using shear waves generated on the backwall of the sample. The time difference between the signals corresponding to reflection of the shear wave from the corner and tip of the defect was used to calculate the defect depth.

A problem arises for smaller defects as the signals from the top and bottom of the defect overlap and become indistinguishable when using conventional piezoelectric transducers. Morgan (1974) and Hudgell et al. (1974) describe two methods for overcoming this problem by processing the data in the frequency domain. One method involves manipulation of the complex frequency spectra from which a time

signal is reconstituted and the other uses modulus spectra from which a cepstrum is generated.

Burger and Testa (1981) recognised that a Rayleigh wave containing a range of frequency components would have all frequencies at the surface and only lower frequencies deeper down. The deeper, low frequency, long wavelength portion of the incident wave will tend to pass underneath a defect with little or no reflection whilst the near surface, high frequency, short wavelength components will interact strongly with it. In effect the defect acts as a low pass filter for the deeper portions of the Rayleigh waves. By performing an FFT on the transmitted Rayleigh wave signal and observing the power spectrum, a cut - off frequency could be determined and related to the defect depth. Cooper et al. (1986a, 1986b) performed an FFT on the laser - generated Rayleigh wave signals representing reflection from and transmission through a 0.75 mm slot and compared these power spectra to the power spectrum of the incident Rayleigh wave. The spectra showed that the high frequency, small wavelength, components were reflected by the slot whilst the low frequency, large wavelength, components were transmitted through the slot. Slot depths could be estimated from these spectra but the choice of cut - off frequency appears to be arbitrary and thus suspect to large errors.

5. 3 : MODELLING OF THE RAYLEIGH WAVE SCATTERING PHENOMENON

To obtain a better understanding of the complex interaction of Rayleigh waves with surface - breaking defects, Mendelsohn et al.

(1980) and Achenbach et al. (1980) investigated theoretically the scattering phenomenon. The authors developed a theory which described the scattering of incident surface waves by a surface - breaking defect in a two - dimensional geometry. Achenbach et al. (1980) presented a more simple approximate approach to the problem. A Rayleigh wave propagating on a crack face is reflected and diffracted by the edge of the crack. For convenience two systems of symmetric and antisymmetric Rayleigh waves, with respect to the plane of the crack, propagating on both crack faces were considered. For a system of symmetric (antisymmetric) Raylaigh waves the tangential (normal) displacements are continuous across the crack faces and the normal (tangential) displacements are discontinuous. These symmetric (antisymmetric) Rayleigh waves are reflected as a system of symmetric (antisymmetric) Raylaigh waves with specific reflection coefficients. The pairs of symmetric and antisymmetric Rayleigh waves thus generated at the edge of the crack are reflected and transmitted by the mouth of the crack. The transmitted surface is equivalent to the superposition of a pair of symmetric surface waves with displacements normal to the crack face and a pair of antisymmetric surface waves with displacements tangential to the crack face.

These surface motions generated by the incident ray are reflected back and forth between the crack edge and crack mouth and they are also transmitted to the free surface half - space. Thus the total back - scattered field can be considered as the superposition of the direct reflection from the crack and the transmission from the surface motion on the crack faces back onto the free surface. Similarly the forward - scattered field is obtained by superimposing the various transmissions to the other side of the crack on the crack - face motions.

The exact back - scattered and forward - scattered vertical displacements obtained by Mendelsohn et al. (1980) are shown in Fig. 5. 1 as a function of the dimensionless parameter $k_R d$ where k_R is the Rayleigh wavenumber and d is the crack depth. Note the existence and spacing of distinct maxima and minima at specific frequencies. These frequencies correspond to resonant modes of vibrations of surface waves propagating on the faces of the crack. The spacing between successive peaks or troughs can be directly related to the crack depth, d, if the wavelength of the incident Rayleigh wave is unchanged. For sufficiently large $k_R d$, the spacing is nearly equal to $k_R d = \pi$. Thus if Δk_R is the spacing between successive peaks or troughs then the depth of a crack can be determined from

$$d = \frac{\pi}{\Delta k_R} \qquad (5.1)$$

This relation is thought to be valid for $k_R d > 6$. Other theoretical and experimental studies into this phenomenon have been reported by Yew et al. (1984), Doyle (1986) and Doyle and Scala (1987, 1990).

5. 4 : EXPERIMENTAL INVESTIGATIONS INTO THE RAYLEIGH WAVE RESONANT PHENOMENON

Experimental plots of the back - scattered and forward - scattered displacement fields as a function of the dimensionless parameter $k_R d$ can be obtained in two ways. Either by keeping the Rayleigh wavelength fixed and using different sized slots (Yew et al. (1984)) or by using a

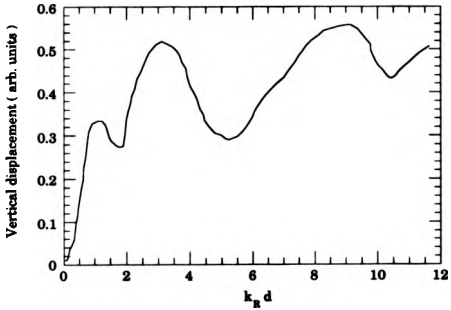

Figure 5. 1a : Vertical displacement of the back - scattered (reflected) Rayleigh wave (after Mendelsohn et al. (1980))

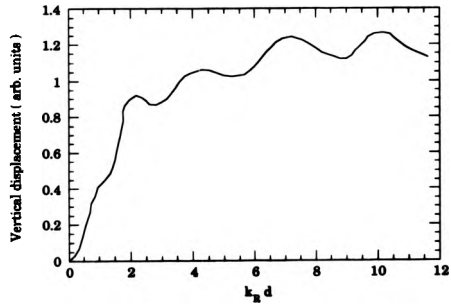

Figure 5. 1b : Vertical displacement of the forward - scattered (transmitted) Rayleigh wave (after Mendelsohn et al. (1980))

slot with a fixed depth and varying the frequency of the incident Rayleigh wave (Doyle (1986), Doyle and Scala (1987, 1990)). Doyle (1986) extended the theory described above to consider corners containing cracks. Initially vertical and horizontal cracks in right - angle corners were considered and expressions derived for the forward - and back - scattered Rayleigh wave displacement fields. These were of the same shape as those shown in Fig. 5. 1 and thus the depth of the defect could be determined from measurements of the spacing between successive peaks or troughs. The theory was extended to cracks and corners with arbitrary angles. Doyle (1986) concluded that the crack depth could be determined for any crack or corner angle although it was not possible to determine the angle of inclination of the crack.

Doyle and Scala (1987, 1990) reported experimental studies on corner cracks of arbitrary angle to verify the theoretical predictions. Broadband Rayleigh waves, with frequency components in the low MHz range, were generated thermoelastically by a Q - switched Nd:YAG laser with a half width pulse duration of 25 ns. The incident and reflected Rayleigh waves were detected using a piezoelectric transducer 0.6 mm in radius with a flat Rayleigh wave frequency response between 0.2 and 1.4 MHz. This frequency response sensibly matched the laser - generated Rayleigh wave frequency range. Modulation in the frequency domain was observed and, within error, compared favourably to the measured crack depth. The angle of the crack relative to the surface was not determined however.

An investigation into the use of this technique for defect sizing using laser generation and interferometric detection was conducted by the author. Fig. 5. 2 illustrates the experimental arrangement. Rayleigh waves were generated with the Q - switched Nd:YAG laser pulse at a fixed energy of ~ 200 mJ / pulse and focussed to a ~ 2 mm diameter spot

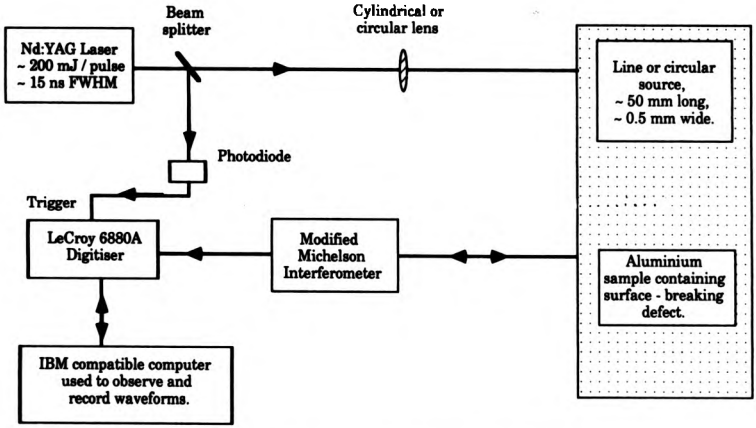

Figure 5. 2 : Experimental arrangement for the investigation of Rayleigh wave interactions with surface - breaking defects

size. A series of aluminium blocks with different sized slots normal to the surface ranging in depth from 0.6 mm to 5 mm and width of ~ 0.25 mm were used to represent surface - breaking defects. This range of slot depths was chosen so as to assess experimentally the range of validity of the technique. An aluminium block with no surface defects was used as the reference sample and Rayleigh waves were recorded at a set distance from the source. The source to detector distance for the recording of the reference Rayleigh waves was chosen to be the same as the distance that the reflected Rayleigh wave would travel from the source to the defect and back to the detector spot. Thus any differences in the Rayleigh waves would be due to the defect only. The laser source was positioned 50 mm from the slot and the detector spot 10 mm from the slot. This was to ensure that both source and detector were in the far field region of the slot. Transmitted Rayleigh waves were not used for this particular investigation as the signal - to - noise ratio was too low for the subsequent data processing.

Data processing similar to that described by Doyle and Scala (1990) was used to produce plots of reflected Rayleigh wave displacement as a function of frequency. The first step was to perform an FFT on both the incident and the reflected Rayleigh waves and to calculate the power spectra for the two signals. The digitiser has a sampling interval of 742 ps and the waveforms were effectively zero filled to 16384 points giving a frequency increment of 0.08 MHz. A Gaussian window was applied to the waveform before it was Fourier transformed. The incident Rayleigh wave power spectrum, Fig. 5. 3b, illustrates that significant frequency components up to ~ 3 MHz are present within the waveform. Using a representative frequency of ~ 1 MHz, corresponding to a wavelength of ~ 3 mm in aluminium (V_R = 2.906 mm / μs), the relation $k_R d > 6$ is satisfied for slot depths $d \geq 3$ mm.

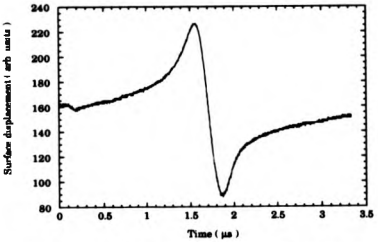

Figure 5. 3a : Incident laser - generated Rayleigh wave before interacting with a surface discontinuity.

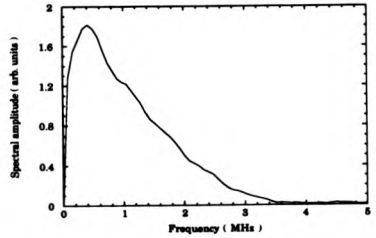

Figure 5. 3b : Power spectrum of incident Rayleigh wave.

The logarithm (to the base 10) of the incident Rayleigh wave power spectrum was calculated and subtracted from the corresponding logarithm (to the base 10) of the reflected Rayleigh wave power spectrum. The result was plotted as a function of frequency over the useful frequency range for each slot size investigated and are shown in Figs. 5. 4 - 5. 6.

Oscillations in the plots are seen for all slot depths and they are similar in shape to those predicted by theory. The plots also illustrate that as the slot depth increases the frequency of the oscillations decreases in agreement with the theory. Using the frequency of oscillation, it is possible to estimate the slot depth using

$$d = \frac{V_R}{2\Delta f_R} \qquad (5.2)$$

where V_R is the Rayleigh wave velocity,

and Δf_R is the frequency of the oscillations.

This equation comes from rearranging and substituting for the wavenumber, k_R, in the original expression given by Achenbach et al. (1980), Mendelsohn et al. (1980). Table 5. 1 compares the slot depth calculated using the frequency of oscillation from Figs. 5. 4 - 5. 6 and (5. 2) with the measured slot depth. Unfortunately the calculated slot depth for slots of > 2 mm deep vary significantly from the actual slot depth. The expected frequency of the oscillations becomes < 0.6 MHz and this is not observed in the Log (Power) - Frequency plots. The reasons for this discrepancy are, at present, unclear. For slot depths of ≤ 2 mm the agreement between measured and calculated slot depth is good indicating that the region of validity extends beyond the relation $k_R d > 6$.

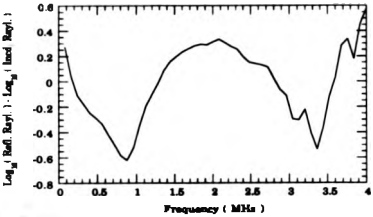

Figure ii. 4a : Rayleigh wave resonance spectrum for 0.6 mm deep slot

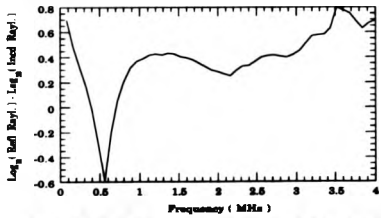

Figure 5. 4b : Rayleigh wave resonance spectrum for 1 mm deep slot

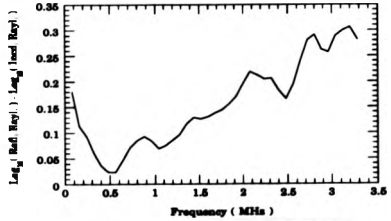

Figure 5. 4c : Rayleigh wave resonance spectrum for 1.5 mm deep slot

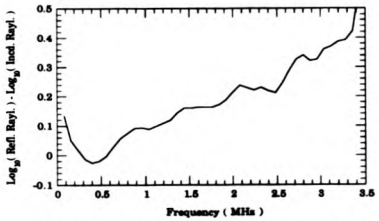

Figure 5. 5a : Rayleigh wave resonance spectrum for 2 mm deep slot

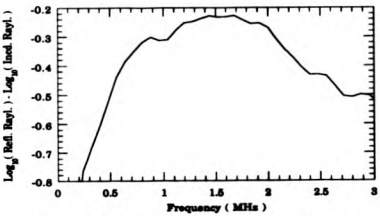

Figure 5. 5b : Rayleigh wave resonance spectrum for 2.5 mm deep slot

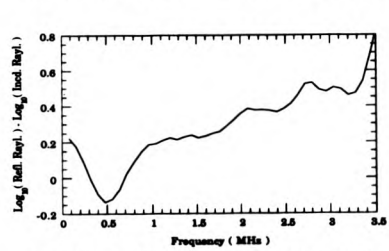

Figure 5. 5c : Rayleigh wave resonance spectrum for 3 mm deep slot

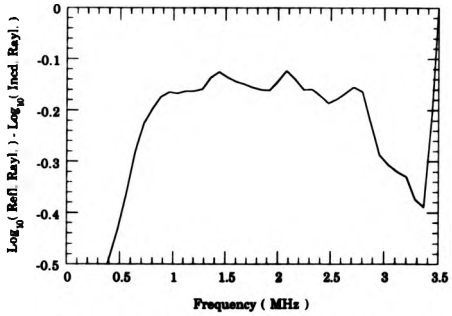

Figure 5. 6a : Rayleigh wave resonance spectrum for 3.6 mm deep slot

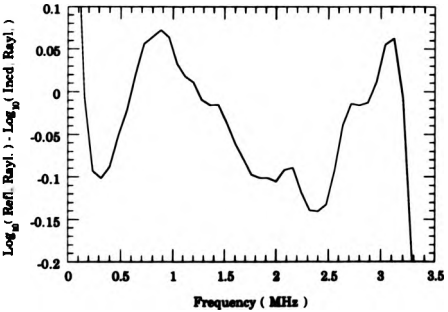

Figure 5. 6b : Rayleigh wave resonance spectrum for 5 mm deep slot

Note that the frequency of oscillation could be obtained more accurately by performing an additional Fourier transform on the Log (Power) - Frequency plots.

Average Δf_R (MHz)	Calculated slot depth (mm)	Measured slot depth (mm)
2.6 ± 0.1	0.56 ± 0.02	0.6 ± 0.1
1.42 ± 0.05	1.02 ± 0.04	1.0 ± 0.1
1.00 ± 0.03	1.44 ± 0.04	1.5 ± 0.1
0.63 ± 0.04	2.3 ± 0.2	2.0 ± 0.1
?	?	2.5 ± 0.1
0.78 ± 0.05	1.9 ± 0.1	3.0 ± 0.1
0.63 ± 0.05	2.3 ± 0.2	3.6 ± 0.1
?	?	5.0 ± 0.1

Table 5. 1 : Comparison between the calculated and measured slot depths.

5. 5 : REFLECTION AND TRANSMISSION COEFFICIENTS

Important to the theoretical work on Rayleigh wave scattering by surface - breaking defects are the reflection and transmission coefficients for the various corners of a defect and for the defect as a whole. Both theoretical and experimental investigations have been undertaken to determine the values of these coefficients.

Investigations were undertaken by the author to determine reflection and transmission coefficients using laser - generated Rayleigh waves and interferometric detection. When a Rayleigh wave

reaches an abrupt change in the surface over which it is propagating, other Rayleigh waves with different amplitude and phase are generated. For example, when a Rayleigh wave interacts with a 90° corner (or a quarter space), the corner effectively becomes a secondary source producing a Rayleigh wave which propagates back towards the source, a Rayleigh wave which propagates along the other surface around the corner and bulk (compression and shear) waves. The reflected and transmitted Rayleigh waves from this 90° corner have a different amplitude and phase than the incident Rayleigh wave.

The aim of this investigation was to determine both the amplitude and phase change of the reflected and transmitted Rayleigh waves after interacting with the 90° and 270° corners of an aluminium step and with various sized slots in aluminium. The amplitude reflection and transmission coefficients were determined by calculating the ratio

$$\frac{\text{Reflected / Transmitted Rayleigh wave peak - peak displacement}}{\text{Incident Rayleigh wave peak - peak displacement}}$$

for the same propagation distance in both cases, for the reasons cited in the previous section. Using the modified Michelson interferometer to record the incident and reflected / transmitted Rayleigh waves it is possible to calculate the surface displacement from the output voltage of the interferometer using (McKie (1987))

$$x = \frac{\lambda V}{4\pi V_o} \qquad (\text{nm}) \qquad (5.3)$$

where x is the surface displacement (in nm),

V is the stabilised (signal) output voltage,

V_o is the unstabilised output voltage,

and λ is the wavelength of the He - Ne laser (= 632.8 nm).

Thus the different unstabilised output voltages from the interferometer at different points on the sample surface can be normalised by converting voltages into displacements.

The source used (~ 200 mJ / pulse, ~ 2 mm diameter spot size) was positioned 50 mm away and the detector spot positioned at distances of ≥ 10 mm away from the surface discontinuity under investigation. Previous investigations (Reinhardt and Dally (1970), Vu and Kinra (1985)) have indicated that the coefficients change with distance from a surface discontinuity. A steady value for the coefficient is obtained only in the far field region, ≥ 10 mm from the discontinuity in this case. This phenomenon is investigated further in the section on reflection and transmission coefficients for various sized slots.

The phase change was determined using data processing similar to that described in Chapter Four. For a particular propagation distance, an FFT was performed on both the incident and reflected / transmitted Rayleigh waves. The phase change algorithm was not implemented using transmitted Rayleigh waves through slots as the signal - to - noise ratio of the recorded signal was insufficient. For each waveform the maximum absolute displacement point was positioned at the centre + 1 of the waveform and the waveform effectively zero filled to 16384 points. A Gaussian window was applied to the 16384 point waveform and the FFT algorithm implemented. The phase difference spectrum is obtained by subtracting the phase spectrum of the incident Rayleigh wave from the phase spectrum of the reflected / transmitted

Rayleigh wave, over the useful frequency range (~ 3 MHz), for a particular surface discontinuity size. A best straight line fit to the data was obtained and extrapolated to zero frequency. This intercept was the phase change produced by the surface discontinuity only. Achenbach et al. (1980) determined the phase of the reflected and transmitted Rayleigh waves from the location of the peaks and troughs in their displacement as a function of k_R d plots. This method was not adopted in this investigation as the errors involved in the location of the peaks and troughs would be too large.

5. 5. 1 : Determination of the Reflection and Transmission coefficients at various stages around a step

Surface - breaking defects may be modelled as a combination of 90° and 270° solid corners. To understand the complex interaction of Rayleigh waves with such defects it is worthwhile splitting the defect into its component parts and investigating the interaction of Rayleigh waves with these component parts. Lapwood (1961) considered the problem of the interaction of a Rayleigh wave with a 90° corner. On transmission of the Rayleigh pulse round a corner it was shown that the shape of the pulse changes. There is a change both in the amplitude and phase of the pulse. Other authors (Viktorov (1967), Munasinghe and Farnell (1973), Farnell (1978), Bond (1979), Gautesen (1985) and Blake and Bond (1989a, 1989b) have concerned themselves with the determination of the amplitude and phase change on reflection from and transmission around a 90° corner. Their theoretical and experimental investigations have in some cases been extended to 270°

corners. The main results from these investigations are summarised in Table 5. 2.

The experimental arrangement used to investigate Rayleigh waves at various stages around a step is similar to that shown in Fig. 5. 2 with the slotted sample replaced by an aluminium step. The height of the step is very much greater than the largest wavelength contained in the Rayleigh wave. Thus it may be considered as an infinite step height in that the incident Rayleigh wave is not perturbed by the bottom of the step. Various configurations of the source and detector beam around the step were used to investigate the change in the Rayleigh wave as it propagated around the step. The shape of the Rayleigh wave sampled at various locations around the step is shown in Fig. 5. 7 for the source on the higher level (the incident Rayleigh wave first interacts with the 90° corner - a downstep) and in Fig. 5. 8 for the source on the lower level (the incident Rayleigh wave first interacts with the 270° corner - an upstep).

When the incident Rayleigh wave interacts with the 90° corner first (Fig. 5. 7), a Rayleigh wave, similar in shape to the incident wave, is reflected back towards the source and a surface displacement is propagated around the corner. The shape of this transmitted Rayleigh wave is unipolar and similar in shape to the in - plane displacement of the incident Rayleigh wave as predicted by Lapwood (1961). When this 90° corner transmittad Rayleigh wave propagates around the 270° corner it remains unipolar but its polarity changes by approximately 180°. Less than 5 % of the incident Rayleigh wave amplitude is reflected back towards the 90° corner at this juncture.

When the incident Rayleigh wave interacts with the 270° corner first (Fig. 5. 8), less than 5 % of the incident Rayleigh wave amplitude is reflected back towards the source and the transmitted Rayleigh wave

Model used / author	90° / 270° corner	Poisson's ratio : σ	Trans. coeff.	Trans. energy : E_t	Refl. coeff.	Refl. energy : E_r	Trans. phase shift	Refl. phase shift	Energy lost to bulk modes
Experiment (Knopoff & Gangi (1960))	270°	0.266	0.28	0.08	< 0.1	< 0.01			0.91
Theoretical (Mal & Knopoff (1965))	270°	0.25	0.25	0.06			135°		
Finite diff. (Munasinghe and Farnell (1973))	270°	0.245	0.28 ± 0.02	0.079	0.09 ± 0.01	0.008	(140 ± 10)°	-(125 ± 10)°	0.91

Model used / author	90° / 270° corner	Poisson's ratio : σ	Trans. coeff.	Trans. energy : E_t	Refl. coeff.	Refl. energy : E_r	Trans. phase shift	Refl. phase shift	Energy lost to bulk modes
Experiment (de Bremaecker (1958))	90°	0.17	0.63 ± 0.06	0.40	0.38 ± 0.04	0.14			0.46
Experiment (Pilant et al. (1964))	90°	0.25	0.67	0.45	0.252	0.06	(0.054 ± 0.017) radians	-(0.208 ± 0.017) radians	0.49
Experiment (Viktorov (1967))	90°	0.34	0.70	0.49	0.60	0.36			0.15
Finite diff. (Munasinghe and Farnell (1973))	90°	0.245	0.64 ± 0.02	0.41	0.36 ± 0.02	0.13	-(79 ± 5)°	(38 ± 5)°	0.46

Model used / author	90° / 270° corner	Poisson's ratio : σ	Trans. coeff.	Trans. energy : E_t	Refl. coeff.	Refl. energy : E_r	Trans. phase shift	Refl. phase shift	Energy lost to bulk modes
Analytical (Cuozzo et al. (1977))	90°	0.33	0.75	0.56	0.38	0.14	- 0.63	- 0.84	0.3
Finite diff.	90°	0.29	-	-	0.43 ± 0.05	0.19			-
(Bond (1979))		0.34	0.6 ± 0.1	0.36	0.37 ± 0.05	0.14			0.5
Pseudo - node model	90°	0.24	0.65 ± 0.05	0.42	0.39 ± 0.05	0.15			0.43
		0.29	0.47 ± 0.05	0.22	0.56 ± 0.05	0.31			0.47
(Bond (1979))		0.34	0.64 ± 0.05	0.41	0.49 ± 0.05	0.24			0.35
2nd order	90°	0.24	0.57 ± 0.05	0.33	0.43 ± 0.05	0.19			0.50
(Bond (1979))		0.34	0.59 ± 0.05	0.35	0.47 ± 0.05	0.22			0.44
Analytical (Achenbach et al. (1980))	90°	0.33	0.60	0.36	0.40	0.16	- 1.60 radians	0.60 radians	0.48

Model used / author	90° / 270° corner	Poisson's ratio : σ	Trans. coeff.	Trans. energy : E_t	Refl. coeff.	Refl. energy : E_r	Trans. phase shift	Refl. phase shift	Energy lost to bulk modes
Tone Burst (Kinra & Vu (1983))	90°	0.34	0.61	0.37	0.43	0.19			0.44
Spectroscopy (Kinra & Vu (1983))	90°	0.34	0.59	0.35	0.43	0.19			0.46
Theoretical	90°	0.17	0.68	0.46	0.27	0.07	-(85 ± 5)°	(51 ± 5)°	0.47
(Gautesen		0.25	0.68	0.46	0.32	0.10	-(85 ± 5)°	(40 ± 5)°	0.44
(1985))		0.33	0.67	0.45	0.39	0.15	-(85 ± 5)°	(28 ± 5)°	0.40
Finite diff.	90°	0.29	0.68 ± 0.01	0.46	0.35 ± 0.01	0.12			0.42
(Bond (1988a))	270°	Mild Steel	0.27 ± 0.01	0.07	0.072 ± 0.002	0.005			0.93

Table 5. 2 : Summary of the main results for Rayleigh wave interactions with 90° and 270° corners

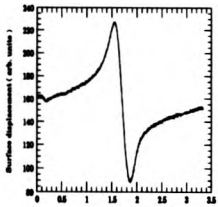

Figure 5. 7a : Incident Rayleigh wave

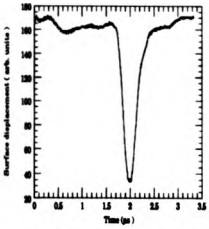

Figure 5. 7c : Rayleigh wave transmitted through 270° corner

SOURCE

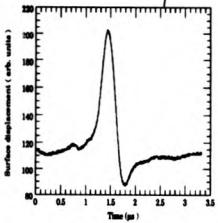

Figure 5. 7b : Rayleigh wave reflected from 90° corner

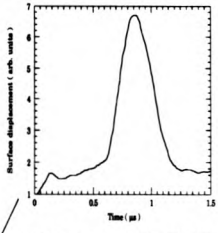

Figure 5. 7d : Rayleigh wave transmitted through 90° and 270° corners

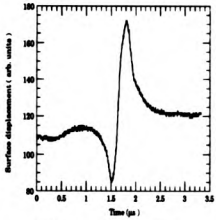

Figure 5. 8b : Rayleigh wave transmitted through 270° corner

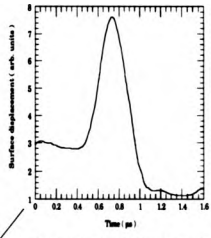

Figure 5. 8d Rayleigh wave transmitted through 270° and 90° corners

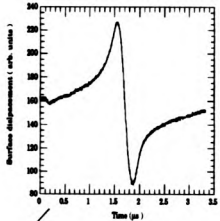

Figure 5. 8a : Incident Rayleigh wave

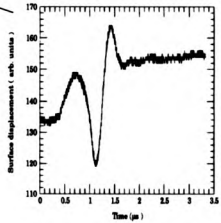

Figure 5. 8c : Rayleigh wave reflected from 90° corner

SOURCE

remains bipolar but goes negative first. The Rayleigh wave reflected from the 90° corner remains bipolar whilst the transmitted Rayleigh wave becomes unipolar and similar in shape to the Rayleigh wave transmitted through the 90° and 270° corners respectively.

In addition to observing the shape of the Rayleigh waves at various locations around the step more quantitative measurements of the amplitude were made and the phase change on interacting with the various discontinuities determined. The phase spectra were determined by aligning the maximum absolute displacement in each waveform to the centre + 1 point. It is unclear whether this corresponds to a similar point of a waveform for the calculations reported in the published papers containing phase change values. The phase difference spectra for the Rayleigh waves reflected from and transmitted around 90° and 270° corners are shown in Fig. 5. 9. The coefficients obtained for the Rayleigh wave interaction with a 90° and 270° corner are summarised in Figs. 5. 10 and 5. 11 respectively. Other results for Poisson ratios similar to aluminium may be found in Table 5. 2.

5. 5. 2 : Determination of the Reflection and Transmission coefficients of various sized slots.

The reflection and transmission coefficients of various sized slots perpendicular to the sample surface and ranging in depth from (0.6 - 5) mm were determined. In addition the phase change of the Rayleigh wave reflected from each slot was determined using the algorithm previously described. Theoretical values for the reflection and transmission coefficients are normally plotted as a function of the ratio

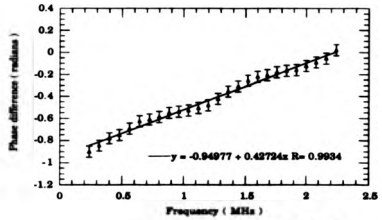

Figure 5. 9a : Phase coherence spectrum for Rayleigh wave reflected from 90° corner

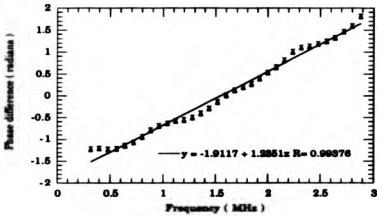

Figure 5. 9b : Phase difference spectrum for Rayleigh wave transmitted through a 90° corner

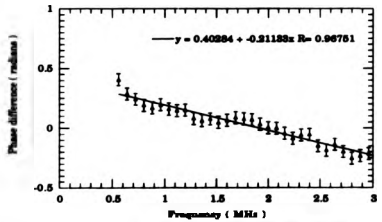

Figure 5. 9c : Phase difference spectrum for Rayleigh wave transmitted through a 270° corner

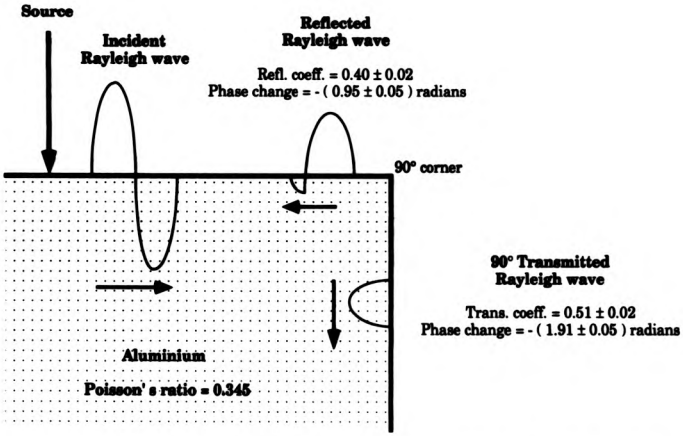

Figure 5. 10 : Reflection and Transmission coefficients for Rayleigh wave incident upon a 90° corner.

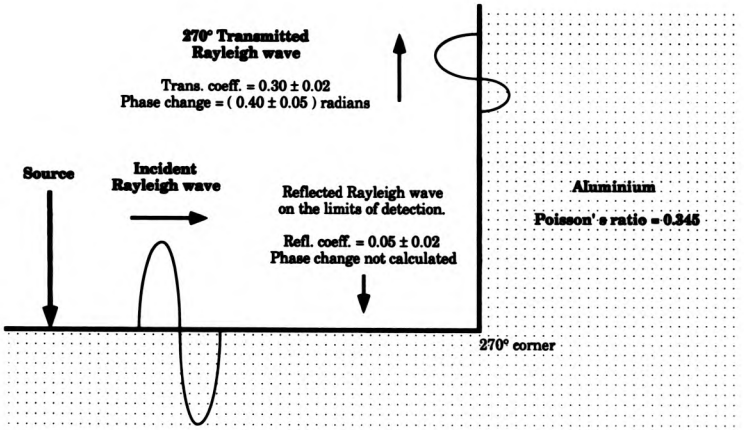

Figure 5. 11 : Reflection and Transmission coefficients for Rayleigh wave incident upon a 270° corner

defect depth / Rayleigh wavelength (e. g. Angel and Achenbach (1984), Hirao et al. (1982)). To compare the results obtained in this investigation with the theoretical values, a suitable wavelength near to the maximum in the laser - generated Rayleigh wave power spectrum was chosen. For convenience, a frequency of ~ 1 MHz (from Fig. 5. 3) was chosen which corresponds to a wavelength of ~ 3 mm. Plots of the amplitude reflection and transmission coefficients as a function of the ratio defect depth / Rayleigh wavelength using a 3 mm wavelength were plotted and compared with the theoretical values available in the literature.

The experimental arrangement is as shown in Fig. 5. 2 with the source positioned 50 mm from the slot in the far - field region. Previous investigations (e.g. Reinhardt and Dally (1970), Vu and Kinra (1985)) have indicated that the amplitude reflection and transmission coefficients vary as a function of distance away from a particular surface - breaking defect. The reflected and transmitted Rayleigh wave amplitudes appear to oscillate in the near - field region of the defect and attain a steady - state value in the far - field region of the defect which is (Vu and Kinra (1985)) distance / wavelength ratios ~ 4. The variation may be accounted for by the contribution to the scattered amplitude of the Rayleigh wave oscillations of the sides of the defect. These oscillations would be expected to extend to a thickness of approximately twice the Rayleigh wavelength from the defect sides. For the defect sizes used in this investigation and using a wavelength of 3 mm the far - field region is at distances of $\geq$ 10 mm. Preliminary investigations by the author have indicated that the amplitude reflection and transmission coefficients do vary in the region of the defect and thus measurements were made at distances of $\geq$ 10 mm from the defect. Vu and Kinra (1985) noted that this variation in the scattered amplitude of the

Rayleigh wave could be potentially useful in the characterisation of surface - breaking defects.

Figs. 5. 12 and 5. 13 illustrates the amplitude reflection and transmission coefficients respectively as a function of the ratio defect depth / Rayleigh wavelength. Also shown are the theoretical calculations of Angel and Achenbach (1984) for a Poisson' s ratio of 0.3 and Hirao et al. (1982) for a Poisson' s ratio of 0.29. The agreement between the experimental results and the theoretical values is generally good when the slightly different Poisson ratios are taken into account. In addition Hirao et al. (1982) modelled their Rayleigh wave interaction with a surface - breaking defect using a Ricker pulse and thus some difference is to be expected.

In association with the measurement of the Rayleigh wave amplitude on the reflected (detector in between source and defect) and transmitted (defect in between source and detector) side of various sized slots, the algorithm for the determination of the phase change was also implemented. Few papers (e. g. Angel and Achenbach (1984), Hirao et al. (1982)) have considered the phase change of the Rayleigh wave on interacting with a surface - breaking defect and little experimental data are available to support the theoretical predictions. Only the phase change of the reflected Rayleigh wave was determined as the transmitted Rayleigh wave amplitude was inadequate, at the larger defect depths, for an accurate determination of the transmitted Rayleigh wave phase change. As with the previous section, the maximum absolute displacement of the reflected Rayleigh wave was positioned at the centre + 1 of a 16384 point waveform. The FFT algorithm and the determination of the phase change was implemented as before. The resulting phase difference spectra for the variety of slots sizes used in this investigation are shown in Figs. 5. 14 and 5. 15. The phase

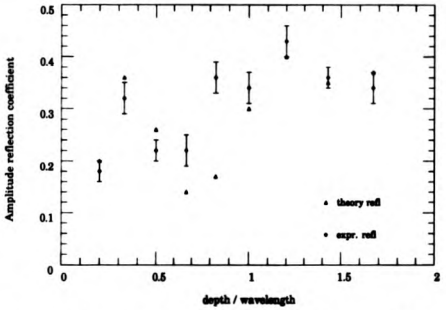

Figure 5. 12a : Comparison of experimental amplitude reflection coefficients for aluminium with theoretical values after Hirao et al. (1982) for a Poisson' s ratio of 0.3

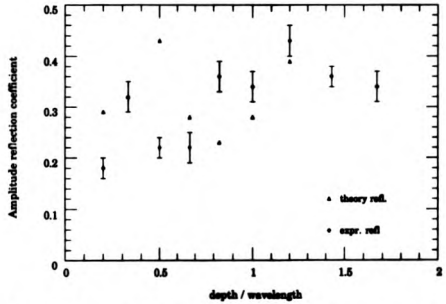

Figure 5. 12b : Comparison of experimental amplitude reflection coefficients for aluminium with theoretical values after Angel and Achenbach (1984) for a Poisson' s ratio of 0.3

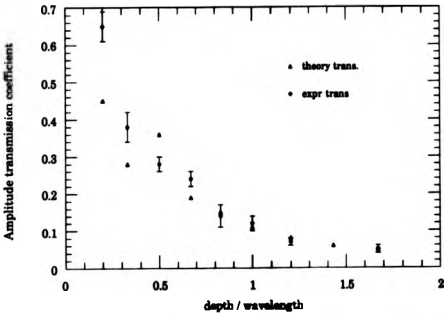

Figure 5. 13a : Comparison of experimental and theoretical (after Hirao et al. (1982) for a Poisson' s ratio of 0.3) amplitude transmission coefficients

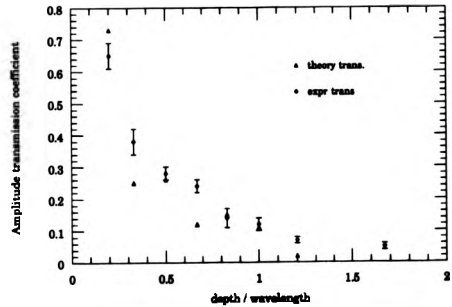

Figure 5. 13b : Comparison of experimental and theoretical (after Angel and Achenbach (1980) for a Poisson' s ratio of 0.3) transmission coefficients

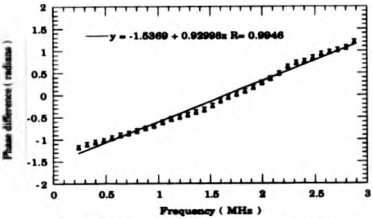

Figure 5. 14a : Phase difference spectrum for Rayleigh wave reflected from 1.5 mm deep slot

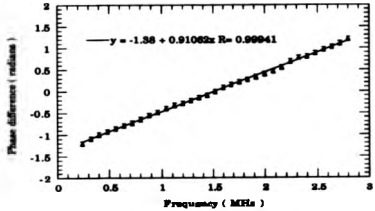

Figure 5. 14b : Phase difference spectrum for Rayleigh wave reflected from 2 mm deep slot

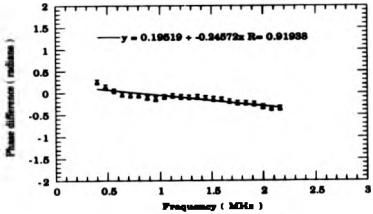

Figure 5. 14c : Phase difference spectrum for Rayleigh wave reflected from 2.5 mm deep slot

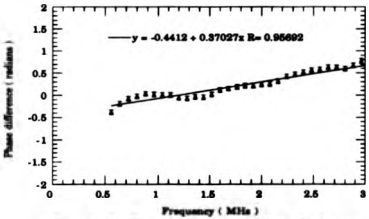

Figure 5. 15a : Phase difference spectrum for Rayleigh wave reflected from 3 mm deep slot

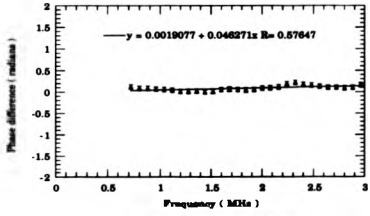

Figure 5. 15b : Phase difference spectrum for Rayleigh wave reflected from a 2.5 mm deep slot

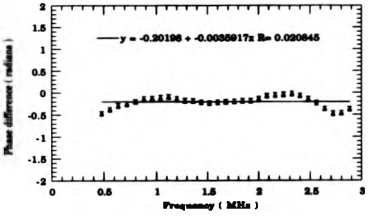

Figure 5. 15c : Phase difference spectrum for Rayleigh wave reflected from 5 mm deep slot

difference spectra for slots ≤ 1 mm deep were not constructed as the reflected Rayleigh waveform contained a component representing a Rayleigh wave emanating from the slot tip (Cooper (1985)). Over the useful frequency range for the remaining slot sizes the phase difference spectra are observed to be linear. The phase change of the reflected Rayleigh waves determined by this method is plotted in Fig. 5. 16 as a function of the ratio defect depth / Rayleigh wavelength. Also shown are the phase change values predicted by the theoretical work of Hirao et al. (1982) and Angel and Achenbach (1984). For clarity they are also compared in Table 5. 3.

Slot depth (mm)	Depth / wavelength	Phase change (after Hirao et al. (1982)) (radians)	Phase change (after Angel et al. (1984)) (radians)	Experimental phase change (radians) Error ± 0.1rd
1.5	0.5	1.37	0.98	- 1.5
2.0	0.67	1.29	1.22	- 1.4
2.5	0.83	0.73	0.84	0.2
3.0	1.0	0.32	0.45	- 0.4
3.6	1.2	0.48	0.38	0.0
5.0	1.67	0.45	-	- 0.2

Table 5. 3 : Comparison of the experimental and theoretical phase change values for various slot sizes.

Note that the relative point on the Rayleigh waveform for the determination of the theoretical phase change is unclear and that the

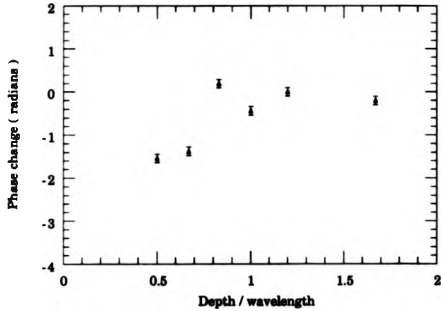

Figure 5. 16a : Experimental Phase change of reflected Rayleigh as a function of defect depth / wavelength

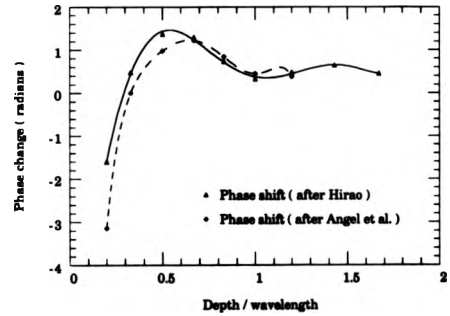

Figure 5. 16b : Theoretical phase change of reflected Rayleigh wave as a function of defect depth / wavelength

Poisson ratios differ between the theoretical and experimental results. If the magnitude of the experimental phase change values are considered then some correlation between theory and experiment is obtained. The distribution of the experimental phase change values as a function of the ratio defect depth / Rayleigh wavelength (Fig. 5. 16a) is also similar to the theoretical distribution.

5. 6 : USE OF RAYLEIGH WAVE MODE - CONVERSION FOR SURFACE - BREAKING DEFECT CHARACTERISATION

The techniques described so far for characterising surface - breaking defects have used only the Rayleigh wave signal (s) after interaction with a defect. In addition to a change in the Rayleigh wave amplitude and phase on interacting with a defect, some of the available Rayleigh wave energy is mode - converted into bulk waves. The generation of mode - converted shear and compression waves radiating from the tip of a defect has been predicted by various authors, for example, Freund (1971), Kundu and Mal (1981) and Tittman et al. (1986). Kundu and Mal (1981) and Tittman et al. (1986) analysed theoretically and experimentally the reflection and transmission of elastic waves from a surface - breaking defect. They obtained experimentally the directivity pattern of the radiated shear and compression waves from the crack tip and good agreement was obtained between theory and experiment. Such information is important as it can indicate the optimum position of the source and detector for accurately sizing the defect. More recently Lokhov (1989) obtained theoretical

directivity patterns of the shear and compression waves generated as a result of mode conversion of a Rayleigh wave at the defect tip.

Reinhardt and Dally (1970) and Hall (1976) used photoelastic visualisation to illustrate the complex interaction of Rayleigh waves with surface - breaking defects. Their illustrations showed that, in addition to a Rayleigh wave reflected from and transmitted through a slot, mode - converted compression and shear waves were generated. Most of the energy radiating from the slot tip goes into shear waves rather than compression waves. Early use of these mode - converted waves to size surface - breaking defects have been described by, for example, Hudgell et al. (1974).

The use of laser - generated Rayleigh waves in the characterisation of surface - breaking and near surface defects has particular advantages. The laser ultrasonic source is very efficient at producing broadband Rayleigh waves which, by using appropriate optics, may have a specific directivity. Circular, line and axicon shaped sources have been used for a variety of defect characterisation applications (e. g. Aindow et al. (1982), Cooper et al. (1986a) and Maldague et al. (1986)).

Cooper (1985) showed that the depth of the surface - breaking defect could be determined from analysis of the reflected Rayleigh waveform. To extend this work, an investigation of Rayleigh wave mode conversion upon interaction with a surface - breaking defect was undertaken, with particular emphasis on the waveforms recorded on the transmitted side of a defect. The aim of this investigation was to determine whether similar features on the transmitted Rayleigh waveform could also be used to determine the defect depth. Initially the experiments were conducted on samples with slots perpendicular to the

sample surface and ranging in depth from (1 - 5) mm. It was then extended to samples with inclined surface - breaking defects.

5. 6. 1 : Analysis of the reflected Rayleigh waveform for the determination of surface - breaking defect depth

Cooper (1985) reported that the depth of a surface - breaking defect could be determined from measurements of the time difference between the portion of a laser - generated Rayleigh wave reflected from the top of a defect and a defect depth related feature which follows the path illustrated in Fig. 5. 17. The time difference, Δt, between the defect top reflected Rayleigh and this defect depth related feature is given by (Cooper (1985))

$$\Delta t = d\left[\frac{1}{V_R} + \frac{1}{V_S \cos\phi_c} - \frac{\tan\phi_c}{V_R}\right] \qquad (5.4)$$

where $V_{R,S}$ are the Rayleigh and shear wave velocities respectively,

and ϕ_c is the angle of incidence of the mode - converted shear wave to the surface.

Using $\phi_c = 30°$ (Cooper (1985)) gives

$$\Delta t = \frac{d}{\sqrt{3}}\left[\frac{\sqrt{3}-1}{V_R} + \frac{2}{V_S}\right] \qquad (5.5)$$

Using equation (5. 5) it is possible to determine the depth of the defect, d, assuming it is perpendicular to the surface. Fig. 5. 18

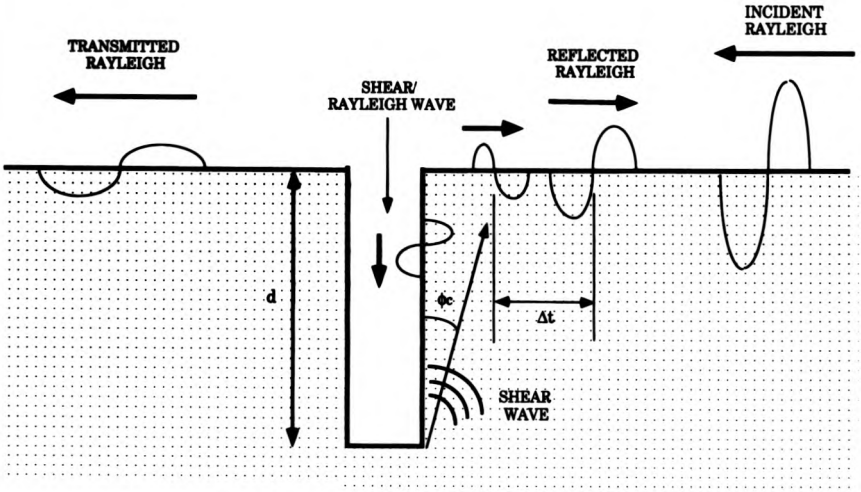

Figure 5. 17 : A proposed reflection interaction of a rayleigh wave with a rectangular surface breaking slot (after Cooper (1985))

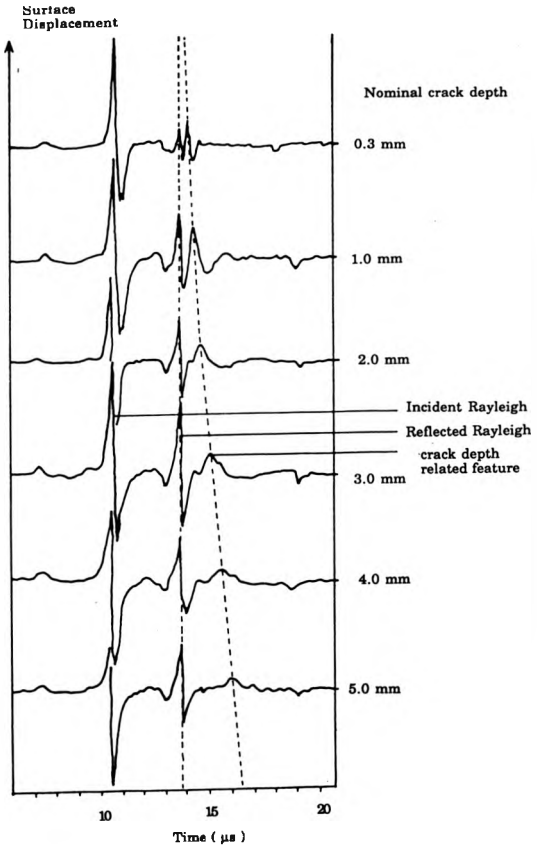

Figure 5. 18 : Variation of reflected Rayleigh waveform with crack depth (after Cooper (1985))

illustrates the variation in the reflected Rayleigh waveform as a function of defect depth. The waveforms indicate that the technique is appropriate for defect depths of ≤ 3 mm. The next section outlines how analysis of the transmitted Rayleigh waveforms enables defect depths in the range (1 - 5) mm to be determined.

5. 6. 2 : Analysis of the transmitted Rayleigh waveform for the determination of surface - breaking defect depth

The experimental arrangement for this investigation is as shown in Fig. 5.2. The position of the laser source remained fixed relative to the defect location and at a distance of 50 mm away. The interferometer He - Ne detector beam was scanned on the transmitted side of the defect at increments of 5 mm. For each source to detector distance, the transmitted Rayleigh waveform was recorded.

The displacement waveforms recorded, at various source to detector distances, when a Rayleigh wave has propagated through a 2.5 mm deep surface - breaking slot perpendicular to the surface are shown in Fig. 5. 19. The waveforms show the broadened transmitted Rayleigh wave and a consistent feature which occurs, on average, (2.19 ± 0.04) μs after the transmitted Rayleigh wave. Fig. 5. 20 illustrates the corresponding waveforms after transmission of a Rayleigh wave through a 3.6 mm deep surface - breaking slot. Again a consistent second feature occurring after the transmitted Rayleigh wave was observed. The average time difference between the transmitted Rayleigh wave and this second feature was (3.3 ± 0.2) μs. Note that the amplitude of the transmitted Rayleigh wave is much reduced and this introduces larger errors in the measurement of the time interval. The

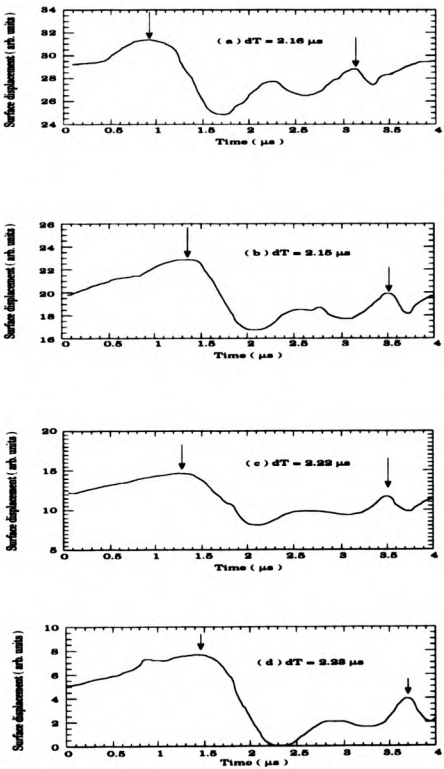

Figure 5. 19 : Rayleigh wave transmitted through a 2.5 mm deep slot for source to detector distances of (a) 60 mm, (b) 65 mm, (c) 70 mm and (d) 75 mm

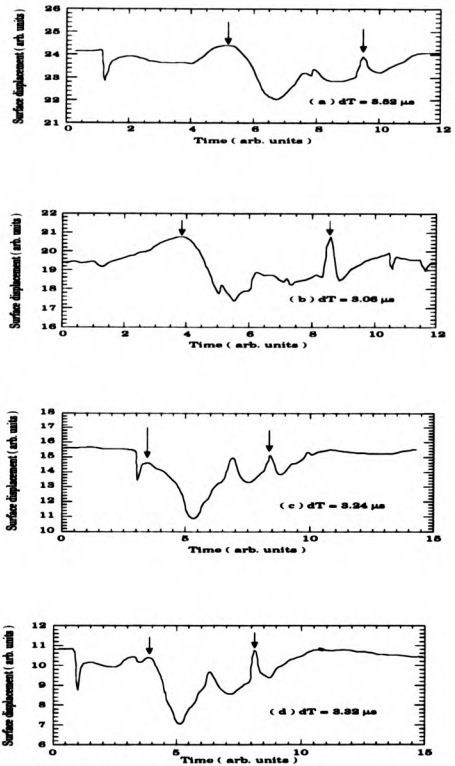

Figure 5. 20 : Rayleigh wave transmitted through a 3.6 mm deep slot for source to detector distances of (a) 60 mm, (b) 65 mm, (c) 70 mm and (d) 75 mm

increase of this time interval with increasing depth implies it is a depth related feature and the constant value of the time interval, for a particular defect depth, as a function of source to detector distance indicates that this second feature has Rayleigh wave characteristics.

A path was sought to explain the existence of this second feature in accordance with previous investigations into Rayleigh wave scattering phenomenon. Paths were considered which resulted in a similar magnitude for the time difference as obtained experimentally. The path proposed to explain the existence of this second feature is illustrated in Fig. 5. 21.

The incident Rayleigh wave interacts with the defect tip resulting in a Rayleigh wave which travels up the far side of the slot to the surface. At this 90° corner a proportion of the Rayleigh wave is reflected back down the defect side. When it reaches the defect tip, mode conversion to a shear wave occurs in a similar manner to that proposed by Cooper (1985) to explain the reflected case. This has also been shown theoretically by, for example, Lokhov (1989). Part of the shear wave energy propagates up to the surface where further mode conversion to a Rayleigh wave occurs. This Rayleigh wave propagates along the surface away from the defect. The time difference, Δt, between the transmitted Rayleigh wave and this consistent second feature for the path outlined is given by

$$\Delta t = d\left[\frac{2}{V_R} + \frac{1}{V_S \cos\phi_c} - \frac{\tan\phi_c}{V_R}\right] \qquad (5.6)$$

Using $\phi_c = 30°$ (Cooper (1985)) gives

$$\Delta t = \frac{d}{\sqrt{3}}\left[\frac{2\sqrt{3}-1}{V_R} + \frac{2}{V_S}\right] \qquad (5.7)$$

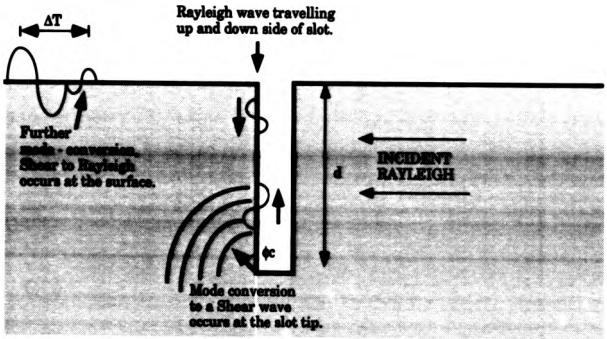

Figure 5. 21 : Proposed path to explain the feature which occurs after a Rayleigh wave has propagated through a rectangular surface - breaking defect.

Rearranging equation (5. 7) gives

$$d = \frac{\sqrt{3}\Delta t}{\left[\frac{2\sqrt{3}-1}{V_R} + \frac{2}{V_S}\right]} \qquad (5.8)$$

The lower frequency (larger wavelength) components of the laser - generated Rayleigh wave contain the largest amplitude components (Fig. 5. 3). It is these low frequency components of the incident Rayleigh wave which interact with the defect tip producing secondary Rayleigh waves which propagate up the far side of the defect. To obtain the proportion of the Rayleigh wave amplitude which propagates up the far side of the defect it is useful to model it as a Rayleigh wave interaction with a 270° corner. Referring to Fig. 5. 11, the transmission coefficient is (0.30 ± 0.02). The reflection coefficient on interaction with the 90° corner at the surface is, from Fig. 5. 10, (0.40 ± 0.02). Thus the proportion of the incident Rayleigh wave amplitude propagating back towards the defect tip is 0.30 x 0.40 = 0.12. At the defect tip further reflection of the Rayleigh disturbance back towards the surface occurs as predicted by, for example, Achenbach et al. (1980). As expected, the amplitude becomes much reduced on further propagation up and down the defect sides.

The efficiency of the mode conversion of the Rayleigh wave to a shear wave at the defect tip may be approximated by assuming a Rayleigh wave interaction with a 270° corner. The energy of the Rayleigh wave lost to bulk modes (Table 5. 2 and Fig. 5. 11) is 1 - (0.40 + 0.05) = 0.65. This is an approximate mode conversion coefficient of 0.43 which implies that at least 5 % of the incident Rayleigh wave energy propagates as shear waves emanating from the defect tip. This may be an underestimate as it considered the defect tip as a 270° corner. The

efficiency of conversion of the shear wave to a Rayleigh wave at the critical angle of 30° is 100 % i. e. the shear wave is completely mode - converted into a Rayleigh wave (Couchman and Bell (1978)).

The time interval, Δt, was measured for a variety of surface - breaking defect depths up to 5 mm deep and perpendicular to the surface. Using equation (5. 8) the depth of each defect was calculated and compared to the measured depth. This comparison is shown in Fig. 5. 22 and Table 5. 4. It is clear that there is good agreement between the calculated and measured values in the surface - breaking defect depth range (1 - 5) mm. It is not possible to use the technique for defect depths of less than 1 mm as the second feature is lost in the transmitted Rayleigh wave signal. For defect depths of more than 5 mm the amplitude of the transmitted Rayleigh wave becomes much diminished and it is difficult to make an accurate measurement of the time interval, Δt.

5. 6. 3 : Analysis of the reflected and transmitted Rayleigh waveforms on interacting with inclined surface - breaking defects

Rayleigh waveforms were recorded on transmission through inclined surface - breaking defects at angles ranging from 20° to 75° to the sample surface. The aim of this investigation was to assess whether it was possible to determine both the angle of inclination and the length of the defect from the Rayleigh waveforms recorded on the transmitted side of the inclined defect. The determination of these two quantities using Rayleigh wave information has been described by Silk (1976), Date et al. (1982), Kinra and Vu (1986) and Doyle and Scala (1989). Zhang and Achenbach (1988) considered theoretically the scattering of

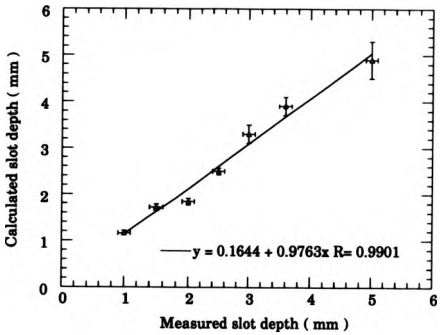

Figure 5. 22 : Graph of the calculated defect depth as a function of measured slot depth

Measured slot depth (mm) ± 0.1 mm	Calculated slot depth (mm)
1.0	1.16 ± 0.05
1.5	1.72 ± 0.07
2.0	1.84 ± 0.07
2.5	2.49 ± 0.07
3.0	3.3 ± 0.2
3.6	3.9 ± 0.2
5.0	4.9 ± 0.4

Table 5. 4 : Comparison of calculated slot depth using equation (5. 8) with measured slot depth

body waves by an inclined surface - breaking crack, whilst Blake and Bond (1989a), using a mixed finite element - finite difference formulation, considered the ultrasonic scattering of Rayleigh waves by wedges of arbitrary interior angle.

Transmitted Rayleigh waveforms were recorded, using the experimental arrangement illustrated in Fig. 5. 2, for both the slot tip directed away from and directed towards the source. The length of the inclined surface - breaking defects was the same for all angles of inclination. The waveforms were detected with the interferometer He - Ne detector spot in the far field region of the inclined surface - breaking defect , $\geq$ 10 mm away. Preliminary investigations of the reflected Rayleigh waveform were conducted.

With the slot tip directed away from the source, the amplitude of the reflected Rayleigh wave increased as the angle of the inclined slot increased in general accordance with the theoretical modelling of Blake and Bond (1989a). For an inclined slot angle of 20° (interior wedge angle of 160°) no reflected Rayleigh wave was observed. It is expected that a reflected Rayleigh feature similar to that described by Cooper (1985) would exist for defect tips within 3 mm of the surface. Fig. 5. 23 shows the amplitude reflection and transmission coefficients as a function of interior wedge angle as calculated by Blake and Bond (1989a). For an interior wedge angle of 160° the amplitude reflection and transmission coefficients are approximately 0.07 and 0.64 respectively. With the slot tip directed towards the source the reflected Rayleigh wave was observed for all inclined slot angles. As far as the author is aware no modelling of Rayleigh wave scattering by wedges with interior angles of $< 90°$ has been published. For these interior wedge angles it is expected that a large proportion of the incident Rayleigh wave amplitude will be reflected back towards the source or

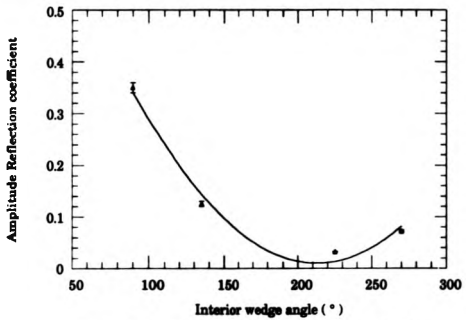

Figure 5. 23a : Reflection coefficient as a function of wedge angle (after Blake and Bond (1989a)

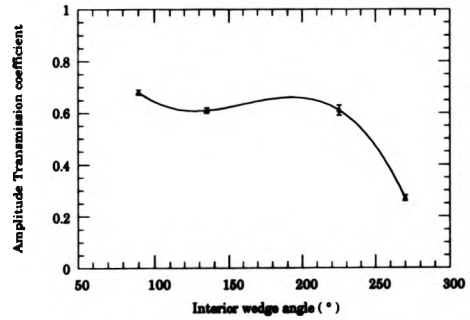

Figure 5. 23b : Transmission coefficient as a function of wedge angle (after Blake and Bond (1989a))

mode - converted into bulk modes. The proportion of the incident Rayleigh energy transmitted around the wedge is expected to be small (≤ 10 %).

The waveforms recorded after Rayleigh wave transmission through a 20° inclined surface - breaking defect with the defect tip directed away from and towards the source are shown in Figs. 5. 24 and 5. 25 respectively as a function of the source to detector distance. The waveforms recorded with the slot tip directed away from the source (Fig. 5. 24) contain the transmitted Rayleigh waveform and an associated consistent second feature which occurs, on average, (2.23 ± 0.04) μs after the transmitted Rayleigh wave. Also seen on the transmitted waveform is a backwall compression wave reflection, which is observed to appear at different times for different source to detector distances, and a secondary Rayleigh wave, which is a result of reflection from the edge of the sample followed by transmission through the 20° inclined slot. In some instances a consistent second feature is observed after the arrival of this transmitted secondary Rayleigh wave.

Similar features are observed on the transmitted Rayleigh waveform for the slot tip directed towards the source (Fig. 5. 25). The time difference between the transmitted Rayleigh wave and the consistent second feature for this arrangement tends to increase with increasing source - to - detector distance at ~ 16 ns / mm. There is also evidence to suggest that this occurs for the other slot angles with the slot tip directed towards the source. The magnitude of the time difference increases with increasing angle.

Transmitted Rayleigh waveforms were recorded for the remaining inclined surface - breaking defect angles and are shown in Fig. 5. 26 for the slot tip directed away from the source and in Fig. 5. 27 for the slot tip directed towards the source. For all waveforms shown,

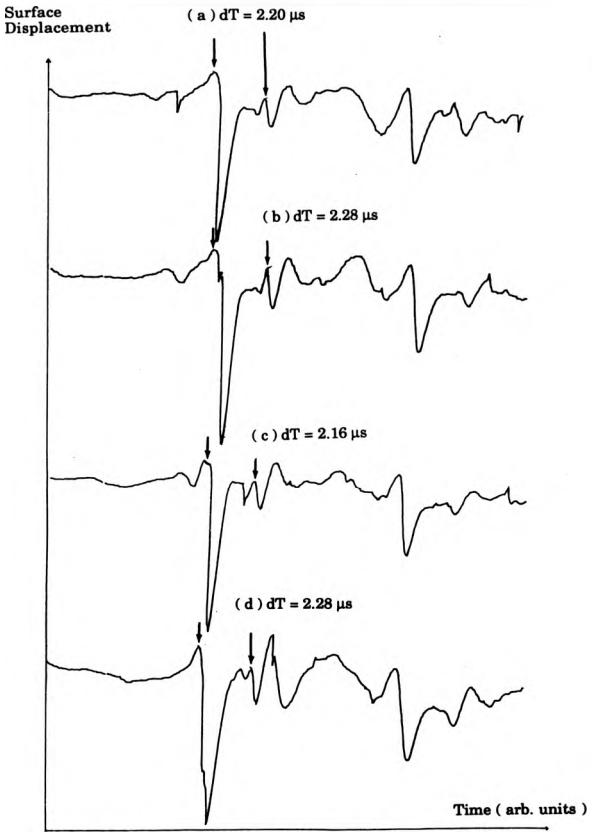

Figure 5. 24 : Rayleigh waveforms after transmission through a 20° inclined slot, with slot tip directed away from source, for various source to detector distances

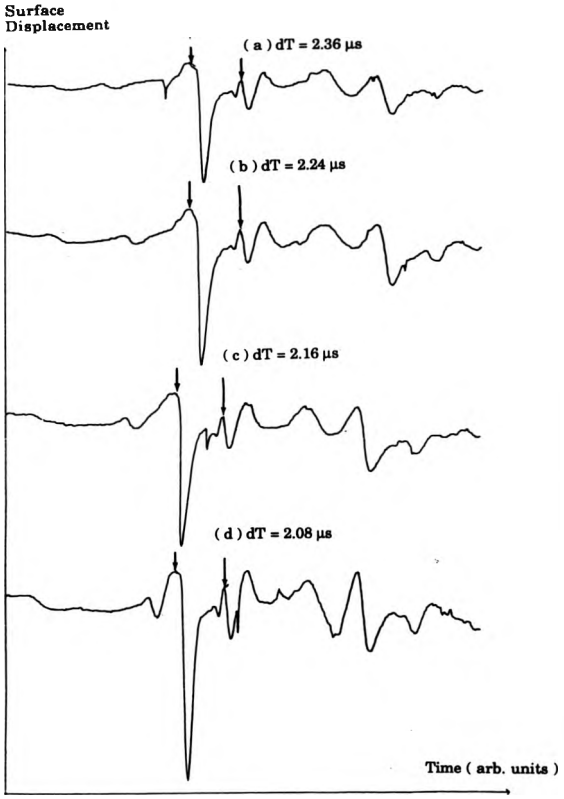

Figure 5. 25 : Rayleigh waveforms after transmission through a 20° inclined slot, with slot tip directed towards source, for various source to detector distances

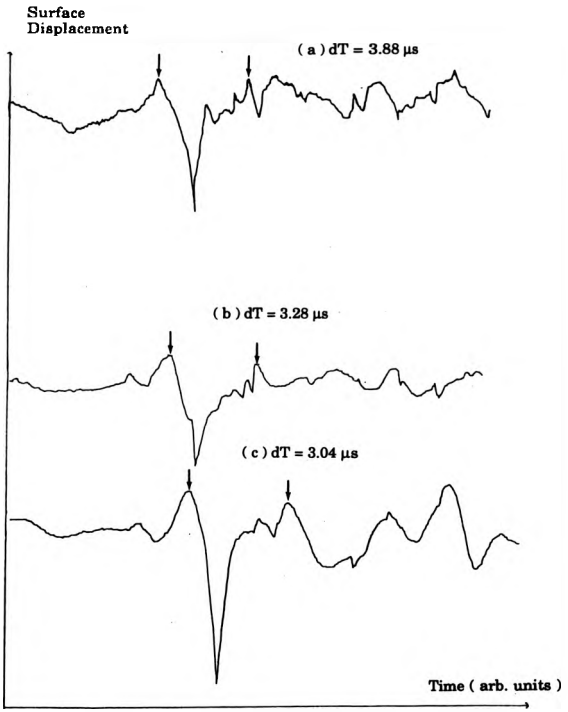

Figure 5. 26 : Rayleigh waveforms after transmission through (a) 75°, (b) 45° and (c) 30° inclined slots, slot tip away from source, for a fixed source to detector distance

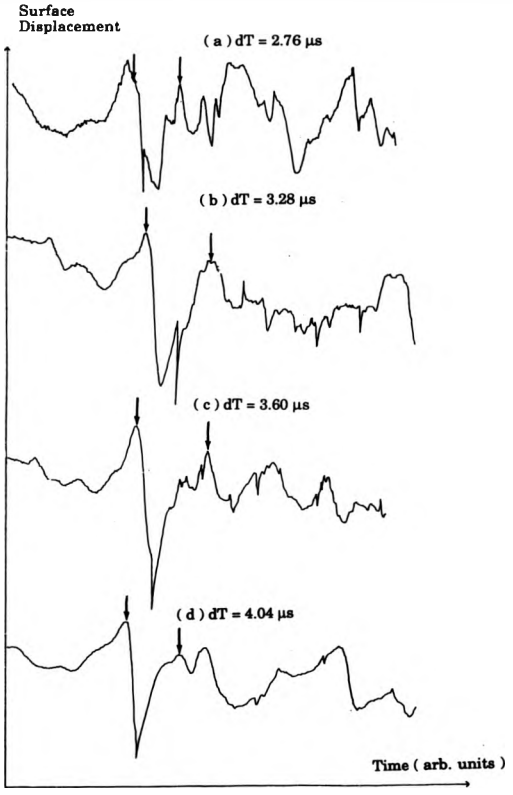

Figure 5. 27 : Rayleigh waveforms after transmission through (a) 75°, (b) 60°, (c) 45° and (d) 30° inclined slots, slot tip towards source, for a fixed source to detector distance

the source to detector distance was 65 mm. The average time intervals between the transmitted Rayleigh wave and the consistant feature for each defect angle with the slot tip directed away from the source are also shown in Fig. 5. 26. The time differences recorded at each source to detector distance for the slot tip directed towards the source as a function of defect angle are given in Table 5. 5.

	Time difference for each inclined angle (in μs)				
Source - to - detector distance (mm)	20°	30°	45°	60°	75°
55 ± 2	2.08 ± 0.04	4. 00 ± 0.05	3.52 ± 0.04	?	3.64 ± 0.04
60 ± 2	2.16 ± 0.04	4.00 ± 0.05	3.80 ± 0.04	?	3.84 ± 0.04
65 ± 2	2.24 ± 0.04	4.04 ± 0.05	3.92 ± 0.04	3.28 ± 0.05	4.00 ± 0.04
70 ± 2	2.36 ± 0.04	3.92 ± 0.05	3.92 ± 0.04	3.92 ± 0.05	4.16 ± 0.04

Table 5. 5 : Summary of the time interval, Δt, for the tip of various inclined surface - breaking defects toward the source as a function of source - to - detector distance.

It was originally envisaged that the Rayleigh interaction with the inclined surface - breaking defect would be similar to that proposed in Fig. 5. 21. For a particular angle, there would be a difference in the time interval, Δt, owing to the different propagation distances of the shear wave component of the path with the defect tip directed away from and towards the source. When the defect tip is directed away from the source

a path similar to that proposed in Fig. 5. 21 may be followed. The time intervals expected for this arrangement of the defect as a function of defect angle are listed in Table 5. 6 along with the experimentally recorded time intervals. The expected and recorded time intervals are of the same magnitude implying that the proposed path is followed for this arrangement of the inclined surface - breaking defect.

Inclined surface - breaking defect angle	Expected time interval, Δt_{the} (μs)	Recorded average time interval, Δt_{exp} (μs)
20°	2.5	2.23 ± 0.04
30°	3.7	3.91 ± 0.05
45°	3.7	3.72 ± 0.04
60°	4.4	-
75°	5.0	3.87 ± 0.04
90°	5.2	5.1 ± 0.4

Table 5. 6 : Comparison of the expected time interval with the recorded time interval for the tip of an inclined surface - breaking defect directed away from the source.

The reason for the increase in the time interval with increasing source - to - detector distance when the slot tip is directed towards the source is not apparent. The incident Rayleigh wave first encounters the slot tip and is expected to transfer some of the Rayleigh wave energy to the movement of the slot tip in the elastic medium. The interaction is assumed to produce secondary Rayleigh waves which propagate along both sides of the slot. The secondary Rayleigh wave incident on the

obtuse interior angle on the transmitted side of the slot would reflect little and most of the energy would be transmitted onto the free surface (Blake and Bond (1989a) and Fig. 5. 23). The time interval between the transmitted Rayleigh wave and a Rayleigh wave which follows this path would be expected to be approximately defect length / Rayleigh velocity. For the defect lengths used in this investigation this time interval is ~ 1.7 μs which is significantly different from the experimental time interval. In addition, such a process would not exhibit a significant variation in the time interval with varying source - to - detector distance.

Consideration of the time that a shear wave would take to reach the detector directly from the slot tip results in a travel time which is almost equivalent to the transmitted Rayleigh wave travel time. Compression waves which follow the same path result in faster travel times. Further experiments, such as keeping the detector fixed and moving the source to see if similar waveforms are obtained and using smaller slot lengths, are required to investigate this effect more fully. The increasing time interval with increasing source to detector distance can be used to indicate that a defect tip is directed toward the source.

5. 7 : CONCLUSIONS

Various techniques for the characterisation of surface - breaking defects have been described in this chapter. The techniques described have been implemented using remote generation and detection of surface displacements. A laser ultrasonic source generates broadband, highly repeatable (~ 5 % variation) Rayleigh waves which interact with surface - breaking defects in a variety of ways. Used in association with

interferometric detection, direct comparisons with theoretical surface displacements may be achieved.

The potential range of applicability of each technique for sizing a particular surface - breaking defect may be assessed. The techniques described in this chapter are summarised in Table 5. 7. The various techniques are able to size surface - breaking defects over the range of defect sizes found in most industrial components. Sizing very small ($\leq 10^{-6}$) defect depth / Rayleigh wavelength ratio surface - breaking defects which may occur on ceramic components may be impossible for some of the techniques e. g. the Rayleigh wave resonance technique. Such defect sizes on metallic surfaces are generally insignificant and do not weaken the structure. On ceramic components, however, these defect sizes may have catastrophic consequences. Current NDT techniques used to characterise surface - breaking defects on ceramics include Acoustic Microscopy and Dye Penetrant methods. At present no detailed investigations on defective ceramic components using laser generation and detection have been published. The laser ultrasonic source has an immediate advantage in that by choosing a suitable laser pulse profile with a fast (~ ps) risetime, Rayleigh waves with wavelengths ~ 1 μm can be generated. It is also possible to use the interference of two laser beams method for producing high (~ GHz) frequency ultrasound (Ishikawa et al. (1990) in Chapter Two).

Characterisation of a surface - breaking defect using laser generation and detection can be achieved by conducting an initial rough scan with either a constant source to detector distance sweep or with the source fixed and scanning the detector over the sample surface. With no defect between the source and detector only the incident Rayleigh wave will be recorded. In the presence of a defect, a reflected and transmitted Rayleigh wave will exist. As the detector passes over the defect the

Technique	Procedure	Theoretical applicability	Experimental applicability	Comments
Rayleigh wave resonance	Measurement of the frequency of resonance in the Log10 (Power spectrum) - frequency plot.	$k_R d > 6$	Good for defect lengths ≤ 2 mm. Less good for defect lengths > 2 mm.	Disadvantage is that it requires data processing of the recorded signal.
Refl. / Trans. coefficients	Variation in the reflected and transmitted Rayleigh wave amplitude and phase as a function of defect depth / Rayleigh wavelength.	All defect depths	All defect depths. Limited only by displacement resolution of detector.	Using both the amplitude and phase change values it may be possible to obtain an accurate determination of defect depth.

Analysis of reflected Rayleigh waveform	Use the time interval between the Rayleigh wave reflected from the top of defect and a depth related feature to size defect.	All defect depths	Useful for defect depths ≤ 3 mm.	This technique is more amenable to defect depth determination directly from the recorded waveform.
Analysis of transmitted Rayleigh waveform	Use the time interval between the Rayleigh wave transmitted through the defect and a depth related feature to size defect	All defect depths	Defect depths (1 - 5) mm.	As above

Table 5. 7 : Summary of the various techniques used to characterise surface - breaking defects in this chapter.

reflected and then the transmitted Rayleigh wave will be detected. Thus, knowing that the transmitted Rayleigh wave is more broadened than the reflected Rayleigh wave, it is possible to estimate the defect location. Using the amplitude of these scattered Rayleigh waves and determining the phase change enables an approximation of the defect depth to be made by referring to theoretical values of the reflection and transmission coefficients. It would be useful for future theoretical investigations of the reflection and transmission coefficients to include calculations on inclined surface - breaking defects. In addition, if the reflected and transmitted Rayleigh waveforms contain the consistent depth related features another estimate of the defect depth can be made.

Once the approximate location and length of the surface - breaking defect has been determined, a more accurate scan in the vicinity of the defect may be conducted for different incident Rayleigh wave directions. The technique best suited to size the defect, determined by the defects approximate depth, may then be implemented. Owing to the repeatability of the laser - generated Rayleigh wave it is possible to obtain an accurate assessment of the surface - breaking defect.

For an inclined surface - breaking defect both the reflected and transmitted Rayleigh waveforms, for different incident Rayleigh wave directions, may be used. A larger proportion of the incident Rayleigh wave will be reflected when the Rayleigh wave first interacts with the acute angular side of the defect than when it first interacts with the obtuse angular side of the defect. Knowledge of the location of the defect tip relative to the source may also be obtained by determining whether any variation in the time interval, between the transmitted Rayleigh wave and the consistant second feature, occurs with varying source - to - detector distance. Also, if information on the variation in reflection coefficient as a function of wedge angle were available, the angle of

inclination may be determined. When the time interval, between the transmitted Rayleigh wave and the consistent second feature on the transmitted Rayleigh waveforms, does not significantly vary as a function of source - to - detector distance it is possible to obtain an estimate of the defect length using equation (5. 8) if it is assumed that the path proposed in Fig. 5. 21 is followed.

Laser - generated Rayleigh waves have been shown to be useful probes of near surface and surface - breaking defects. They have extended the range of applicability of Rayleigh waves to the characterisation of such defects. Further fundamental research into the complex interaction of Rayleigh waves with surface - breaking defects is required in addition to its use in more practical NDT applications.

5.8 : REFERENCES

Achenbach, J. D. et al. (1980)	IEEE SU - 27, 124 (1980)
Aindow, A. M. et al. (1982)	Opt. Comm., 42, 116 (1982)
Angel, Y. C. and Achenbach, J. D. (1984)	J. A. S. A., 75, 313 (1984)
Blake, R. J. and Bond, L. J. (1989a)	Daresbury Lab. preprint DL / SCI / P632T
Blake, R. J. and Bond, L. J. (1989b)	Daresbury Lab. preprint DL / SCI / P652T
Bond, L. J. (1979)	Ultrasonics, 17, 71 (1979)
Burger, C. P. and Testa, A. J. (1981)	Ultra. Int. 81 Conf. Proc., 271 (1981)
Cooper, J. A. (1985)	PhD Thesis, University of Hull (1985)
Cooper, J. A. et al. (1986a)	Phil. Trans. R. Soc. Lond., A 320, 319 (1986)
Cooper, J. A. et al. (1986b)	IEEE UFFC - 33, 462 (1986)
Couchman, J. C. and Bell, J. R. (1978)	Ultrasonics, 16, 272 (1978)
Cuomo, F. C. et al. (1977)	IEEE SU - 24, 280 (1977)
Date, K. et al. (1982)	NDT Int., 15, 315 (1982)
De Bremaecker, J. Cl. (1958)	Geophysics, 23, 253 (1958)
Doyle, P. A. (1986)	J. Nondestr. Eval., 5, 179 (1986)

Doyle, P. A. and Scala, C. M. (1987) Ultra. Int. 87 Conf. Proc., 407 (1987)

Doyle, P. A. and Scala, C. M. (1990) Ultrasonics, **28**, 77 (1990)

Farnell, G. W. (1978) in ' Acoustic Surface Waves ', Edited by A. A. Oliner (Springer - Verlag) (1978)

Freund, L. B. (1971) Int. J. Solids Struct., **7**, 1199 (1971)

Gautesen, A. K. (1985) Trans. ASME : J. Appl. Mech., **52**, 664 (1985)

Hall, K. G. (1976) NDT, 121 (1976)

Hirao, M. et al. (1982) J. A. S. A., **72**, 602 (1982)

Hudgell, R. J. et al. (1974) Brit. J. NDT, **16**, 144 (1974)

Ishikawa, K. et al. (1990) Opt. Comm., **76**, 81 (1990)

Kinra, V. K. and Vu, B. Q. (1983) Mech. Res. Comm., **10**, 193 (1983)

Kinra, V. K. and Vu, B. Q. (1986) J. A. S. A., **79**, 1688 (1986)

Knopoff, L. and Gangi, A. F. (1960) Geophysics, **25**, 1203 (1960)

Kundu, T. and Mal, A. K. (1981)	Trans. ASME : J. Appl. Mech., **48**, 570 (1981)
Lapwood, E. R. (1961)	Geophys. J. R. Astr. Soc., **4**, 174 (1961)
Lidington, B. H. and Silk, M. G. (1975)	Brit. J. NDT, **17**, 165 (1975)
Lokhov, V. P. (1989)	Sov. J. NDT, **25**, 189 (1989)
Lloyd, E. A. (1975)	Brit. J. NDT, **17**, 172 (1975)
Mal, A. K. and Knopoff, L. (1965)	Bull. Seism. Soc. Am., **55**, 319 (1965)
Maldague, X. et al. (1986)	Mat. Eval., **44**, 1120 (1986)
Mendelsohn, D. A. et al. (1980)	Wave Motion, **2**, 277 (1980)
Morgan, L. L. (1974)	Acustica, **30**, 222 (1974)
Munasinghe, M. and Farnell, G. W.	J. Appl. Phys., **44**, 2025 (1973)
Pilant, W. L. et al. (1964)	J. Geophys. Res., **69**, 291 (1964)
Reinhardt, H. W. and Dally, J. W.	Mat. Eval., 213 (1970)
Sharpe, R. S. et al. (1984)	' Quality Technology Handbook', 4th Ed., (Butterworth) (1984)
Silk, M. G. (1976)	NDT Int., **9**, 290 (1976)

Tittmann, B. R. et al. (1986) Appl. Phys. Lett., 49, 1333 (1986)

Viktorov, I. A. (1967) ' Rayleigh and Lamb Waves ', (Plenum Press) (1967)

Vu, B. Q. and Kinra, V. K. (1985) J. A. S. A., 77, 1425 (1985)

Yew, C. H. et al. (1984) J. A. S. A., 75, 189 (1984)

Zhang, Ch. and Achenbach, J. D. (1988) Ultrasonics, 26, 132 (1988)

Chapter Six

CONCLUDING REMARKS AND FUTURE WORK

The various properties of laser - generated ultrasound have been utilised in the investigations described in this thesis. The review of laser - generated ultrasound given in Chapter Two summarised, in chronological order, the determination of the various characteristics of the acoustic source to date in both the thermoelastic and plasma regimes. Knowledge of these properties is required if they are to be fully implemented in further research. Characteristic of research in many branches of physics, the laser source was initially investigated experimentally and then theoretically modelled in association with further experimentation. Modelling from other branches of physics was employed, particularly from the field of geophysics, where similarities between the characteristics of an earthquake source and the laser source were identified.

A majority of present day research conducted using laser - generated ultrasound aims to find suitable applications for this unique ultrasonic source. The most immediate application is for the non - destructive testing of components, for which the use of remote generation and detection of ultrasound has been demonstrated successfully in a laboratory environment. At present it has not been successfully implemented in an industrial setting. The high cost and safety requirements for a portable laser ultrasonic system, in comparison to a piezoelectric based inspection system, means that it will not immediately replace those areas of

applicability where piezoelectric transducers are sufficient. In some cases piezoelectric transducers are much more convenient to use.

Laser ultrasonics will demonstrate its usefulness in areas of applicability where it is not possible to use piezoelectric transducers. In addition it has a potential role in improving and extending already established techniques for the non - destructive testing of components. One advantage is the improvement in the resolution of defect tips or a collection of defects owing to the wideband nature, compared to piezoelectric transducers, of the laser - generated ultrasound. Other advantages, such as its non - contact nature, repeatability and adaptability, have also been outlined in Chapter Two.

It was generally assumed that the frequency content of ultrasound generated in the plasma regime was directly dependent upon the properties of the incident laser pulse. The faster the risetime of the incident laser pulse the higher the frequency content of the ultrasonic compression wave produced. Few quantitative investigations had been conducted, however, to investigate this relationship more fully. In Chapter Three, the various processes involved in the production of a stress upon a solid surface when irradiated with a laser pulse of sufficient power density to eventually cause vapourisation were considered. The aim of the investigation was to determine whether the risetime of the ultrasonic compression wave was dependent solely on the risetime of the incident laser pulse or, in addition, to the properties of the irradiated solid also.

The ultrasonic generation model followed indicated that the highest ultrasonic frequency components would be generated when the profile of the stress approaches that of a δ - function with zero rise and fall time and infinite amplitude. The Fourier transform of a δ - function is a Heaviside

function with infinite bandwidth. Analysis of the various parameters involved in the generation process concluded that a solid which would most closely approach a δ - function stress profile requires a large thermal conductivity and vapourisation temperature with the remaining relevant mechanical and thermal properties low valued.

An experimental investigation into the risetime of the ultrasonic compression wave pulse, generated in various solids by lasers of different pulse profiles and wavelengths and recorded using wide bandwidth modified Michelson interferometers, was conducted. The fastest risetimes were recorded in aluminium, mild steel and silicon using the 430 MHz bandwidth interferometer to detect the epicentral displacements. A significant variation in the recorded risetime on different solids was observed in this investigation in keeping with the predictions of the theoretical analysis.

The technique for the measurement of the ultrasonic compression wave risetime can be improved. A major problem in obtaining accurate risetime measurements is the finite size of the source and detector. The incident generating laser pulse may be focussed to a smaller diameter using a lens with a small focal length to enable a more pointlike source. Placing various neutral density filters in turn in the path of the incident laser pulse enables an investigation of the variation in the risetime in a particular solid as a function of the incident power density. An increasing power density for a particular solid would be expected to decrease the time to reach vapourisation. This, in turn, would be expected to result in smaller risetimes. Preliminary investigations by the author have indicated that, within the plasma regime, the risetime does not vary with varying power

density. It would also be of interest to investigate the effect upon the risetime when laser pulses with risetimes ~ (10^{-11} - 10^{-10}) s are used.

Focussing of the interferometer He - Ne beam will also result in potentially recording a faster risetime. The bandwidth of the photodiodes and amplifier in the interferometer is required to be larger than the bandwidth of the incident laser pulse also. If the risetimes are to be corrected for the error associated with the finite size of the detector then the detection sensitivity across the beam has to be evaluated. The correction may be implemented using convolution in the frequency domain.

Larger propagation distances will also reduce the error associated with the finite size of the source and detector. Ultrasonic attenuation, which is generally frequency dependent, may increase the risetime of the compression wave pulse with increasing propagation distance. The risetimes of the compression wave pulses recorded on the 5 mm thick samples were, in most cases, the same as the risetimes recorded on the thinner samples. The amplitude of the compression wave was diminished in accordance with an increased propagation distance. The optimum sample thickness is required to be large enough to consider the source and detector as pointlike and small enough to enable sufficient signal to be obtained for a single generating laser pulse incidence. Pitting of the surface owing to the generation mechanism results in a decreased source - to - detector distance. Consecutive incident generating pulses would tend to blur the actual risetime if an average waveform is recorded. This effect was observed in the data recorded using the picosecond laser pulse to generate ultrasound.

The wide bandwidth nature of laser - generated ultrasound was used in the characterisation of bulk defects for data recorded with the source and

detector in the Time - of - Flight Diffraction arrangement. Ultrasonic compression waves scattered from various sized slots and cylindrical holes were compared to a reference backwall reflection in the frequency - phase domain. In the time domain the slot and hole scattered signals were similar. A significant difference in the phase difference spectra for the slots and holes existed which could be used to characterise the type of defect.

One drawback of this investigation was the inability of the detection system to obtain sufficient signal amplitude for ultrasound scattered from a real fatigue crack. As data in Chapter Four illustrated, the amplitude of the scattered compression wave back towards the surface is relatively small. To record this signal with sufficient amplitude an interferometer with a smaller displacement resolution is required. Since these data were recorded, an improved interferometer has been developed in the laboratory and thus it would be advantageous to record the scattered ultrasound from the crack using this interferometer. The phase change value determined from a crack scattered signal would be expected to more closely match the theoretical value.

The potential usefulness of the technique for defect characterisation has been demonstrated. Further investigations on samples which introduce noise to the scattered signal, from, for example, grain boundary scattering or a defect embedded in a welded section, are required to fully evaluate the technique. If the phase change of the scattered pulse can be extracted from the recorded data, by utilising certain signal processing techniques to reduce the noise level, an assessment of the type of defect present may be made aiding in its characterisation.

Chapter Five describes various techniques for the characterisation of surface - breaking defects using laser - generated Rayleigh waves. These

include Rayleigh wave resonance, reflection / transmission coefficient determination and analysis of the reflected or transmitted Rayleigh waveform. Measurements of the reflection and transmission coefficients of 90° and 270° corners and surface - breaking slots of various depths included calculations of the phase change of the Rayleigh wave on interacting with the various surface discontinuities. The phase change was determined using an algorithm similar to that described in Chapter Four. The experimentally determined phase change values were compared with published theoretical data. Direct comparison of these data was uncertain as it was unclear which relative point on the Rayleigh waveforms in the theoretical analyses was used to determine the phase change. Further analysis of the theoretical Rayleigh wave scattering process is required to determine this point so that direct comparisons can be made. It would also be useful to obtain phase change data for Rayleigh waves transmitted through various sized slots. It was not possible to determine the transmitted Rayleigh wave phase change in this investigation as the signal - to - noise ratio was too low for the phase change determination algorithm to be implemented.

The waveform recorded after propagation of a laser - generated Rayleigh wave through a surface - breaking slot perpendicular to the surface contained the transmitted Rayleigh wave followed by a consistent second feature. A path was proposed to explain this consistent second feature in accordance with all the theoretical and experimental investigations into Rayleigh wave scattering by surface - breaking defects. The proposed path was used to size defect depths in the range (1 - 5) mm.

The Rayleigh waveforms obtained after propagation through inclined surface - breaking defects exhibited a similar consistent feature. The time

interval between the transmitted Rayleigh wave and the consistent second feature for the slot tip directed toward the source tended to increase with increasing source - to - detector distance whereas it remained constant, within experimental error, for the slot tip directed away from the source. As yet this increase in time interval with increasing source - to - detector distance has not been fully accounted for and further investigations into the laser - generated Rayleigh wave scattering by inclined surface - breaking defects is required.

It is hoped that the investigations described in this thesis have extended the knowledge of laser - generated ultrasound and highlighted areas of potential applicability. Laser ultrasonics is at its development stage with some fundamental research into the generation mechanism but with the majority of the research concerned with potential applications. The results from the various investigations described have demonstrated its usefulness in improving and extending already established techniques for the non - destructive testing of components. Suggestions for future work have been given to enable further comprehension of some of the aspects of the research described.